Metals and Ceramics Division

Heavy Vehicle Propulsion Materials Program
Quarterly Progress Report for
January through March 2005

D. R. Johnson
Technical Project Manager

Prepared for
U.S. Department of Energy
Assistant Secretary for Energy Efficiency and Renewable Energy
Office of FreedomCAR and Vehicle Technologies Program
VT 05 01 020

Prepared by the
OAK RIDGE NATIONAL LABORATORY
Oak Ridge, Tennessee 37831-6066
Managed by
UT-Battelle, LLC
for the Department of Energy
Under contract DE-AC05-00OR22725

CONTENTS

Materials for Fuel Systems

High Toughness Materials (ORNL)

Materials for Exhaust Aftertreatment

Materials for Exhaust Aftertreatment (Caterpillar Inc.)

Development of Materials Analysis Tools for Studying NO_x Adsorber Catalysts (ORNL)

Development of NO_x Sensor for Heavy Vehicle Applications (ORNL and Ford Motor Company)

Microstructural Changes in NO_x Trap Materials Under Lean and Rich Conditions at High Temperatures (ORNL)

Durability of Particulate Filters (ORNL)

Materials for Air Handling, Hot Section, and Structural Components

Lightweight Valve Train Materials (Caterpillar Inc.)

Thick Thermal Barrier Coatings (TTBCs) for Low Emission, High Efficiency Diesel Engine Components (Caterpillar)

Nanoengineered Materials (North Carolina A&T State University)

NDE of Diesel Engine Components (Argonne National Laboratory)

Durability of Diesel Engine Component Materials (ORNL)

Life Prediction of Diesel Engine Components (ORNL and Caterpillar)

Low-Cost Manufacturing of Precision Diesel Engine Components (ORNL)

Advanced Machining and Sensor Concepts (University of Michigan)

Advanced Cast Austenitic Stainless Steels for High-Temperature Components (ORNL and Caterpillar Inc.)

TiAl Nanolaminate Composites (Lawrence Livermore National Laboratory)

High-Density Infrared Surface Treatment of Materials for Heavy-Duty Vehicles (ORNL)

High Temperature Aluminum Alloys (Cummins)

Titanium Alloys for Heavy-Duty Vehicles (ORNL)

Mechanical Behavior of Ceramic Materials for Heavy Duty Diesel Engines (ORNL)

Deformation Processes for the Next Generation Ceramics (ORNL)

High Speed Machining of Titanium Project (Third Wave Systems, Inc.)

Synthesis of Nanocrystalline Ceramics (Pennsylvania State University)

Development of Titanium Components for a Heavy-Duty Diesel Engine Turbocharger (Caterpillar Inc.)

Test and Materials Standards

IEA – Rolling Contact Fatigue (ORNL)

IEA Implementing Agreement for a Programme of Research and Development on Advanced Materials for Transportation Applications (ORNL)

Testing Standards (NIST)

Surface Modification of Engineering Materials for Heavy Vehicle Applications (NIST)

Low Cost-High Toughness Ceramics

T. N. Tiegs, F. C. Montgomery, and P. A. Menchhofer
Oak Ridge National Laboratory

Objective/Scope

Significant improvement in the reliability of structural ceramics for advanced diesel engine applications could be attained if the critical fracture toughness (K_{Ic}) were increased without strength degradation. Currently, the project is examining toughening of ceramics by incorporation of ductile intermetallic phases.

Technical Highlights

Previous studies have shown that the properties of the aluminide-bonded ceramics are attractive for diesel engine applications and consequently, development of these materials was started. At the present time, TiC-based composites with 40-60 vol % Ni_3Al are being developed because they have expansion characteristics very close to those for steel. The development effort is being done in collaboration with CoorsTek, Inc.

A new NiAl commercial source has been identified, procured, and characterized. A large batch (3 kg) of TiC-50 vol % Ni_3Al powder was processed with the new NiAl powder and shipped to CoorTek for injection molding (IM) trials. Test parts were fabricated and shipped back to ORNL. Initial sintering results indicated the shrinkage and densification behavior was essentially identical to the earlier composites.

Based on those results, new IM tooling was designed and fabricated at CoorsTek. Several large batches (>15 kg total) of TiC-50 vol % Ni_3Al powder were milled, homogeneously mixed and shipped to CoorsTek. Parts with the new tooling have been IM and returned to ORNL. The specimens are currently awaiting sintering when the furnace is repaired.

Status of Milestones

On schedule.

Communications/Visits/Travel

Travel by T. N. Tiegs to Cocoa Beach, FL, Jan. 23-27 to attend American Ceramic Society Conference on Advanced Ceramics and Composites and present invited paper entitled “Aluminide Bonded Ceramic Composites.”

Problems Encountered

The sintering furnace used for processing studies is out of service for two months because of a faulty pressure control valve.

Publications

T. N. Tiegs, F. C. Montgomery, P. A. Menchhofer, and P. F. Becher, “Aluminide Bonded Ceramic Composites,” to be published in Ceram. Eng. Sci. Proc., Am. Ceram. Soc., Westerville, OH (2005).

Advanced Diesel Aftertreatment Program

Christie Ragle, Herbert DaCosta, Julie Faas, Matt Stefanick, Ron Silver, Paul Park and Craig Habeger
Caterpillar Inc.

Objective/Scope

The objective of the effort is to develop and evaluate materials that will be utilized in aftertreatment systems for diesel engine applications. These materials include catalysts for CO and hydrocarbon oxidation, NO_x reduction, and filtration media to improve particulate abatement capabilities in the exhaust system. The project is a part of Caterpillar strategy to meet EPA requirements for regulated diesel emissions in 2007 and beyond.

This year's focus is to assess durability of various catalyst technologies in terms of phosphorous, sulfur and thermal degradation, and to identify diesel particulate trapping materials that have high durability and filtration efficiency to comply with future emission regulations for heavy-duty diesel engines.

Technical Highlights

Diesel Particulate Filter (DPF).

A non-disclosure agreement (NDA) has been in place with an identified supplier in order to assess their catalyzed and un-catalyzed DPF samples. The un-catalyzed DPF obtained from the supplier showed promising results in our bench test measurements. High filtration efficiencies (97.5 - 99%) and moderate backpressure increase (1 kPa for a load of 3.5g soot/L DPF) were achieved. However, small sizes of particulates passed through the un-catalyzed DPF in the early stages of soot loading. A catalyzed DPF will be tested to compare with the results of the un-catalyzed DPF.

Catalyst Durability.

NO_x Adsorber Durability: A test plan has been developed to evaluate the durability of NO_x Adsorbers (LNTs) in terms of phosphorous degradation. Model LNTs incorporating a NO oxidation function, a NO_x storage element and a NO reduction function have been prepared and tested for fresh performance to establish a baseline. Next quarter, samples will be loaded with phosphorous using a previously developed method on a laboratory diesel fuel burner and a doped fuel. The oxidation, storage and reduction function of the NO_x adsorbers will be tested after loading with 4 g/L and then 10 g/L phosphorus, with and without a blank monolith in front. The potential interaction between phosphorus deactivation and sulfur degradation will also be investigated. An abstract of a presentation including some of the preliminary results from this study was submitted to the North American Catalysis Society for their 19th annual meeting.

Lean-NO_x durability: Durability studies using sulfur and phosphorus aging have been performed on Lean- NO_x catalysts. Phosphorus was introduced to the sample using a diesel fuel burner burning phosphorus-blended zero-sulfur fuel, and the NO_x reduction performance was tested after each exposure increment. NO_x reduction of the catalyst maintained more than 40% NO_x conversion after reaching 30,000 hours engine-equivalent (C15 engine) phosphorus exposure. Phosphorus content of the aged samples is being quantified using XRF.

Sulfur was introduced by SO_2 exposure directly using a bench test system, monitoring the NO_x reduction performance as a function of time-on-stream with SO_2. Sulfur content of the exposed samples has been quantified using a LECO CS-200 Carbon/Sulfur Determinator. NO_x reduction performance of the catalyst was reduced to ~30% NO_x reduction after 5,000 hours engine-equivalent (C15 engine) sulfur exposure, but maintained that level of performance through the test period of 20,000 hours.

The negative impact of sulfur exposure is more pronounced than that of phosphorus exposure, both in magnitude and rate of degradation. Understanding the effects of sulfur and phosphorus provides insight into the development of catalyst materials and mitigation options best suited for the intended environment.

Future Plans

1. Capture intellectual properties and document technical reports (Lean- NO_x project).
2. Study catalyst durability (P, S and thermal sintering) of oxidation catalyst technologies.
3. Load samples of LNTs with varying levels of P to determine durability relative to fresh performance.
4. Continue searching for and testing new substrate materials for DPF filters.

Travel

Herbert DaCosta made two trips (Minneapolis, MN, and Chicago, IL) to attend training sessions on the FEMLAB software that is a simulation tool for designing and modeling DPF systems.

Status of FY 2005 Milestones

1. The durability study of various catalyst technologies for P and S degradation begins.
2. Tested 1-in. x 3-in. core samples uncatalyzed DPF for filtration efficiency and backpressure.

Development of Materials Analysis Tools for Studying NO_x Adsorber Catalysts

Thomas Watkins, Larry Allard, Doug Blom, Michael Lance, Harry Meyer, Larry Walker, and Chaitanya Narula
Oak Ridge National Laboratory

Bill Eppling and Roger England
Cummins, Inc.

Objective

The objective of this effort is to produce a quantitative understanding of the processing and in-service effects on NO_x adsorber catalyst technology leading to an exhaust aftertreatment system with improved catalyst performance capable of meeting the 2007 emission requirements.

Samples and Approach

A Cummins catalyst supplier provided new catalyst materials, which are being examined with diagnostic tools developed under the CRADA. Investigations of these candidate-production materials are being implemented on both the bench and engine research scale. These investigations include the examination of unused, reactor and engine-aged catalyst samples. Investigative tools included transmission electron microscopy (TEM), X-ray diffraction (XRD), X-ray photoelectron spectroscopy (XPS), Raman spectroscopy and infrared spectroscopy (IR).

Technical Highlight

A baseline oxidation catalyst sample has been partially examined with XRD to determine the particle size as a function of length along the sample. Eight 10-mm areas are being examined while the remaining 70 mm is masked off with (100) Si wafer parts. The Pt crystallite size is 13, 51 and 43 nm for the first, second and eighth 10-mm segments.

A "FRESH" Pt/Ba/gamma-Al_2O_3 was examined in the JEOL 8200 electron microprobe. Elemental maps and quantitative line-scans for this sample were performed. Figure 1 shows the major components while Figure 2 has an expanded ordinate to better illustrate the distribution of S, Ba and Pt in the sample. Ba was uniformly distributed throughout the thickness of the washcoat. The Pt concentration was highest at the outer surface, while S was present as a diffuse layer in the outer half of the washcoat. Elemental maps of Pt, Ba, Al and S are shown in Fig. 3. The same trends as seen in the line-scans are evident.

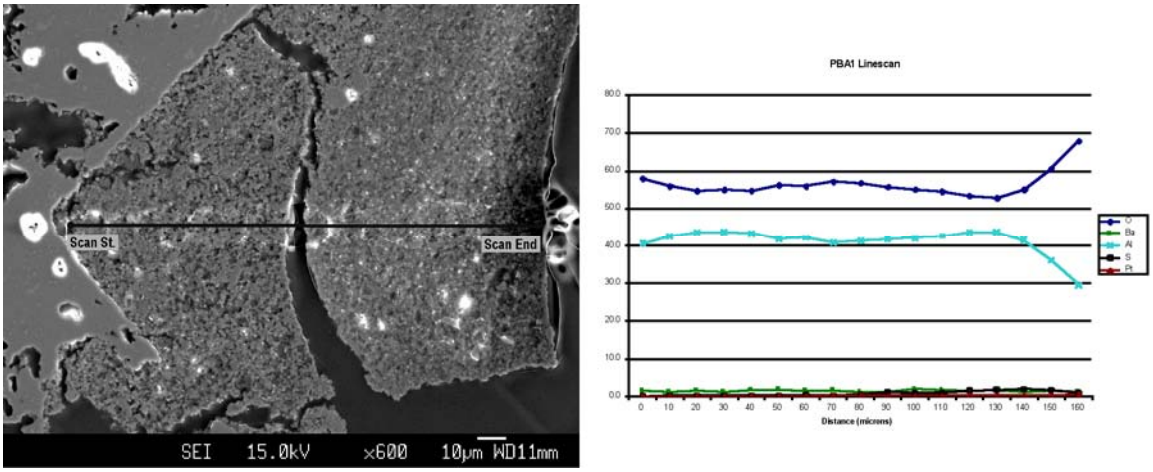

Figure 1: Secondary electron image and quantitative linescan of sample PBA1. A 10-micron beam was stepped 10 microns at a time from the cordierite monolith out to the outer surface of the washcoat. The circular marks in the SE image are evidence of the damage caused during the data collection.

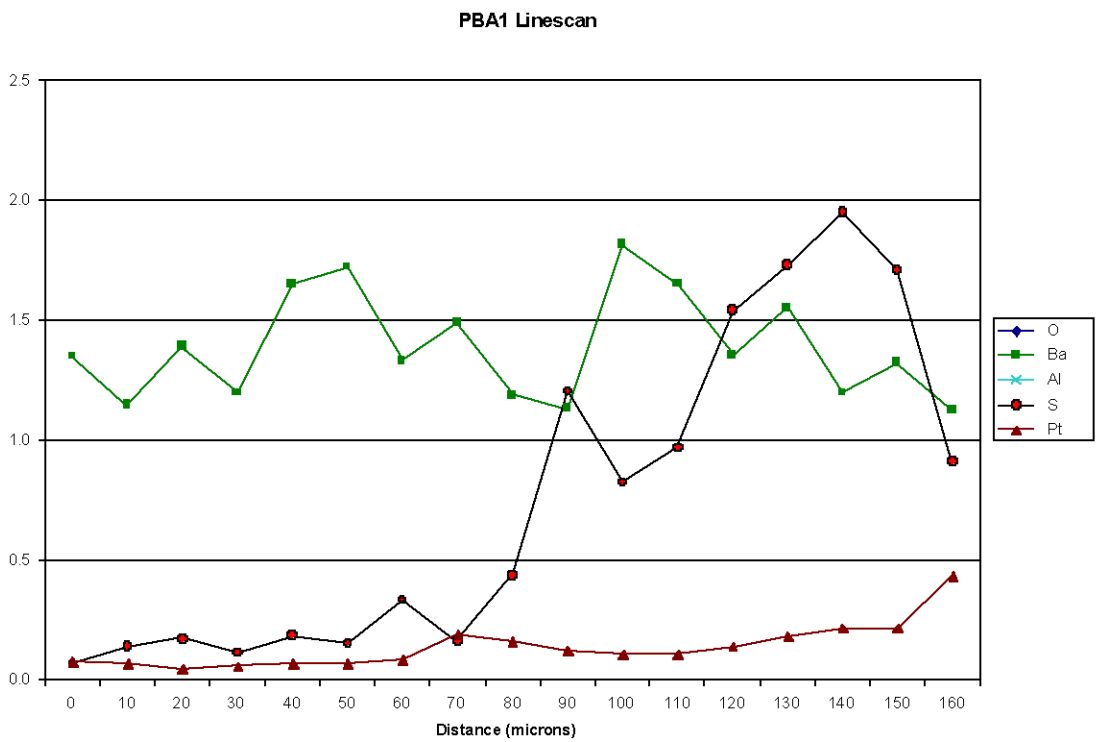

Figure 2: Quantitative linescan with an expanded y-axis to show the variation of Ba, S, and Pt throughout the washcoat. Pt is highest at the outer surface of the washcoat with a relatively uniform distribution of Ba and S being present as a diffuse layer in the outer half of the washcoat layer.

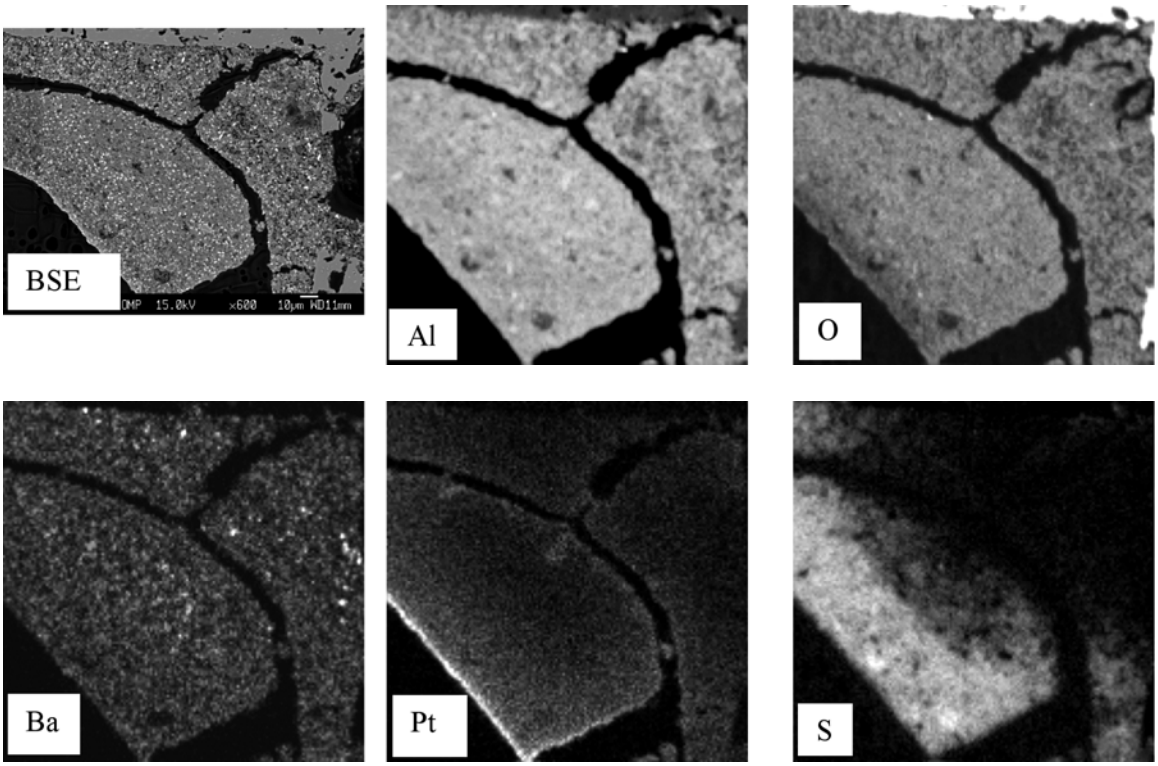

Figure 3: Backscattered electron image and X-ray maps for PBA1.

Development of NOx Sensors for Heavy Vehicle Applications

Timothy R. Armstrong, David L. West, and Fred C. Montgomery
Oak Ridge National Laboratory
CRADA No. ORNL 01-0627
with Ford Motor Company

Objective

The proposed project seeks to develop technologies and materials that will facilitate the development of NO_x and ammonia sensors. The development of low-cost, simple NO_x will facilitate the development of ultra-low NO_x emission engines, directly supporting the OHVT goals.

Technical Highlights

1. Studied longer-term sensing performance under both "dry" and "wet" (~1–3 % H_2O). This was in response to CRADA partner requests.
    a. Element resistance appears to "plateau" under both "dry" and "wet" conditions.
    b. Changes due to NO_x variations (between 20 and 190 ppm_V) are clearly distinguishable against "background".
    c. Varying H_2O (Fig. 1b) causes changes in element resistance.

2. Discovered that current electrode material (Sr-modified $LaCrO_3$) decomposes when exposed to H_2O, NO_2 (and perhaps NO), and electrical bias.
    a. Decomposition not observed when electrode powder only subjected to moisture and elevated temperature (600°C).
    b. Decomposition also not observed in absence of H_2O.
    c. Indicates some "synergy" between electrical stimulus, presence of NO_x, and H_2O.

3. Pursuant to discovery above, have re-opened investigation into new materials.
    a. Results in Fig. 2 (obtained testing in dry air with $La_{0.75}Sr_{0.25}Cr_{0.5}Mn_{0.5}O_3$) are promising, indicate that "total NO_x" behavior may be possible with a variety of oxides.
    b.

Future Plans

- Investigate use of Mg-modified electrodes. This will help determine whether decomposition problem mentioned above is caused by use of alkaline earth modifiers.

- Work with CRADA partner to develop a screening test for sensitivity to moisture and bias.

- Initiate collaboration with Georgia Tech on Raman, FTIR investigation of NO_x species, crystallography of electrode material at sensor surface.

Status of FY 2005 Milestones

(1) Optimize the electrode design (geometry) to maximize output signal. **(03/05)**
(2) Optimize the electrode morphology for the current class of lanthanum chromite electrocatalysts to maximize output signal. **(05/05)**
(3) Evaluate sensor sensitivity to steam and develop protocol to minimize. **(09/05)**
Ford recently indicated during a phone call that milestone 3 is to be the focus of this year's activity. They further indicated that humidity has been the major cause of failure in most NO_x sensors developed to date and they wish us to develop an understanding of humidities' effects on our materials immediately. ***On track***

Communications/Visits/Travel

1. Biweekly teleconference were initiated this quarter between DOE, Ford, LLNL, and ORNL.
2. A meeting was held at LLNL in March with all members attending to discuss technical progress and continue to define the path towards commercialization.

Problems Encountered

None to date.

Publications

None.

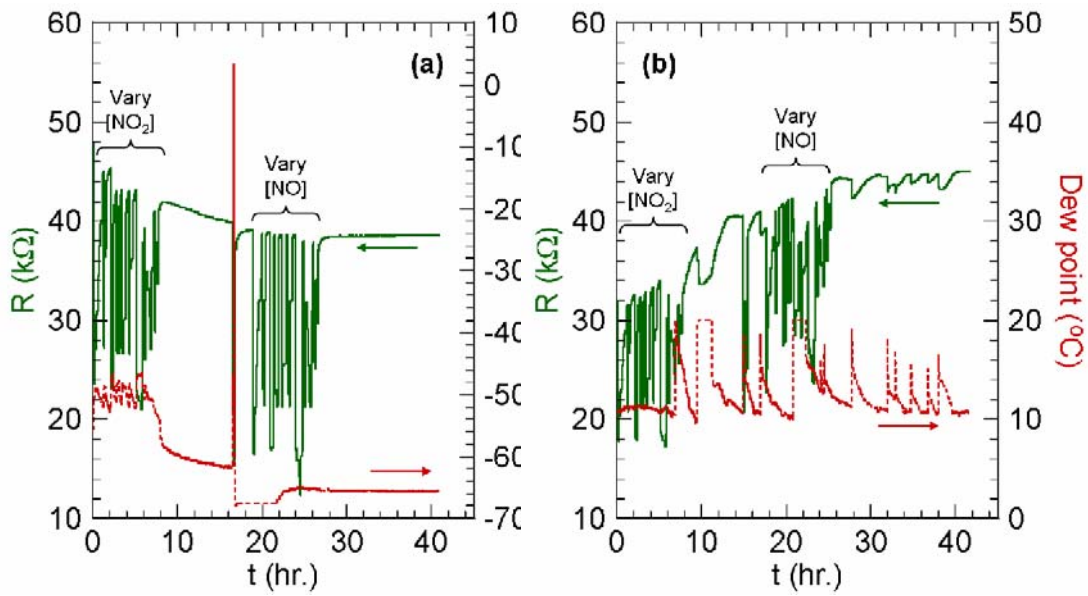

Figure 1. Sensing element performance under continuous operation for ~50 h in "dry" (a) and "wet" (b) conditions. Data collected at 600°C, 7 vol % O_2.

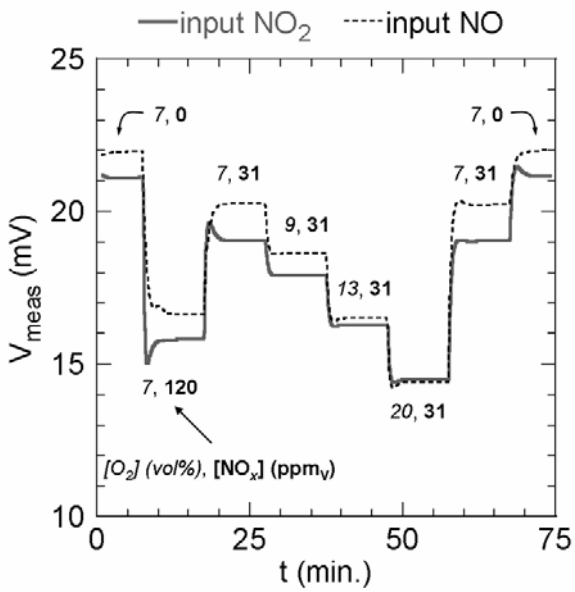

Figure 2. Sensing performance of $La_{0.75}Sr_{0.25}Cr_{0.5}Mn_{0.5}O_3$ electrodes. Data collected in 7% O_2, balance N_2 (no added H_2O) at 600°C.

Microstructural Changes in NO_x Trap Materials under Lean and Rich Conditions at High Temperatures

C.K. Narula, M. Moses, and L.F. Allard
Oak Ridge National Laboratory

Objective/Scope

The introduction of diesel-engine-based heavy-duty trucks and passenger vehicles depends on the successful development of a strategy to treat nitrogen oxides (NO_x) emissions. A catalyst or a combination of catalysts that can convert NO_x into inert gases under oxidizing conditions over a complete range of exhaust temperatures does not presently exist. Among NO_x treatment strategies, lean NO_x traps (LNT) are the most likely candidates for early deployment because they are consumer transparent (no action needed on the part of consumers) and can be system-integrated into current vehicle control strategies [1].

NO_x traps collect engine out NO_x during lean operation and treat it during short rich operation cycles [2]. The NO_x traps can be considered to be derived from commercial three-way catalysts (TWC) installed to treat stoichiometric emissions from engines operating at air-fuel ratios of ~14. As such, the basic components of NO_x traps are identical to three-way catalysts. The advance version of three-way catalyst is a two layer system on a honeycomb substrate with the inner layer based on platinum-alumina and the outer layer on rhodium-ceria-zirconia. The NO_x traps derived from advanced three-way catalysts are identical to these with the exception of high baria content (the upper limit being close to 20%) in the alumina layer.

Fresh NO_x traps work very well but cannot sustain their high efficiency over the life-time of vehicles. The gradual and persistent deterioration in the performance of commercial TWC is quite well known [3]. The performance deterioration in NO_x traps is believed to be caused by aging due to high-temperature operation and sulfation-desulfation cycles necessitated by the sulfur oxides in the emissions from the oxidation of sulfur in fuel. The formation of barium aluminate is also considered to be a cause of performance deterioration since barium aluminate forms on thermal aging and is an inefficient NO_x adsorber. Until last year, the aging related microstructural changes in precious metals component were not available in open literature. In our previous reports, we summarized our studies of fresh and aged supplier samples that clearly show changes that occur on aging under various operating conditions. The prominent changes are sintering and migration of precious metals and migration of barium leading to reduced precious metal-adsorber surface area available for NO_x adsorption in lean cycles.

In order to design a thermally durable NO_x trap, there is a need to understand the changes in the microstructure of materials that occur during various modes of operation (lean, rich, and lean-rich cycles). This information can form the basis for selection and design of new NO_x trap materials that can resist the deterioration under normal operation. The first goal of the project is to determine if one or all of the microstructural changes take place during lean, rich, or lean-rich cycles.

The tasks to achieve this goal are as follows:

- Complete microstructural characterization of fresh and thermally aged NO_x trap materials to determine the species formed as a result of aging.
- Complete microstructural characterization of fresh NO_x trap materials after exposure to lean conditions to determine the species formed during lean cycles.
- Complete microstructural characterization of fresh NO_x trap materials after exposure to rich conditions to determine the species formed during rich cycles.

The second goal of the project is to investigate and design new materials that can withstand NO_x trap operating conditions without undergoing detrimental structural changes. The results from the first goal will provide insights into changes that occur in NO_x trap materials at a microstructural level upon extended exposure to NO_x trap operating conditions enabling selection and design of materials for the second goal.

Over the last two years, we determined the microstructural changes that occurred in a supplier lean NO_x trap system (based on Pt/BaO-Al_2O_3 and CeO_2-ZrO_2 materials) upon aging on (1) a pulsator at Ford (2) dyano at Ford, and (3) on vehicles in gasoline DISI engines in Europe.

- After pulsator aging, lean and rich aged samples showed that the sintering of platinum particles occurs during aging and barium migrates into ceria-zirconia layer. Both of these factors reduce platinum-barium oxide surface area where NO_x adsorption and reduction takes place during lean and rich cycles respectively. The stoichiometric aging also leads to the migration of barium into ceria-zirocnia layer but the sintering of platinum is less severe.
- The dyano aged samples showed extensive sintering of platinum and its migration in ceria-zirconia layer. The sintering of rhodium was also observed. The migration of barium into ceria-zirconia and the sintering of precious metal component could explain the deterioration of performance
- The analysis of on vehicle evaluated samples after 32K km and 80 km showed that the bulk of precious metal sintering occurred in the early stages of on vehicle aging.

These results primarily show precious metal sintering and barium migration to be cause of performance deterioration in NO_x trap materials in gasoline engine exhaust conditions. While the laboratory aging protocols for diesel engines are in development, we have compiled a data showing early stage changes in model NO_x trap materials under diesel conditions. We assumed that lower temperature of simulated diesel exhaust would slow down the aging compared with gasoline engine exhaust. Thus, we completed a series of thermal aging, diesel lean aging, and diesel rich aging of model NO_x trap and model NO_x trap modified with manganese oxide as well as Pt/Al_2O_3 for comparison purposes. The results were reported in the last report and are summarized in Table I with updates.

During last six months we have completed an update of ex-situ reactor that is now capable of lean-rich cycling in addition to independent lean and rich cycles. The updated ex-situ reactor incorporates a commercial bench top tube furnace and solenoids into the gas flow pathway. The tube furnace allows for higher temperatures needed for thermal aging under exhaust conditions in addition to attaining continuous and reproducible temperatures. The introduction of two solenoids controlled by LabView software enables the cycling of lean and rich diesel gases at a continuous cycle.

In order to test the updated reactor, we are in the process of reproducing our work on the microstructural changes to fresh NO_x trap catalysts. Currently, reproducibility of results from the old reactor for 2%Pt-98%[10%CeO_2-ZrO_2-90%(2%La_2O_3-98% BaO•6Al_2O_3)] and 2%Pt-5%MnO_2-93%[10%CeO_2-ZrO_2-90%(2%La_2O_3-98% BaO•6Al_2O_3)] catalysts for NO_x traps under lean diesel aging at 500°C for 4 hours on the new reactor are in progress. The results on the new reactor for these two catalysts are expected to be consistent with the changes observed on the old reactor. Lean diesel aging of the Pt/γ-Al_2O_3 material on the updated ex-situ reactor shows microstructural changes that differ from the changes observed on the old reactor. Lean diesel aging of Pt on the updated reactor produced little (ca. 0.5 nm increase) sintering of the Pt particles. This is in contrast with the results on the old reactor where Pt particle size increased from 0.5-1.0 nm to 8.0-10.0 nm. This is not surprising because lean aging of Pt/γ-Al_2O_3 on the old reactor was not consistent with other model LNTs (containing barium oxide).

Interestingly, aging studies under cycling of the lean and rich diesel exhaust gases at a constant 60s/5s cycle, respectively, at 500°C for 4h show that there is only marginal sintering of the Pt particles in the 2%Pt-98%[10%CeO_2-ZrO_2-90%(2%La_2O_3-98% BaO•6Al_2O_3)] (Fig. 1) and 2%Pt, 5%MnO_2-93%[10%CeO_2-ZrO_2-90%(2%La_2O_3-98% BaO•6Al_2O_3)] NO_x trap catalysts.

These results show that there is no significant sintering under either lean, rich, or lean-rich cycle conditions at 500ºC after 4 hours. This observation is consistent with the fact that LNTs are durable under normal operation if there is no sulfur present in the fuel and no desulfation step is required.

Due to the new capabilities of our updated reactor, we have initiated aging studies under lean-rich cycle conditions. These studies are under accelerated aging protocols suggested by our collaborators and consists of a 60s/5s lean/rich diesel gas flow cycle, respectively, at 700°C for a 16 h period. Our ongoing experiment is partially complete and results are reported here. We have not included sulfur dioxide in our simulated diesel exhaust in this experiment but will be included in the next experiment. A comparison of results will allow us to comment on microstructural changes that occur at 700°C with and without desulfation step. Furthermore, we will be able to correlate our results with dyano and vehicle aged lean NOx trap as they become available.

In order to follow the microstructural changes that occur under accelerated aging conditions as a function of time on 2%Pt-98%[10%CeO_2-ZrO_2-90%(2%La_2O_3-98% BaO•6Al_2O_3)], we are carrying out aging in 4 hour steps. Results of the microstructural changes to the Pt particles after the first 4 h of the thermal aging process show a small 0.5-1.0 nm increase in size and no change after the next two 4 h periods. While significant sintering of the Pt particles did not occur in the first 12 h of the simulated lean/rich thermal aging protocol, the location and presence of Pt particles changed significantly in the 1st 4h period, Fig. 2. A significant change in particle presence and location was not observed in the 2nd or 3rd 4h period, Fig. 2.

We will complete this aging study as well as aging study of 2%Pt-98%[10%CeO_2-ZrO_2-90%(2%La_2O_3-98% BaO•6Al_2O_3)] using simulated exhaust containing sulfur oxide shortly. The results, correlated with catalyst evaluation results, will allow us to forecast durability based on microstructural changes.

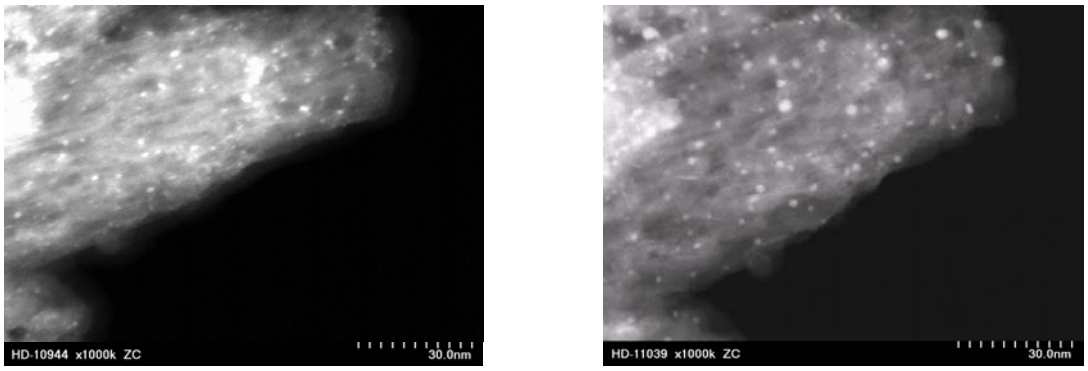

Figure 1. DF-STEM of fresh (left) and lean/rich aged (right) 2%Pt-98%[10%CeO_2-ZrO_2-90%(2%La_2O_3-98% BaO•6Al_2O_3)] at 500°C, 4 h.

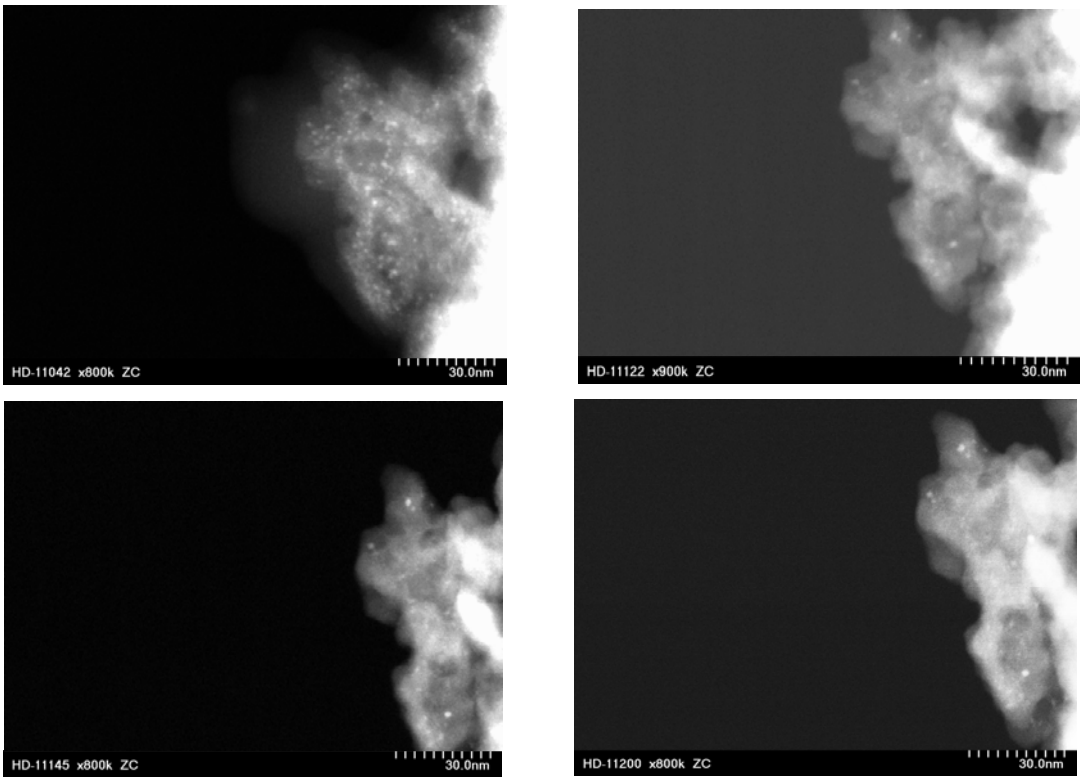

Figure 2. DF-STEM of fresh and lean/rich thermally aged 2%Pt-98%[10%CeO_2-ZrO_2-90%(2%La_2O_3-98% BaO•6Al_2O_3)]; Fresh (left, top), 700°C, 1st 4h period (right, top), 2nd 4h period (left, bottom), and 3rd 4h period (right, bottom).

<u>Other activities</u>

We have completed an update of ex-situ reactor that is capable of lean/rich cycling in addition to lean or rich cycles. We are currently studying the results of lean/rich cycling at 500ºC and the thermal aging protocol on the three catalysts to finish the series summarized in table 1. Tests

employing the updated reactor are also in progress to confirm the reliability of the results obtained on the old reactor under lean and rich conditions. A bench top flow-reactor design is completed, and we will initiate assembly shortly. The bench top flow-reactor will enable us to monitor the activity of the NO_x trap catalysts under varying conditions. We will also be able to screen the activity of modified catalyst in route to establishing a more efficient NO_x trap catalysts resistant to the sintering observed in those currently available.

Communications/Visitors/Travel

1. We are writing an invited review article on "Materials Issues Related to Catalysts for Diesel Exhaust Treatment" jointly with J. Hoard of Ford Motor Co.
2. We will be presenting results in CLEERS workshop to be held at UM, Dearborn in May 2005.

References

1. Miyoshi, N.; Matsumoto, S.; Katoh, K.; Tanaka, T.; Harada, J.; Takahashi, N.; Yokota, K.; Sigiura M., and Kasahra, K.; "Development of New Concept Three-Way Catalyst for Automotive Lena-Burn Engines," SAE paper 95-0809.
2. Takahashi, N.; Shinjoh, H.; Iijima, T.; Suzuki, T.; Yamazaki, K.; Yokota, K.; Suzuki, H.; Miyoshi, N.; Matsumoto, S.; Tanizawa, T.; Tateishi, S.; and Kasahara, K.; "The New Concept 3-Way Catalyst for Automotive Lean-Burn Engine: NO_x Storage and Reduction Catalyst," Catalysis Today, 1996, **27**, 63-69.
3. Gandhi, H.S., Graham, G.W., and McCabe, R.W., "Automotive Exhaust Catalysis," J. Cat., 2003, **216**, 433-442.

Table 1: Summary of Pt particle size change under various treatments to the model catalysts studied to date.

	Fresh Sample[1]	**Thermal Aging In Air (XRD of powder)**	**Lean Diesel Aging 500 °C/ 4h**	**Rich Diesel Aging 500 °C/ 4h**	**Lean/ Rich Cycle (60s/5s) Diesel Aging 500 °C/ 4h**[1]	**Lean/Rich Thermal Diesel Aging 700 °C**[1]
2% Pt / γ-Al_2O_3	0.5 - 1.0 nm (0.9 nm)	600ºC, 3.4 nm 700ºC, 17.1 nm 800ºC, 26.1 nm 900ºC, 39.5 nm	1.0 - 1.5 nm[1] (1.3 nm)	2.0 - 4.0 nm		
2%Pt-98%[10%CeO_2-ZrO_2-90%(2%La_2O_3-98% BaO•6Al_2O_3)]	1.0 – 1.5 nm (1.45 nm)	600ºC, 2.6 nm 700ºC, 21.3 nm 800ºC, 37.2 nm 900ºC, 48.4 nm	1.0 -2.0 nm	1.5 - 3.5 nm	1.0 - 1.5 nm (1.7 nm)	1.0 nm F (1.4 nm) 1.5 – 2.0 nm 4h (2.1 nm) 1.5 - 2.0 nm 8h (2.1 nm) 1.5 nm 12h (2.0 nm) _____nm 16h
2%Pt, 5%MnO_2-93%[10%CeO_2-ZrO_2-90%(2%La_2O_3-98% BaO•6Al_2O_3)]	1.0 - 1.5 nm (1.6 nm)	700ºC, 20.7 nm 800ºC, 27.0 nm 900ºC, 34.0 nm	2 - 3 nm	1 - 2 nm	1.0 – 1.5 nm (1.7 nm)	

1. The distribution is centered on these values. Averages are reported in brackets.

Durability and Reliability of Ceramic Substrates for Diesel Particulate Filters

Edgar Lara-Curzio, Amit Shyam, H-T. Lin and Randy Parten
Oak Ridge National Laboratory

Objectives/Scope

To develop/implement test techniques to characterize the physical and mechanical properties of ceramic Diesel particulate filters (DPFs). To implement a probabilistic-based analysis to quantify the durability and reliability of DPFs.

Highlights

The fracture toughness and slow crack growth behavior of porous cordierite DPF test specimens was determined by the double-torsion test method at ambient temperature.

Technical Progress

During the reporting period the fracture toughness of porous cordierite test specimens was determined according to the double-torsion test method. The material evaluated was received from Corning. The fracture toughness was found to be 0.49 MPam$^{0.5}$. In all cases, cracks propagated parallel to the major axis of the test specimen and the crack was found to interact with the material microstructure, in particular with large pores. Work was also initiated to determine the propensity of porous cordierite to slow crack growth (SCG) using the double-torsion test method and the load relaxation technique. It was found that at ambient temperature the SCG exponent was equal to 30. Work is in progress to investigate the SCG behavior of this material at elevated temperature.

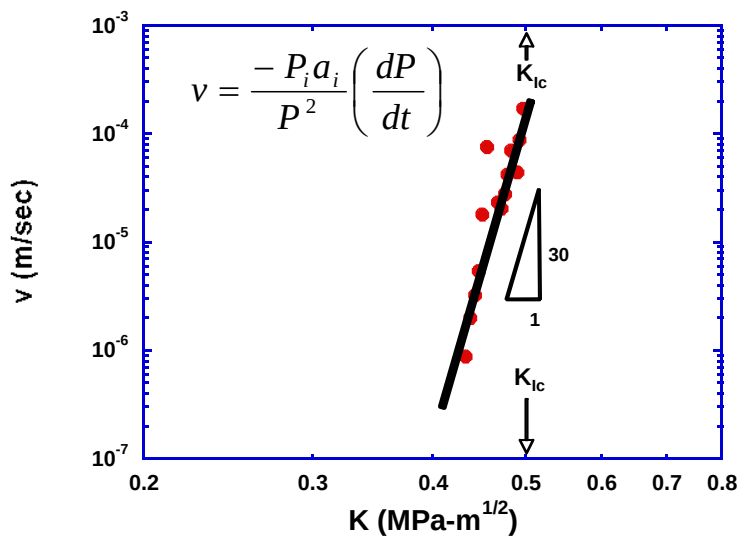

Figure 1. Slow crack growth results for porous cordierite at ambient conditions.

Milestones

To organize a round-robin testing program to determine the precision in the determination of flexural strength of cordierite cellular ceramics used as DPFs. June 2005. **(Completed)**

Meetings

Monthly teleconferences with Cummins and Corning personnel were held during the reporting period.

Lightweight Valve Train Materials

Jeremy S. Trethewey, John. A. Grassi, and Matt P. Fletcher
Caterpillar Inc.

Introduction

Valve train components in heavy-duty engines operate under high stresses and temperatures, and in severely corrosive environments. In contrast, the valve train components in the light-duty engine market require cost-effective reliable materials that are wear resistant and lightweight in order to achieve high power density. For both engine classes, better valve train materials need to be identified to meet market demand for high reliability and improved performance while providing the consumer lower operating costs.

Advanced ceramics and emerging intermetallic materials are highly corrosion and oxidation resistant, and possess high strength and hardness at elevated temperatures. These properties are expected to allow higher engine operating temperatures, lower wear, and enhanced reliability. In addition, the lighter weight of these materials (about 1/3 of production alloys) will lead to lower reciprocating valve train mass that could improve fuel efficiency. This research and development program is an in-depth investigation of the potential for use of these materials in heavy-duty engine environments.

The overall valve train effort will provide the materials, design, manufacturing, and economic information necessary to bring these new materials and technologies to commercial realization. With this information, component designs will be optimized using computer-based lifetime prediction models, verified in rig bench tests and validated in short-and long-term engine tests.

Program Overview -

Information presented in this report is based on previous proprietary research conducted under Cooperative Agreement DE-FC05-97OR22579.

Ceramic Materials:

Silicon nitride materials have been targeted for valve train materials in automotive and diesel industries since the early 1980's. Some silicon nitride material grades have reached a mature level of materials processing, capable of implementation into production. Commercial realizations have been reported in both automotive and diesel valve trains, with large-scale production underway. The silicon nitride valve train components in production are used in high rolling contact stress applications and have exhibited superior wear resistance, and longevity.

Intermetallic Materials:

Titanium aluminide based intermetallics retain their strength to elevated temperature and are highly corrosion-resistant. They are lightweight, and posses high fracture toughness. These alloys are actively being investigated for several aerospace and automotive applications.

Current Quarter Summary

Program Shift from Si_3N_4 to TiAl

At the commencement of this high temperature material investigation the primary material class of interest was structural ceramics. This material class has been investigated from both a technical and economical perspective for several years. After conducting a high level investigation of different types of structural ceramics, a supplier was chosen to supply Si_3N_4 materials for valve blanks. These valves are being finish machined and will be evaluated in several engine and bench tests by 3Q05. However, the brittle nature of Si_3N_4 has led to significant resistance to the implementation of structural ceramics in field applications. Recently, Titanium Aluminide has emerged as an intermetallic that is expected to be an intermediary from a performance standpoint between the current Ni-based production material and a structural ceramic.

Due to the great potential of this emerging material, the emphasis of the project will be shifted from the structural ceramic materials (Si_3N_4) to intermetallics (TiAl). A renewed effort will be initiated to examine the effects of machining damage on the mechanical properties of TiAl test specimens. Cast TiAl samples will be examined at Argonne National Lab (by JG Sun) to investigate NDE opportunities and challenges. In 2004, a preliminary set of TiAl valves was friction welded to Ti-6Al-4V shafts. These valves will be tested in parallel to Si_3N_4 and production Ni-based valves on engine and rig tests.

Development of a Life Prediction Tool for Advanced Materials

In an effort to analyze the lifetime of advanced materials from a theoretical standpoint Caterpillar has been working with Jadaan Engineering & Consulting on the application of the life prediction code NASA/CARES to advanced valves. Several tasks have been completed and are discussed below:

FEA model development

There are several inputs for the life prediction code:

- Axisymmetric FEA model to establish the valve's geometry – see Figure 1
- Mechanical stresses as a function of crank angle for an entire cam cycle (considered as mechanical boundary conditions – see Figure 2)
- Temperature distribution throughout the valve to account for thermal stresses (considered as thermal boundary conditions)
- Mechanical properties of the valve material

These inputs were supplied to Jadaan Engineering & Consulting for a G3406 valve experiencing representative operating conditions. A finite element model was then generated and a transient reliability analysis was performed.

Transient reliability analysis

Subsequent to applying the mechanical and thermal boundary conditions onto the valve geometry, the material properties of Si_3N_4 are assigned to the elements. The mechanical load spectrum (Figure 2) was discretized into a finite number of steps and the stress state was calculated for each set of loads. Figure 3 shows a snapshot of the stress field (maximum principal stress) at a selected crank angle (~13º). This is representative of the stress field at every time step; the maximum principal stress is experienced in the fillet radius of the valve head.

Using this information, a computational transient reliability analysis is performed. In this approach, the material is susceptible to slow crack growth (fatigue) and the probability of failure depends on both the number of cycles and load history sequence. The probability of failure during a given time step is directly impacted by those in the previous time steps. Due to fatigue damage, the probability of failure will increase with time as damage accumulates with additional load cycles. The resulting number of cycles vs. probability of failure chart is shown below.

Safety Factor	Number of cycles	Time (hours)	Probability of failure
1	1	1.58e-5	0.0
	1e9	15800	0.0
	1e15	1.58e10	0.0
	1e20	1.58e15	0.444e-15
3	1	1.58e-5	0.8441e-8
	1000	1.58e-2	0.8524e-8
	1e5	1.58	0.1220e-7
	1e8	1580	0.5667e-7
	1e9	15800	0.9632e-7
	1e12	1.58e7	0.4717e-6
5	1	1.58e-5	0.8130e-3
	10000	0.158	0.9605e-3
	1e6	15.8	0.2351e-2
	1e8	1580	0.6754e-2
	1e9	15800	0.01145
	1e12	1.58e7	0.05432

Surprisingly, at a safety factor of one, there is a very low chance of failure below 10^{20} cycles. Even at a safety factor of five, there is ~0.7% probability of failure after two months of operation (10^8 cycles). Although these may seem to be promising results, they must be interpreted with extreme caution. It must be noted that the loads modeled are not the only ones present. However, this exercise served to explore the capability of the model. Further refinement of the valve loading conditions must be made to more closely model the actual operating conditions of the valve. It is expected that when boundary conditions that are more rigorous are applied, the probability of failure will increase dramatically compared to this preliminary model.

Outline of future work

Several secondary tasks will be performed now that the foundation of the life prediction model has been developed. First, a three-dimensional valve model will be generated. This will allow for non-axisymmetric loading modes (e.g. stem bending due to valve guide misalignment). After a Si_3N_4 model has been fully explored, a TiAl material model will be developed using a three parameter Weibull fit to capture the probabilistic nature of the intermetallic material. Finally, a Probabilistic Design System (PDS) study will be performed on the model to examine the influence that various parameters (material specifications, geometric tolerances) have on the overall lifetime of the valve.

Engine Testing of Silicon Nitride, TiAl and Production Valves
As outlined in the 4Q04 report, a test timeline has been established to evaluate the robustness of three different material classes of G3406 engine valves (i.e. Si_3N_4, TiAl and the Ni-based production valve). In addition to the comparative measurements made between the three materials, the performance of the ceramic and intermetallic valves will be compared to results from the computational analysis outlined above.

A Natural Gas G3406 engine, located at the National Transportation Research Center in Knoxville, TN, will be used to execute the 1000-hour engine durability test. At various intervals of accumulated engine hours, valves will be removed from the engine and evaluated using various analytical methods. The retained strength analysis will be of particular interest, as it will best correlate to the computational results. At ORNL's High Temperature Materials Research Lab (HTML), each valve will be sectioned into five pieces (valve head and four semi-cylindrical shaft sections). Under the supervision of H.-T. Lin, each part will be subjected to an ASTM-defined strength test and the results will be compared to the computational results of the life prediction tool.

Restoration of Thermomechanical Valve Test Rig
In 4Q04 a valve test rig capable of simulating cyclic thermal and combustion loads was internally relocated at the Caterpillar Technical Center. The rig is capable of applying a cyclical hydraulic load to the valve face to simulate combustion pressure loading. It can also apply a cyclic thermal load using an induction heating coil. Thus, a near-engine environment may be simulated on magnetically susceptible valve materials (i.e., metals and most intermetallics but few ceramics).

In order to fully restore the valve test rig, several supporting components must be acquired and the rig's integrated systems must be assembled (hydraulic, electrical, mechanical). A personnel resource will be obtained to support the assembly and daily operation of this rig. By the end of 2Q05, rig development will be in the debugging phase and the first testing will commence in 3Q05.

C15 ACERT Engine Donation
A C15 ACERT engine was donated to Oak Ridge National Laboratory during 1Q05. The engine was procured by Caterpillar's Advanced Materials Technology Division and delivered to the National Transportation Research Center in Knoxville, TN. This engine will support component testing of advanced materials.

Figures -

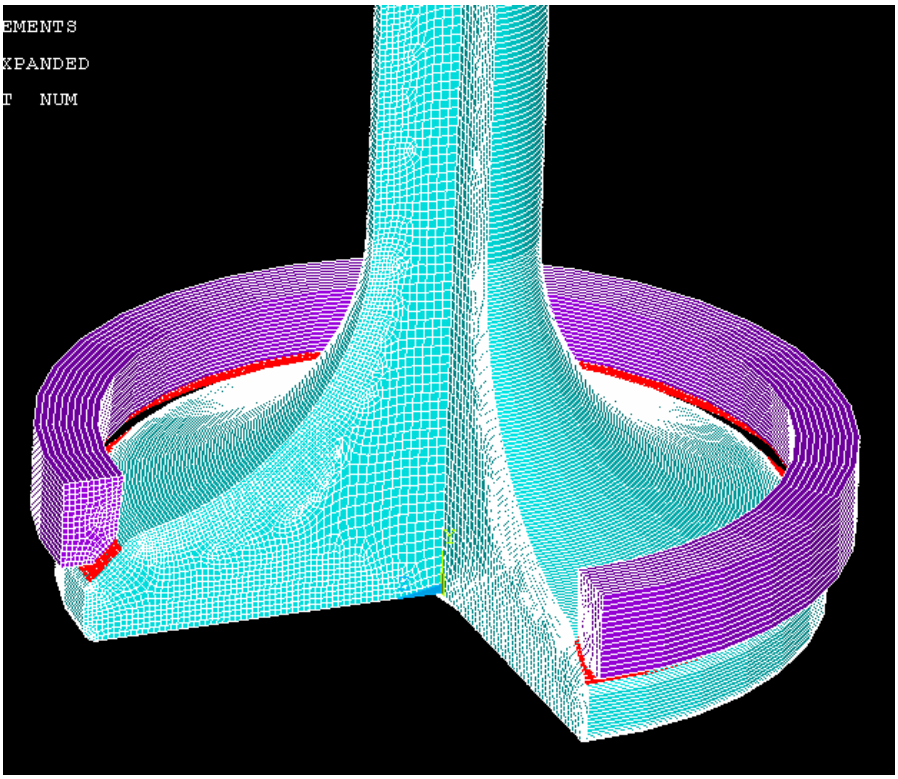

Figure 1: A sectioned view of the axisymmetric finite element mesh used to evaluate the thermo-mechanical deformation of the re-designed G3406 exhaust valve. Note that the seat insert was included to model the mechanical contact of the valve/seat pair.

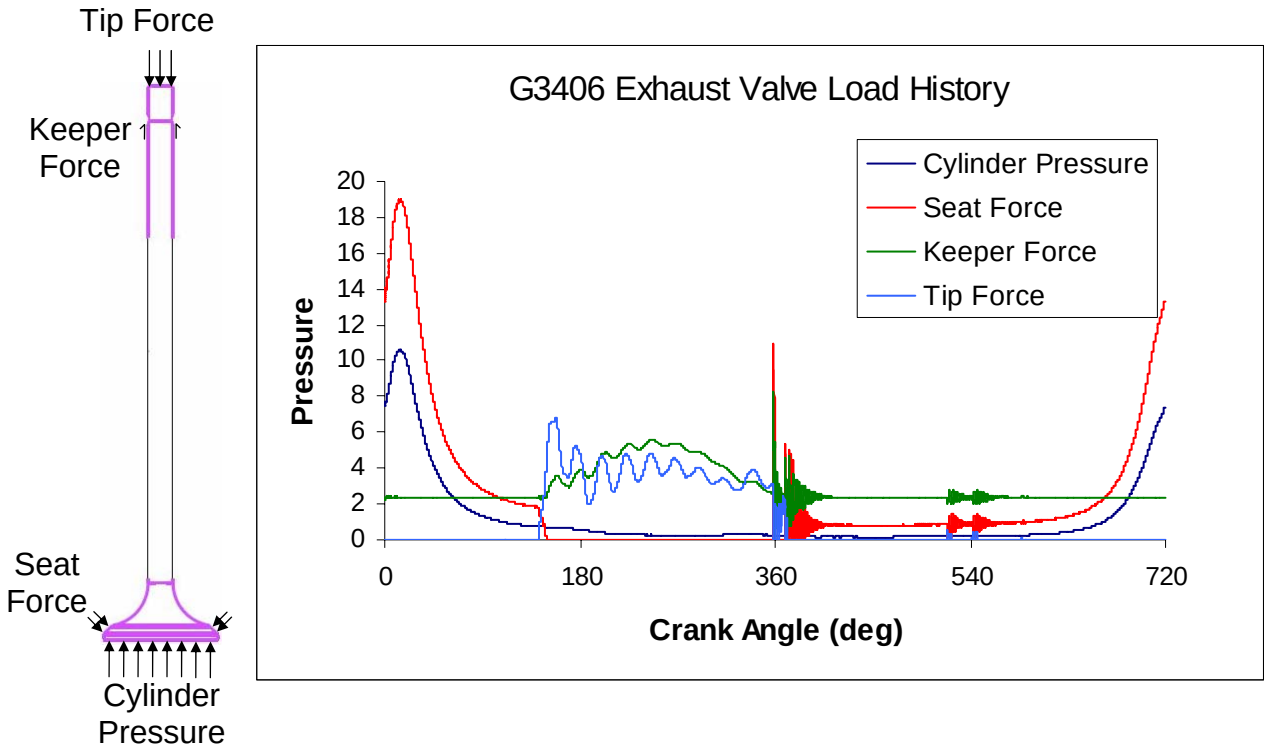

Figure 2: The load history of four primary forces that act upon a valve during a single cam cycle (from stem to face): force from bridge to valve tip, traction force from keeper, valve seat insert contact load and cylinder pressure on valve head. These boundary conditions are prescribed on the finite element model shown in Figure 1.

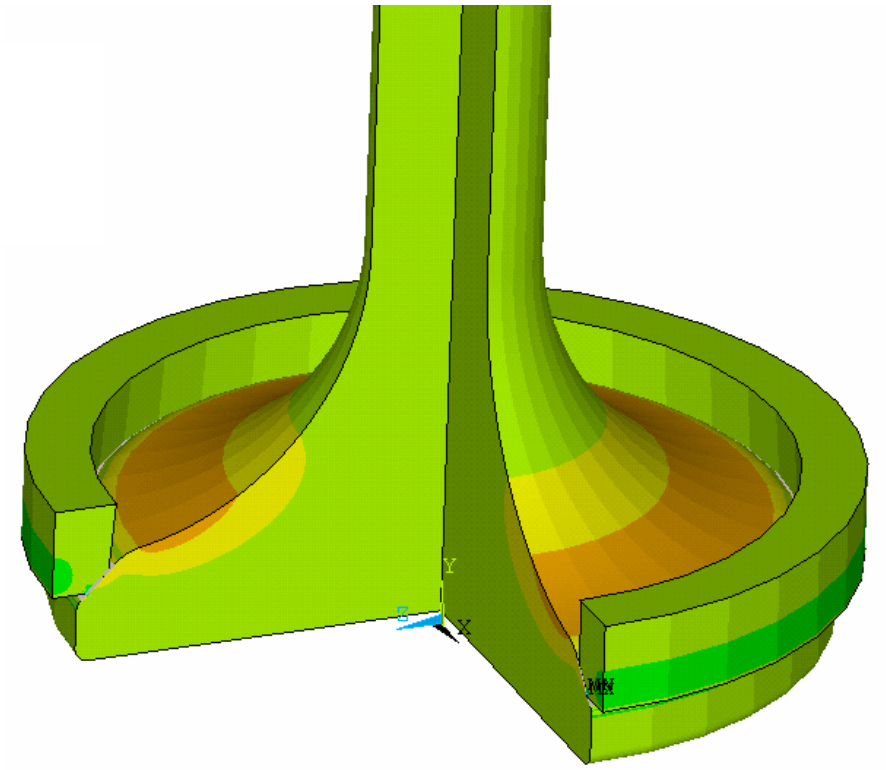

Figure 3: The maximum principal stress distribution within the ceramic valve at crank angle (~13º). This represents the maximum principal stress during the entire transient load history and corresponds to the time when the cylinder pressure peaks.

Thick Thermal Barrier Coatings (TTBCs) for Low Emission, High Efficiency Diesel Engine Components

M. Brad Beardsley
Caterpillar Inc.

Objective/Scope

Engine testing of thermal sprayed coatings has demonstrated their use as thermal barriers and wear coatings can reduce fuel consumption, reduce wear and reduce component temperatures. The durability of thermal sprayed coatings, particularly thermal barrier coatings, remains as the major technical challenge to their implementation in new engine designs. New approaches to coating design and fabrication will be developed to aid in overcoming this technical hurdle. Two new laser technologies, laser cleaning of the surfaces (PROTAL) and laser assisted plasma spraying will be applied to enhance adherence and increase coating strength. New quasicrystalline and amorphous steel materials will be evaluated as thermal barrier coatings. Plasma spraying and HVOF processing will be the primary methods of application.

Technical Highlights

Laser Assisted Thermal Spraying – The move of Caterpillar's 4 kW YAG laser to the thermal spray laboratory at the Technical Center was completed in January, 2005 and will be used to develop the laser assisted thermal spray technique. The fiber optics to the plasma spray cell still need to be installed and are scheduled to be completed by end of May, 2005. Initial laser assisted plasma spraying will begin after installation.

Laser Surface Cleaning - New Q-switched laser systems for laser cleaning of surfaces have been purchased and installed in the thermal spray laboratory. These lasers have very high power densities (~30,000 W/cm2) created by due to the short pulse duration (20 nanosecond) and have high repetition rates of 120 Hz. This laser will be used to investigate the effect on bonding of the plasma sprayed coatings of providing chemically clean surfaces just prior to deposition (PROTAL process).

Quasicrystalline and Amorphous Steel Coatings – Diffusion couples of quasicrystalline coatings sprayed onto three types of bond coatings are being evaluated. Bond coating chemistries were nickel based with two levels of chrome and aluminum and one iron based bond coating. Microprobe analysis of the diffusion couples will be used to determine temperature and time capability of the quasicrystalline material for use as thermal barrier coatings as shown in Figure 1. Three temperatures, 500, 700, and 900 C, and three times, 25, 100, 500 hours, were used and will allow for extrapolation of to longer times.

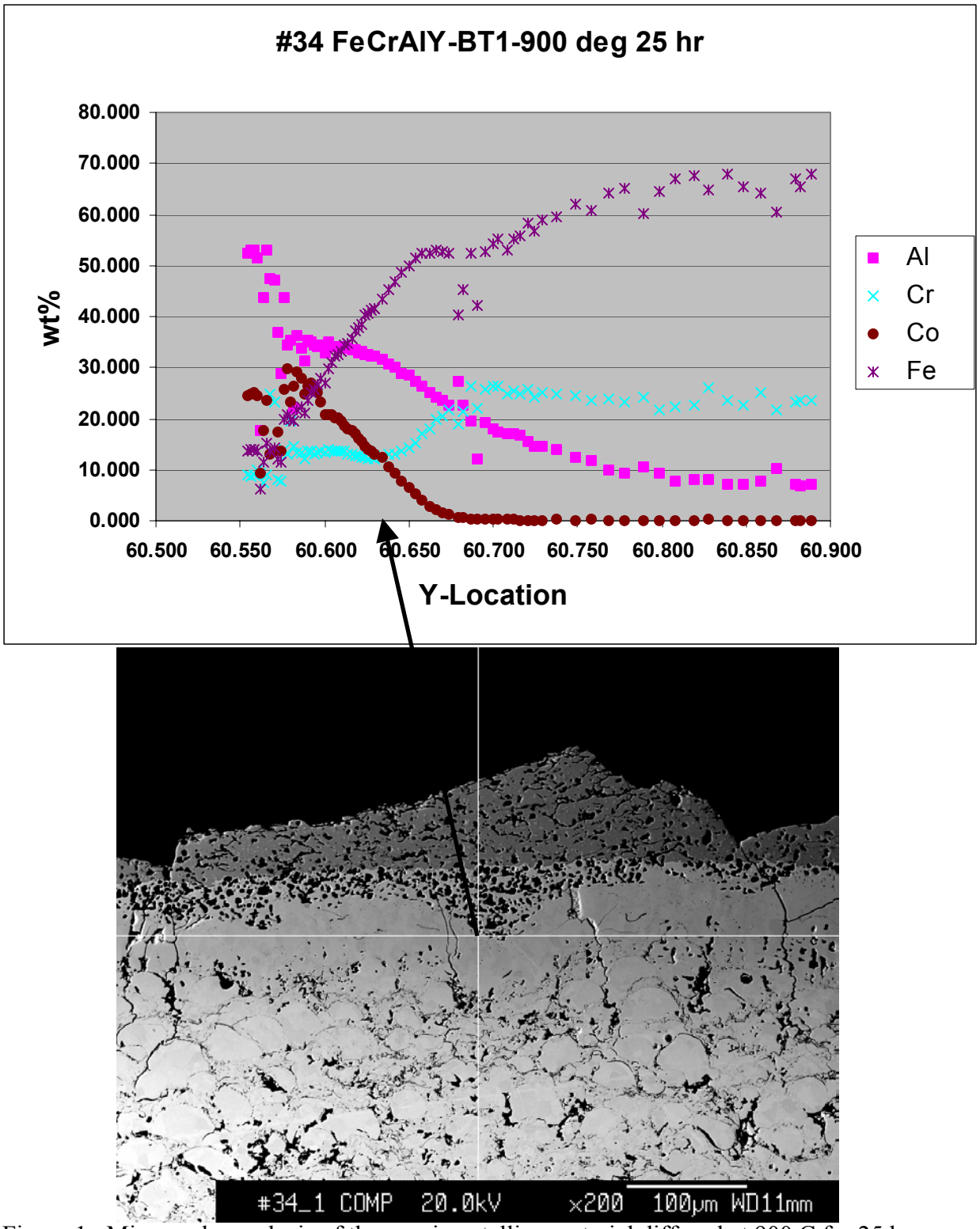

Figure 1. Microprobe analysis of the quasicrystalline material diffused at 900 C for 25 hours on Ni-26Cr-8Al-0.4Y bond coat. Similar analysis underway for the additional diffusion couples.

Future Plans

Analysis of the quasicrystalline diffusion couples will be completed in the next quarter.

Travel

None this period

Status of FY 2005 Milestones

Determine adhesive strength of optimized phosphate coating. (Completed by January 31, 2005)

Determine coating bending strength of quasicrystalline TBC. (Complete by February 28, 2005)

Delayed, will be completed by August, 2005.

Determine quasicrystalline TBC stability at 800 C after 500 hour exposure. (Complete by March 31, 2005)

Diffusion couple testing completed, microprobe measurement of samples completed, analysis of the results in progress, to be completed by August, 2005.

Produce quasicrystalline TBC piston for engine testing. (Complete by April 30, 2005)

Delayed, to be completed by July, 2005.

Publications

None this period.

Processing and Characterization of Structural and Functional Materials for Heavy Vehicle Applications

J. Sankar, Z. Xu, G. Rajaram and S. Yarmolenko
North Carolina A & T State University

Objective/Scope

Study the effect of the processing parameters on the porosity of the NiO/YSZ anode substrates.

Task

Use uniaxial cold press and subsequently sintering to process NiO/YSZ cermets for the anode of solid oxide fuel cells (SOFCs). Study the effect of the processing parameters, such starting powder composition, pressing pressure, amount of graphite, and sintering temperature on the porosity of the final products.

Technical Highlights

A major focus in the solid oxide fuel cell (SOFC) research is the reduction of the cost of the unit cell to an affordable range [1]. Techniques that could help to reduce the overall cost of the fuel cell are: identifying cost-effective, relatively low-purity raw materials, mass production of cell components, use of inexpensive and simplified fabrication processes and enhanced cell life [2-6]. The future of SOFCs greatly depends on the outcome of these techniques. Currently, the cost of the fuel cell is greatly influenced by the number of processing steps during the fabrication process[1], apart from the direct cost of raw materials. Generally, the SOFC is fabricated in either one of the two most common designs, tubular or planar cell[7]. Anode-supported planar cells are the most popular and commercially efficient cell design, due to their high power densities[8]. There are various steps at each stage of this fuel cell fabrication: developing the anode, depositing electrolyte layer, sintering the cell etc. Each step consumes enormous time and cost. This presents a major hindrance in the commercialization of the fuel cell. The cost and time involved in the fabrication can be reduced a lot by careful selection of process parameters. One way in which process parameters can be optimized is by having an experimental design called a factorial design for obtaining data with a minimum expenditure of time and resources and by meticulous analysis of the data, called analysis of variance (ANOVA). The analysis provides detailed insight into the direct effect of process variables on part porosity as well as into the intensity of the numerous interactions between variables. This kind of Response Surface Methodology (RSM) helps to determine, on the basis of one experiment, where to move in the next experiment toward the optimal point on the underlying response surface[9]. The optimized results will help to reduce cost and time involved in the fabrication process.

In this study, NiO and YSZ, the most preferred anode material for SOFCs, were used as the raw materials along with the pore former graphite. A full 2^4 factorial design was used. The four variables that were considered for the experimental design are graphite volume percent, ratio of NiO to YSZ, compaction pressure and sintering temperature. The two levels for each variable are listed in Table 1. A total of 16 sets of experiments with two replicates for each set (32 total experiments) were conducted. Based on the design chart, the total weight of the powder required for each set of experiment was calculated. The calculated amount of powders was carefully measured using a digital balance. Then the powder mixture was ball milled along with ethanol

using the horizontal ball milling machine for 48 hours. The ball milled mixture was removed from the jar and dried on a hot plate. The dried powder was milled again using the mortar and the pestle set. The obtained powder particles were in the range of 80 – 120 nm. The desired amount of the ball milled powder was poured in the half-inch steel die (as shown in Fig. 1) and care taken that the powder was evenly distributed within the die cavity. The powder mixture was uniaxially pressed using a universal testing machine (Material Test System 880). The compaction cycle is shown in Figure 2a. The green samples were sintered (using Applied Test System 3320 furnace) in air for 1 hour. The sintering cycle is shown in Figure 2b. The dimensions and weight of the sintered samples were measured using the laboratory calipers and digital balance respectively. The measured dimensions were used for the porosity calculations.

Table 1 Level design for the experimental parameters

Independent Variable	Treatment Level	
	Level 0	Level 1
Graphite (vol %)	40	30
YSZ / NiO weight ratio	50 : 50	42.5 : 57.5
Compaction pressure (MPa)	150	125
Sintering temperature (°C)	1350	1200

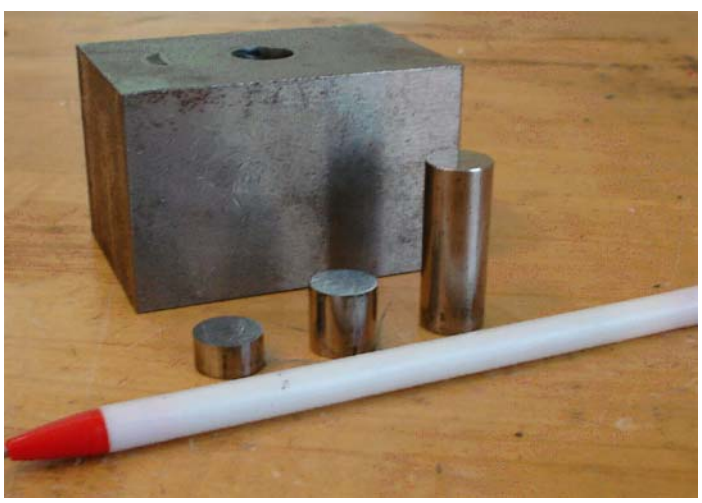

Figure 1. Steel die for clod press of NiO/YSZ pellets.

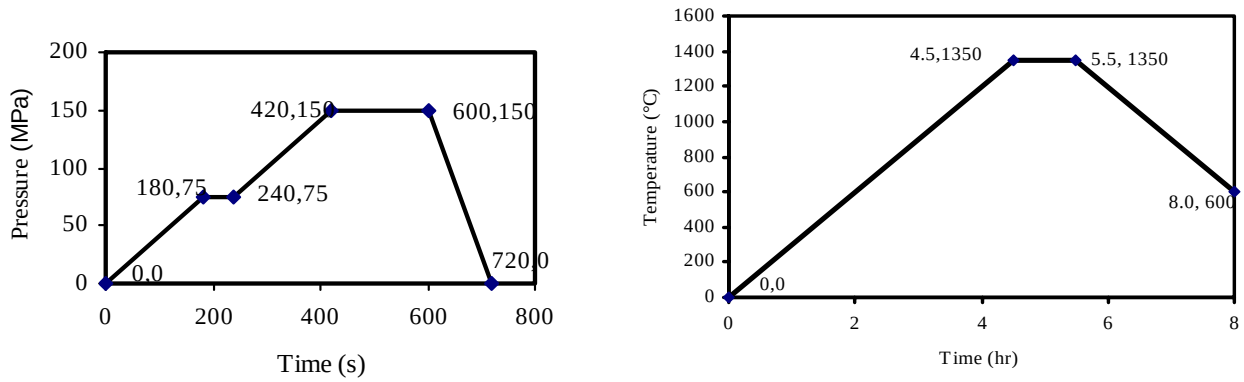

a b

Figure 2. a) Loading cycle for powder compaction, and b) temperature cycle for the sintering.

Results and Discussion

The calculations were based on the following equations (1-4). The obtained porosity values after sintering are shown in Table 2 which will be used as the inputs for the ANOVA subsequently.

$$v = \frac{\pi}{4} d^2 t \tag{1}$$

where

v	=	volume of sintered sample
d	=	diameter of sample
t	=	thickness of sample

$$\rho_a = \frac{m}{v} \tag{2}$$

where

ρ_a	=	actual density of sample
m	=	mass
v	=	volume

$$\rho_t = \left(vol.\%_{NiO} * \rho_{NiO}\right) + \left(vol.\%_{YSZ} * \rho_{YSZ}\right) \tag{3}$$

where

ρ_t	=	theoretical density of sample
ρ_{NiO}	=	density of bulk NiO
ρ_{YSZ}	=	density of bulk YSZ

$$Porosity\ volume\ \% = \left(1 - \rho_a / \rho_t\right) * 100 \tag{4}$$

Table 2. Porosity values of sintered NiO/YSZ samples

Design #		1	2	3	4	5	6	7	8
Porosity (%)	**Set 1**	6.85	40.62	8.00	41.41	10.85	42.94	10.68	40.38
	Set 2	7.09	41.80	8.39	41.41	10.47	42.57	10.03	40.92

Design #		9	10	11	12	13	14	15	16
Porosity (%)	**Set 1**	9.58	34.38	9.38	33.80	11.16	35.15	9.31	33.83
	Set 2	9.75	33.68	10.23	34.13	9.68	35.08	9.69	35.77

The effects of the processing parameter on the porosity of the sintered anode pellets are shown in Fig. 3. It can be noticed that the porosity of the anode increases slightly with the increasing of the NiO component in the mixture and the increasing rates are in accordance with the level of the pressure used to make the pellets. The sintering temperature was found to be one of the very significant factors in the porosity control. The porosity of the anode sintered at 1200°C was four times more than that sintered at 1350°C. The effect of the amount of graphite used as the pore former was shown to be significant, too. The porosity of the anode increased as the graphite amount increased within the experimental range.

Conclusions

The 2^4 factorial design was used for four parameter; i.e., ratio of NiO to YSZ, pressure, sintering temperature, and amount of graphite used as the pore former. The effects of these parameters were examined against the porosities of the sintered anode samples. The sintering temperature and graphite usage were found to have very significant effect, while the ratio of NiO/YSZ and the pressing pressure were found to have less significant effects on the porosity of the anodes. The effects are planned to be further analyzed by ANOVA.

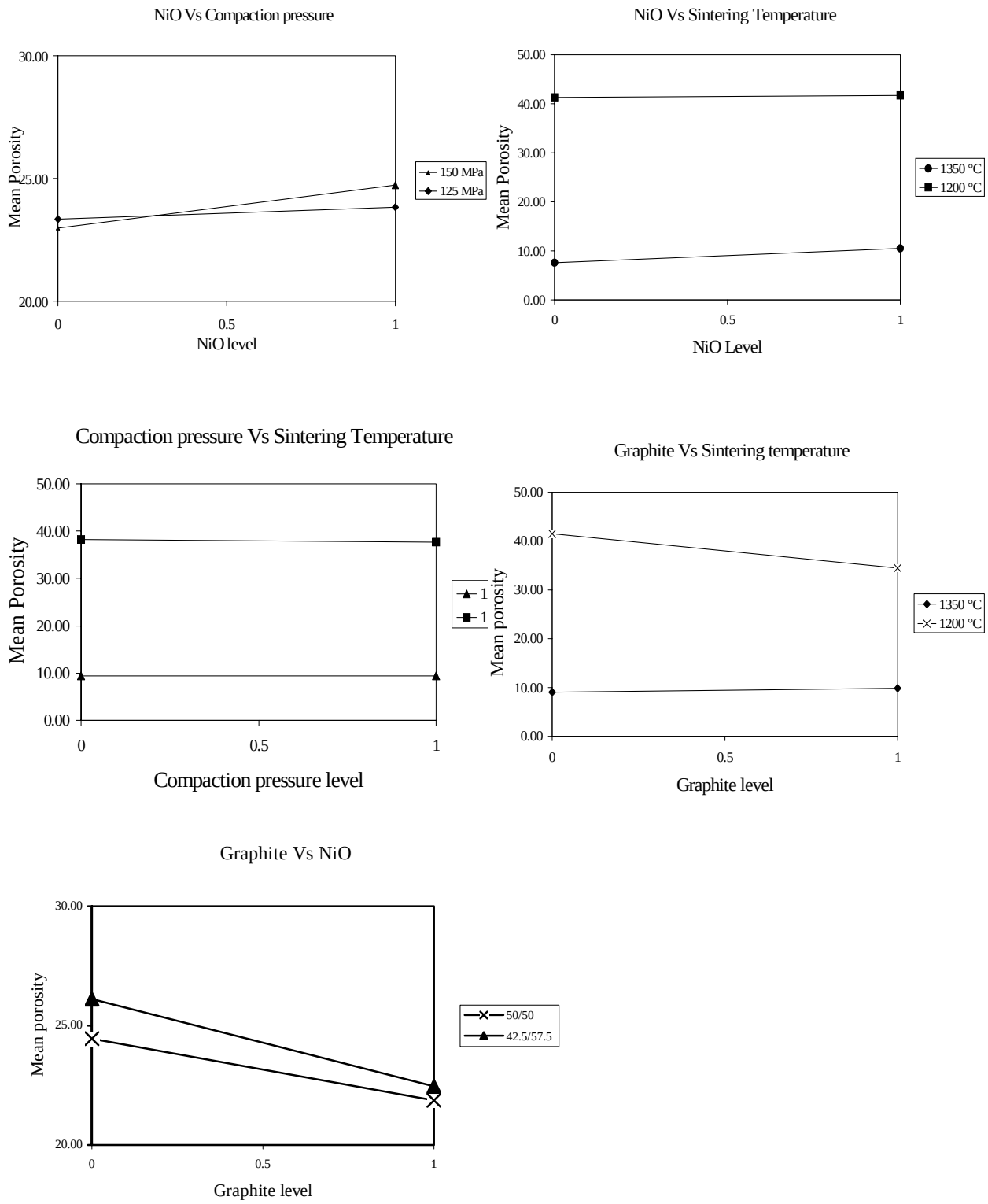

Figure 3. Effect of the processing parameters on the sintered NiO/YSZ anodes.

References

1. R. N. Basu, G. Blass, H. P. Buchkremer, D. Stöver, F. Tietz, E. Wessel, and I. C. Vinke, "Simplified processing of anode-supported thin film planar solid oxide fuel cells," *Journal of the European Ceramic Society*, **25**, 463–471 (2005).
2. S.C. Singhal, "Status of solid oxide fuel cell technology," In *Proceedings of the 17th Risø International Symposium on Materials Science: High Temperature Electrochemistry: Ceramics and Metals*," ed. F. W. Poulsen, N. Bonanos, S. Linderoth, M. Mogensen and B. Zachau-Christiansen. Risø National Laboratory, Denmark, 123–138 (1996).
3. F. Tietz, F.J. Dias, D. Simwonis, and D. Stöver, "Evaluation of commercial nickel oxide powders for components in solid oxide fuel cells," *Journal of the European Ceramic Society*, **20**(8), 1023–1034 (2000).
4. G. Rietveld, P. Nammensma, and J.P. Ouweltjes, "Status of SOFC component development at ECN," In *Proceedings of the Seventh International Symposium on Solid Oxide Cells* (*SOFC-VII*), ed. H. Yokokawa and S. C. Singhal. The Electrochemical Society Proceedings Series (PV 2001-16), Pennington, NJ, 125–130 (2001).
5. R.N. Basu, C.A. Randall, and M.J. Mayo, "Fabrication of dense zirconia electrolyte films for tubular solid oxide fuel cells by electrophoretic deposition," *Journal of the American Ceramic Society*, **84**, 33–40 (2001).
6. T. Ishihara, T. Shibayama, H. Nishiguchi, and Y. Takita, "Nickel–Gd-doped CeO2 cermet anode for intermediate temperature operating solid oxide fuel cells using LaGaO3-based perovskite electrolyte," *Solid State Ionics*, **132**, 209–216 (2000).
7. S.C. Singhal, "Solid oxide fuel cells for stationary, mobile, and military applications," *Solid State Ionics*, **152-153,** 405-410 (2002).
8. J.W. Kim, A.V. Virkar, K.Z. Fung, K. Mehta, and S.C. Singhal, "Polarization effects in intermediate temperature, anode supported solid oxide fuel cells," *Journal of the Electrochemical Society*, **146**, 69-78 (1999).
9. C.R. Hicks, and K.V. Turner Jr., "Fundamental concepts in the design of experiments," *Oxford University Press*, Fifth Edition (1999).

Communications/Visitors/Travel

None

Problems Encountered

None

NDE Development for Ceramic Valves for Diesel Engines

J. G. Sun, J.M. Zhang
Argonne National Laboratory
J. S. Tretheway and J. A. Grassi
Caterpillar, Inc.

Objective/Scope

Emission reduction in diesel engines designated to burn fuels from several sources has lead to the need to assess ceramic valves to reduce corrosion and emission. The objective of this work is to evaluate several nondestructive evaluation (NDE) methods to detect defect/damage in structural ceramic valves for diesel engines. One primary NDE method to be addressed is elastic optical scattering. The end target is to demonstrate that NDE data can be correlated to material damage as well as used to predict material microstructural and mechanical properties. There are three tasks to be carried out: (1) Characterize subsurface defects and machining damage in flexure-bar specimens of NT551 and SN235 silicon nitrides to be used as valve materials. Laser-scattering studies will be conducted at various wavelengths using a He-Ne laser and a tunable-wavelength solid-state laser to optimize detection sensitivity. NDE studies will be coupled with examination of surface/subsurface microstructure and fracture surface to determine defect/damage depth and fracture origin. NDE data will also be correlated with mechanical properties. (2) Assess and evaluate subsurface damage in ceramic valves to be run in bench test and in a single-cylinder-engine test. All valves will be examined at ANL prior to test, during periodic scheduled shut downs, and at the end of the planned test runs. (3) Evaluate healing of subsurface damage by laser glazing on machined surfaces of GS44 ceramics. ANL will perform laser-scattering characterization on machining surfaces at before and after glazing treatment. NDE data will be correlated with glazing parameters and mechanical properties.

Technical Highlights

During this period (January-March 2005), two main tasks were accomplished, including further optimization of the full-valve laser-scatter system and correlation of laser scattering NDE data and fractography results for 8 machined SN235P rods.

1. Optimization of full-valve laser-scattering system

In order to scan the whole valve (including valve head and rod regions, total length of about 200 mm), two linear translation stages with longer ranges were implemented. A 250-mm-range translation stage was used to replace the previous 100-mm-range stage for axial translation of the valve, which makes it possible to scan the entire valve (head and shaft) within one pass. Meanwhile, the 100-mm-range translation stage was used to replace the previous 50-mm-range stage, providing more room during alignment. A few mechanical parts were machined and installed to make the whole system more robust and substantially reduce the time spent on alignment. In addition, data acquisition software was modified to improve synchronization between data acquisition and stage motion along the valve profile. Figure 1 shows a photograph of the new system setup. With all these modifications, it is considered that major development of the valve scan system has been completed.

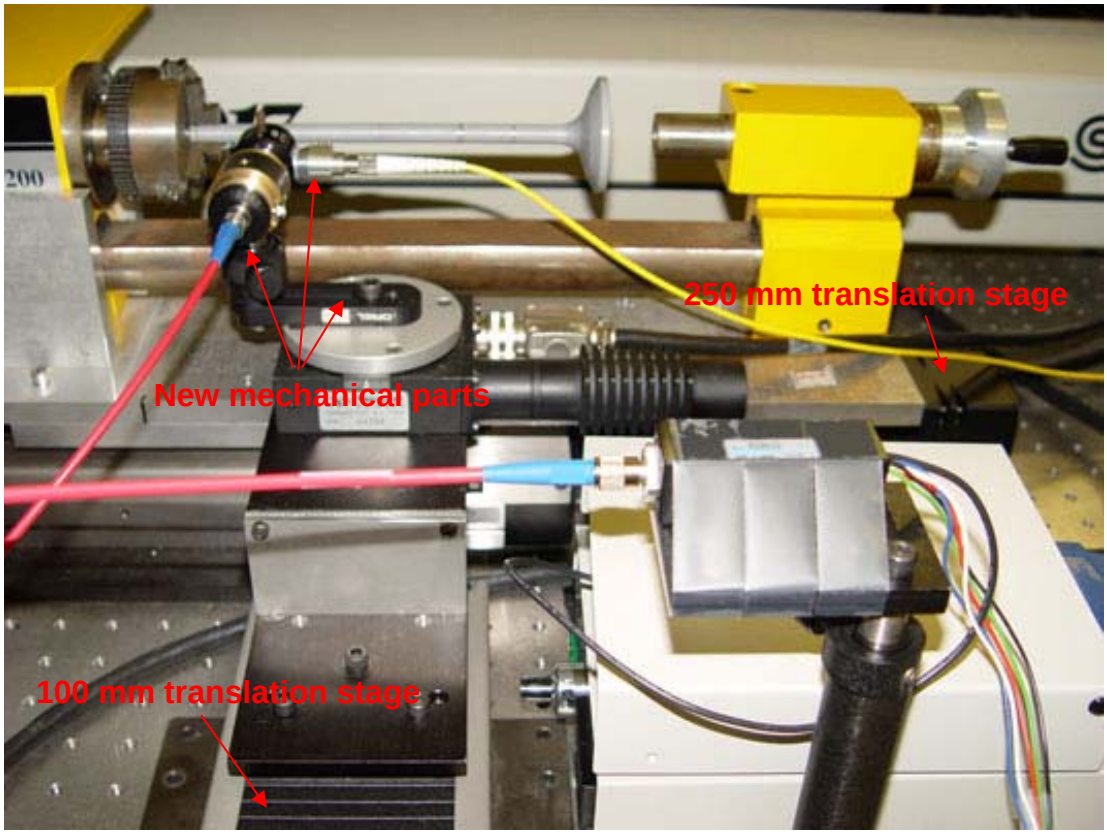

Fig. 1. Photograph of the new laser-scattering system.

Figure 2 shows the laser-scattering scan data of SN235P diesel intake valve #2 using the new system. The scan image of the entire valve-head section with 10 μm scan resolution is shown in Fig. 2a, and some small areas at different locations of the valve are enlarged in Fig. 2b. This result shows an improvement in the uniformity of the background scatter intensity, indicating that the incident angle of laser beam was consistent along the valve-head profile during the scan.

Dr. Tretheway of Caterpillar informed us that all SN235P valves will be re-machined in the next period. These valves will be re-scanned by this new system after the machining. The system is capable for fast scanning of entire valve (head and shaft) within two hours.

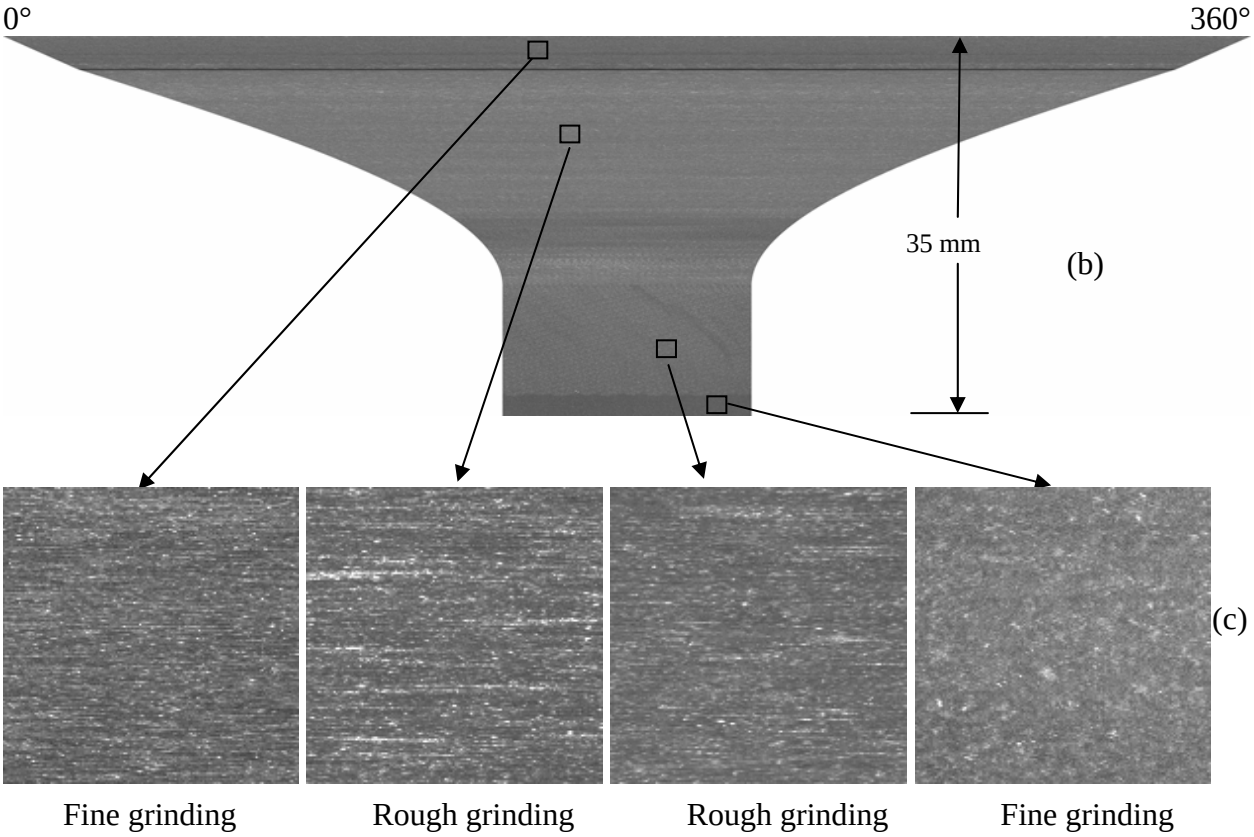

Fig. 2. (a) Laser-scattering image of SN235P diesel intake valve #2 and (b) enlarged areas (image size is 1.5 mm × 1.5 mm).

2. Characterization of ground rods using laser scattering technology and fractography

Laser scattering technology was combined with fractography method to characterize eight ground SN235P rods. Before and after these ground rods were fractured, they were tested by laser scattering technology. Fracture origin where the fracture initiated can be determined by comparing scattering images and fracture photomicrographs. The fracture surfaces were first examined to locate the fracture flaw. Figure 3 shows the fracture surfaces of SN235P rod #2 where the fracture initiation defect can be easily observed. The flaw site was then mapped in the tensile (i.e., cylinder) surface. The correlation of surface photomicrograph with the laser scatter image for rod #2 is shown in Fig. 4. As indicated, the fracture initiation defect in this specimen appears to be a high-porosity material defect.

The results for all 8 SN235P rods are summarized in Fig. 5, which shows the fracture strength of each rod and its corresponding fracture origin in the scanning image. It can be clearly seen that all of the rods fractured from the material flaws, except rod #1 which fractured from a machining damage (likely a lateral machining crack). The lowest fracture strength occurs in rods #2 and #5. For rod #2, there are a group of material flaws along the fracture line, which may explain for its low fracture strength. As for rod #5, its fracture origin is more intensive and slightly bigger (~35 micron) than those on the other rods, indicating that its material flaw is larger and possibly deeper. Other rods with higher fracture strengths have a smaller material flaw size (~25 micron), such as rods 3, 4 and 6. However, from the NDE data shown in Fig. 5b, it is

apparent that fractures were not necessarily initiated from the most prominent NDE indications in the fracture region. This may be due to the differences in configuration and depth of the flaws that should be examined by a longer laser wavelength with deeper penetration. Studies with a laser wavelength of 850nm will be carried out and reported in the next period.

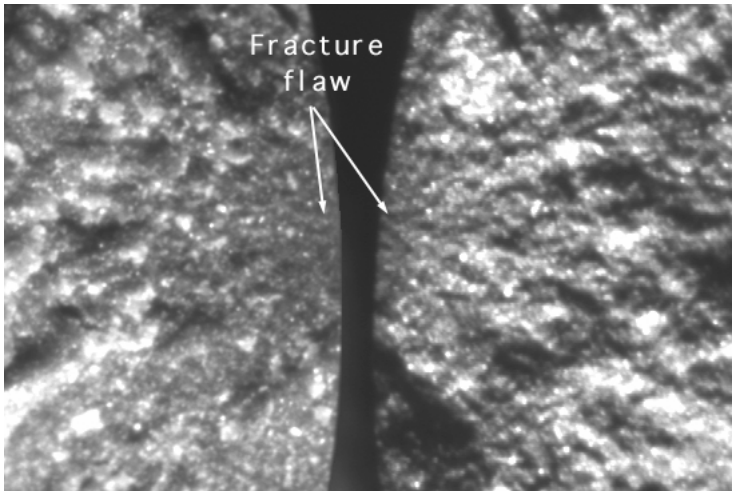

Fig. 3. Photomicrograph of fracture surfaces of fractured SN235P rod #2.

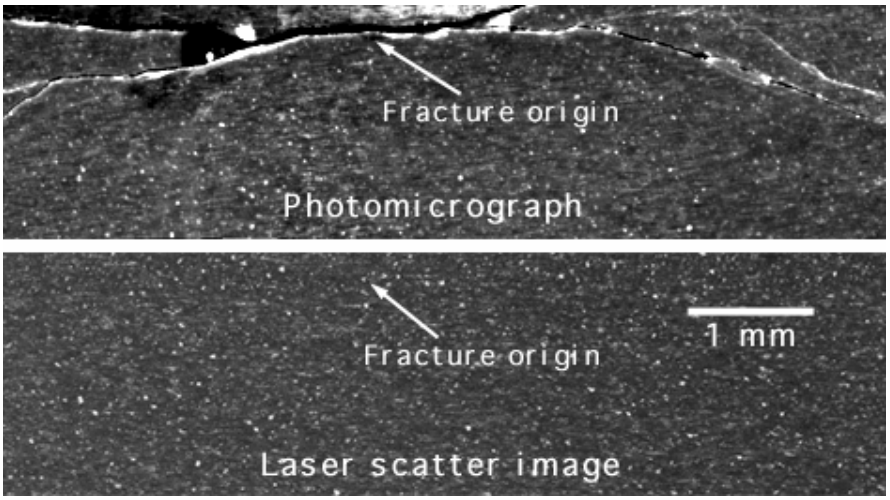

Fig. 4. Photomicrograph and laser-scatter image (before fracture) on tensile surface of fractured SN235P rod #2.

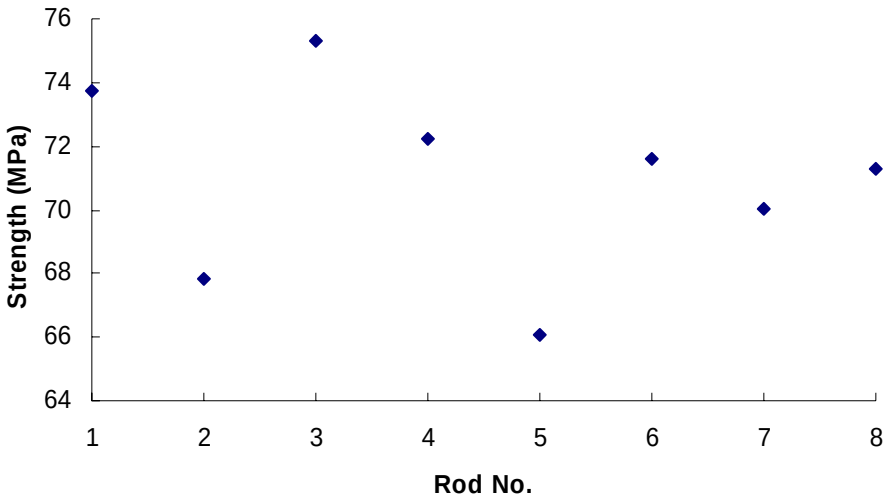

(a)

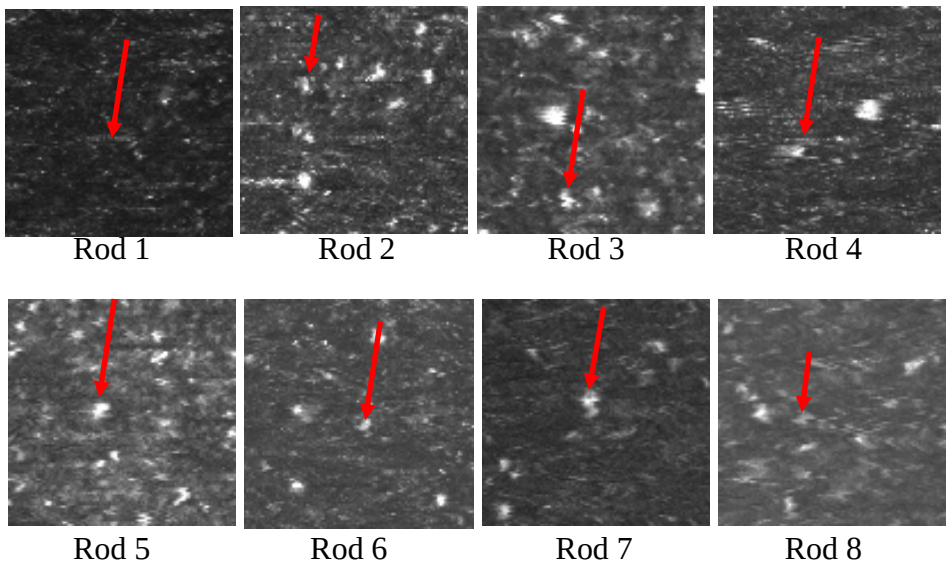

(b)

Fig. 5. (a) Fracture strength for ground rods; (b) Corresponding fracture origins in scattering images (image size is 0.5 mm × 0.5 mm).

Status of Milestones

Current ANL milestones are on schedule.

Communications/Visits/Travel

J. G. Sun attended the American Ceramic Society's 29th International Cocoa Beach Conference and Exposition on Advanced Ceramics & Composites, Cocoa Beach, FL, January 23-28, 2005.

Problems Encountered

None this period.

Publications

- Sun, J. G., Zhang, J. M., Tretheway, J. S., Grassi, J. A., Fletcher, M. P., and Andrews, M. J., 2005, "Nondestructive Evaluation of Machining and Bench-Test Damage in Silicon-Nitride Ceramic Valves," paper was accepted for publication in the Proceeding of the 29th International Cocoa Beach Conference and Exposition on Advanced Ceramics & Composites, Cocoa Beach, FL, Jan. 23-28, 2005.

Durability of Diesel Engine Component Materials

Peter Blau and Jun Qu
Oak Ridge National Laboratory

John Truhan
University of Tennessee

Objective/Scope

The objective of this effort is to enable the development and use of more durable, low-friction moving parts in diesel engines for heavy vehicle propulsion systems. The scope of candidate materials and coatings broadly includes metallic alloys, intermetallic compounds, ceramics, or composite materials depending on which is best-suited for each application. Parts of current interest include scuffing-critical components, like fuel injector plungers and exhaust gas recirculation (EGR) waste gate bushings. Bench-scale simulations of the rubbing conditions in diesel engine environments are developed and used to study the accumulation of surface damage, and to correlate it with the properties and compositions of the surface species. The effects of mechanical, thermal, and chemical factors on scuffing and reciprocating sliding wear are being determined. Results are used to develop graphical methods for scuffing performance mapping and to select materials for durability-critical engine components. In FY 2005 an analytical model for selecting materials for scuffing-critical applications is being developed and validated. Also in FY 2005, a new task was initiated to determine how to engineer the surfaces of titanium alloys to make them more suitable for friction- and wear-sensitive engine components. Approaches include thermal oxidation to create thin lubricating layers.

Technical Highlights

Scuffing model development. A new, three-regime scuffing model is being developed based on microstructural observations and the results previously-reported experimental work on candidate materials for fuel injector plungers. This model represents an interdisciplinary effort to integrate concepts from both lubrication theory and material science. Shown schematically in Figure 1, the model makes use of sub-models whose applicability depends on whether the contact is effectively lubricated (solid surfaces that are not touching), boundary-lubricated, or subjected to significant solid contact. The latter case was described in the previous quarterly report and remains under development. During this reporting period, however, greater attention was paid to the complex situation called Regime II. In this region, the friction and wear of the tribosystem transition from one controlled by lubricant films to one that sees increasing solid contact, leading to the onset of scuffing, and ultimately failure. Examination of test specimens in various stages of sliding damage shows four kinds of contacts that share in supporting the bearing load: (a) surfaces coated with lubricating liquid films, (b) surfaces covered with oxides, tarnishes, or reaction products of additives with the surface, (c) surfaces whose films and coatings have been wiped clean to expose the nascent, underlying solid, and (d) areas in which debris particles have been collecting and consolidating into load-bearing masses. The model being developed considers time-dependent changes in the instantaneous arrangement and effective shear strengths of these four kinds of load-bearing areas. More details about this model and its governing assumptions will be presented in the next report.

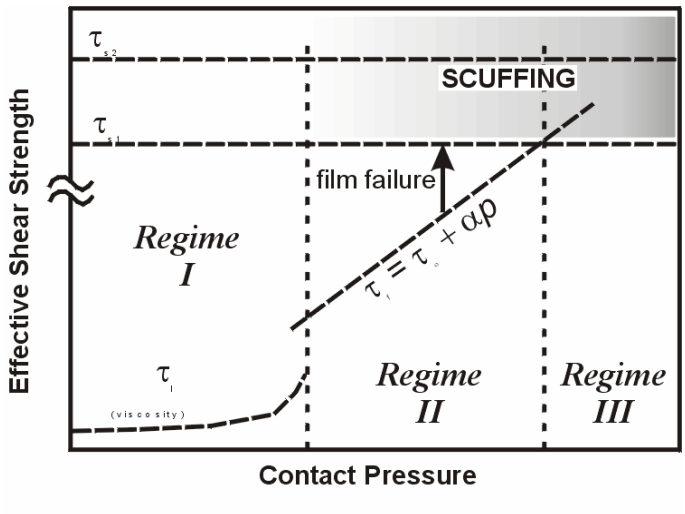

Figure 1. Basic concept for a three-regime model for scuffing. Regime II attempts to bridge the gap between boundary lubrication and the increasing effects of material contact.

New process greatly improves the friction and wear of titanium engine components. A new, relatively simple-to-apply heat treatment has been tested and shown to significantly reduce the friction coefficient and wear rate of titanium alloy 6Al-4V. Using a new ASTM test method, developed by ORNL under DOE/OFHVT sponsorship, reciprocating sliding tests were performed in diesel engine oil. Comparisons were made using production grade, Cr-plated diesel engine piston rings (for a Caterpillar C-15 engine) rubbing against cast iron, non-treated titanium and thermally-treated titanium.

This new heat treatment greatly reduced the wear and friction of the titanium, even to levels comparable to or better than gray cast iron, the traditional cylinder bore material. More information on these highly promising results will be given in the next report (see Milestone 3, listed below). A journal article describing the effects of the treatment, the surface chemistry, and the morphology of wear surfaces is in preparation.

Future Plans

1) Continue to develop stage II of the scuffing model that involves the failure of boundary lubricating films to separate the contacts surfaces and the transition from liquid lubricated contacts to solid contact.

2) Blau, Qu, and Truhan will attend the 15th International Conference on Wear of Materials (San Diego, California – April 24-28) to present one paper on scuffing and three other papers resulting from other DOE and DOT-sponsored projects.

Travel

None this period.

Status of Milestones

1) Prepare transition diagrams for current and promising, new fuel system materials that exemplify the relationship between real contact pressure, surface finish, and the onset of scuffing in diesel fuel environments. (March 31, 2004 - completed)

2) Develop a model for selecting materials and their optimal surface finishes for scuffing applications in diesel engines. (September 30, 2004**)**

3) Report on the results of research to improve the friction and wear characteristics of titanium alloys by applying surface engineering methods like thermal oxidation and controlled surface patterning. (June 30, 2005)

4) Develop mechanistic model for scuffing processes in boundary-lubricated fuel injector plunger materials. (September 30, 2005)

Publications and Presentations

J. Qu, P. J. Blau, T. R. Watkins, O. B. Cavin, and N. S. Kulkarni (2005) "Friction and wear of titanium alloys sliding against metal, polymer, and ceramic counterfaces," *Wear*, Vol. 258, pp. 1348-1356.

J. Qu, J. J Truhan, and P. J. Blau (2005) "Detecting the Onset of Localized Scuffing with the Pin-on-Twin Fuel-Lubricated Test for Heavy Duty Diesel Fuel Injectors," *SAE International Journal of Engine Research*, Vol. 6, No. 1, Mar. 2005, pp. 1-9

J. Qu, J. J. Truhan, and P. Blau (2005) "Investigation of the scuffing characteristics of candidate materials for heavy duty diesel fuel cell injectors," *Tribology International*, Vol. 18, pp. 381-390.

J. Qu, J. J. Truhan, P. J. Blau (2005) Scuffing Transition Diagrams for Heavy Duty Diesel Fuel Injector Materials in Ultra Low-Sulfur Fuel-Lubricated Environment," accepted for presentation at International Conference on Wear of Materials, and publication in the special volume of the journal *Wear*.

Life Prediction of Diesel Engine Components

H. T. Lin, T. P. Kirkland, A. A. Wereszczak, M. K. Ferber
Oak Ridge National Laboratory
and Jeremy Trethewey
Caterpillar

Objective/Scope

The valid prediction of mechanical reliability and service life is a prerequisite for the successful implementation of structural ceramics and advanced intermetallic alloys as internal combustion engine components. There are three primary goals of this research project which contribute toward that implementation: the generation of mechanical engineering data from ambient to high temperatures of candidate structural ceramics and intermetallic alloys; the microstructural characterization of failure phenomena in these ceramics and alloys and components fabricated from them; and the application and verification of probabilistic life prediction methods using diesel engine components as test cases. For all three stages, results are provided to both the material suppliers and component end-users.

The systematic study of candidate structural ceramics (primarily silicon nitride) for internal combustion engine components is undertaken as a function of temperature (< 1200°C), environment, time, and machining conditions. Properties such as strength and fatigue will be characterized via flexure and rotary bend testing.

The second goal of the program is to characterize the evolution and role of damage mechanisms, and changes in microstructure linked to the ceramic's mechanical performance, at representative engine component service conditions. These will be examined using several analytical techniques including optical and scanning electron microscopy. Specifically, several microstructural aspects of failure will be characterized:

(1) strength-limiting flaw-type identification;
(2) edge, surface, and volume effects on strength and fatigue size-scaling
(3) changes in failure mechanism as a function of temperature;
(4) the nature of slow crack growth; and
(5) what role residual stresses may have in these processes.

Lastly, numerical probabilistic models (i.e., life prediction codes) will be used in conjunction with the generated strength and fatigue data to predict the failure probability and reliability of complex-shaped components subjected to mechanical loading, such as a silicon nitride diesel engine valve. The predicted results will then be compared to actual component performance measured experimentally or from field service data. As a consequence of these efforts, the data generated in this program will not only provide a critically needed base for component utilization in internal combustion engines, but will also facilitate the maturation of candidate ceramic materials and a design algorithm for ceramic components subjected to mechanical loading in general.

Technical Highlights

Results of dynamic fatigue behavior of a commercial grade silicon nitride, i.e., SN147-31E, manufactured by Ceradyne Advanced Ceramic, Inc., CA, showed a low fatigue exponent (N) of ~39 at 850°C in air. Note that SN147-31E should contain a crystalline secondary phase that was achieved via a proprietary post heat treatment process. The result of low fatigue exponent suggested that the SN147-31E exhibited an increased susceptibility to slow crack growth process at test temperature, which was similar to the value obtained for the SN147-31N. The obtained mechanical results suggest that an additional post heat treatment needs to be carried out to ensure the complete crystallization of secondary phase, and thus better high temperature mechanical performance.

Mechanical strength testing on sixteen NT551 silicon nitride valves (14 with 30° and 4 with 45° valve seat angle) after 500 h bend rig test at Caterpillar was completed during this reporting period. In general, the optical microscopy examinations showed that there were no apparent surface damages/flaws observed after the bench rig test, except the distinct valve seat markings at the valve and stainless steel valve seat contact point. Strength testing was carried out at room temperature to evaluate the effect of 500 h bench rig test on the mechanical performance with an in-house design compression test fixture (Fig.1). The test results of as-received NT551 valves obtained using a hydraulic chamber facility were used as a baseline for comparison (Fig. 2). Mechanical results of 500h tested valves show that the characteristic strength as well as Weibull strength distribution were similar to those obtained for the as-machined valves, indicative of no surface/subsurface damages were introduced during the bench rig test (Fig. 3). Note that nondestructive evaluations carried out at ANL on these 500 h tested valves also indicated no apparent damages/flaws could be detected, consistent with the present mechanical results.

The final surface machining for SN235P silicon nitride valves that will be employed for actual engine testing is still in progress. The surface roughness and valve dimensions will be well characterized via the CMC prior to the bench rig testing as well as engine test.

Status of Milestones

Milestone: “Complete testing and analysis of prototype silicon nitride valves after bench rig testing.” On schedule.

Communications / Visitors / Travel

Communication with Jeremy Trethewey at Caterpillar on the microstructure analysis and dynamic fatigue results of Ceradyne SN147-31E silicon nitride.

Communication with Jeremy Trethewey at Caterpillar on the mechanical results of NT1551 valves received after 500 h bench rig test.

Monthly telephone conference with Jeremy Trethewey at Caterpillar was carried out to update the preparation of engine testing for SN235P silicon nitride valves.

Problems Encountered
None.

Publications
H. T. Lin, T. P. Kirkland, A. A. Wereszczak, and M. J. Andrews, "Strength Retention of Silicon Nitride After Long-Term Oil Immersion Exposure," submitted to *J. Mater. Sci*.

References
[1] H. T. Lin, T. P. Kirkland, M. K. Ferber, and M. J. Andrews, "Life Prediction of Diesel Engine Components," Heavy Vehicle Propulsion System Materials Program Quarterly Technical Progress Report to DOE Office of Transportation Technologies, Oct. – Dec., 2003.
[2] H. T. Lin, T. P. Kirkland, M. K. Ferber, and M. J. Andrews, "Life Prediction of Diesel Engine Components," Heavy Vehicle Propulsion System Materials Program Quarterly Technical Progress Report to DOE Office of Transportation Technologies, Jan. – March, 2004.
[3] H. T. Lin, T. P. Kirkland, M. K. Ferber, and M. J. Andrews, "Life Prediction of Diesel Engine Components," Heavy Vehicle Propulsion System Materials Program Quarterly Technical Progress Report to DOE Office of Transportation Technologies, Apr. – June, 2004.

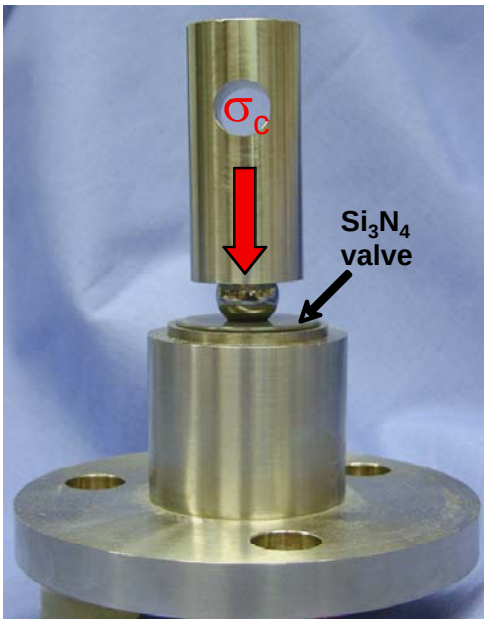

Figure 1. Photo of silicon nitride exhaust valve mechanical testing fixture. The test was carried out via a Universal Instron machine.

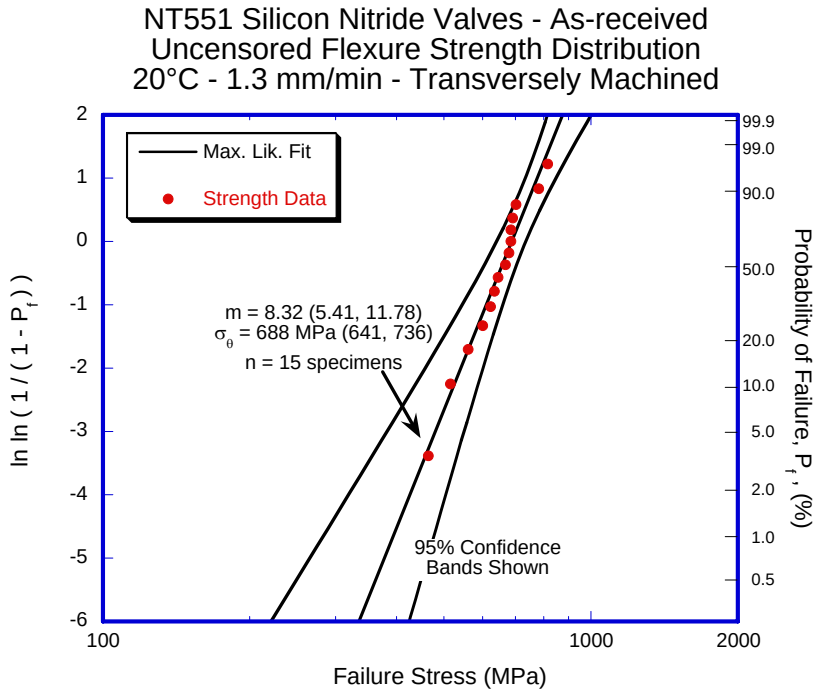

Figure 2. Strength distribution of as-received Norton NT551 silicon nitride valve transversely machined and tested at 20°C.

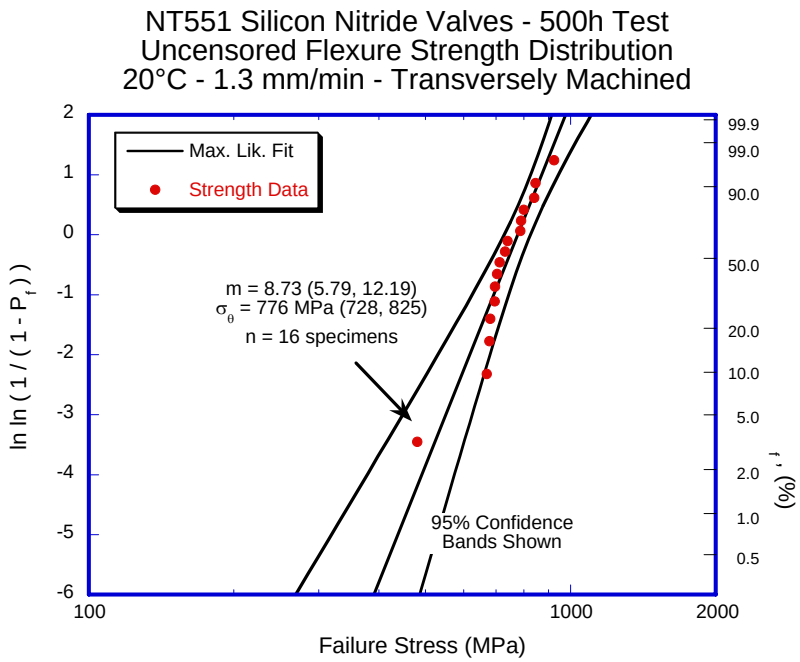

Figure 3. Strength distribution of 500h-tested Norton NT551 silicon nitride valve transversely machined and tested at 20°C.

Low-Cost Manufacturing of Precision Diesel Engine Components

P. J. Blau and Jun Qu
Oak Ridge National Laboratory

Objective/Scope

The objectives of this effort are (1) to identify and investigate cost-effective processes to machine precision components of advanced materials for diesel engines and (2) to develop and use methods to characterize the effects of machining on the surface quality and performance of advanced engine materials.

Technical Highlights

High-Speed Machining of Titanium. In titanium machining, cutting chips can ignite when their temperature rises above 1200°C. To determine whether this situation could be predicted from a model, Third Wave Systems (TWS) *AdvantEdge*^{TM} computer software was used to simulate chip ignition during a turning process, and showed encouraging results. Lathe turning experiments were conducted at ORNL on a Ti-6Al-4V workpiece using a Micrograin AR6 (WC-Co) cutting tool and compared with the temperature predictions from the software. The feed rate was 0.1 mm/rev and the depth of cut (DOC) ranged from 30-150 μm. Results in Table 1 show very good agreement between simulations and experiments. The simulated temperature profiles of the titanium chips for different DOCs are illustrated in Fig. 1.

Table 1. Comparison of Simulated with Experiment Results on Ti chip ignition.

DOC (μm)	30	50	75 – 150
Simulation	No ignition (Chip T_{max} < 1000°C)	Possible ignition (Chip T_{max} ~ 1200°C)	Ignition (Chip T_{max} > 1400°C)
Experiment	No ignition	*Not tested*	Ignition

Tool wear characterization. In Ti machining, the high tool wear, particularly diffusion-controlled wear, significantly limits the usable cutting speed and the tool life. The wear of four WC-Co based turning tools with different coatings and/or corner radii was measured and characterized. The four tool inserts were collected at the point of tool failure (indicated by a dramatic increase in cutting forces) after various durations of titanium machining (see Table 2).

The worn tool tips were measured using laser profilometry (Rodenstock RM600), and their 3D profiles are shown in Fig. 2. Different 'tool failure' mechanisms were observed: the tools with 0.8 mm corner radius showed high crater wear (Figs. 2(a) and 2(b)), while the 0.1 mm corner radius tools failed because the work material transferred and built up on the cutting edge. Energy dispersive spectrum analysis confirmed the high Ti concentration of the build-up material. The volumes of the crater wear and edge build-up were then quantified using the True Map^{TM} 3D image analysis package, and summarized in Table 2. The TiB_2 coated tool (0.8 mm r_c) had a slightly higher wear rate compared to the non-coated tool, but it lasted much longer. That is possibly due to its slower rate of edge build-up, which dramatically reduces the edge sharpness and causes high adhesion to the workpiece material. For a corner radius of 0.1 mm,

the TiB_2 coated tool significantly outperformed the TiAlN coated tool due to the much lower edge build-up rate, as seen in Table 2.

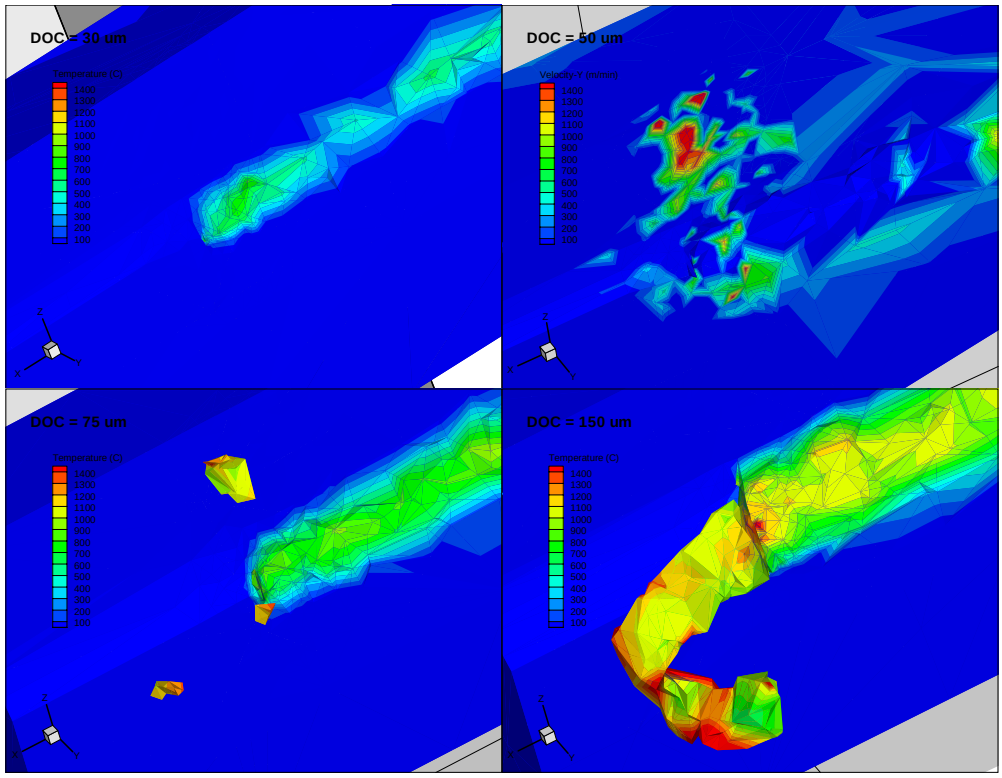

Figure 1. Simulation of ignition conditions during chip formation using four different depths of cut (indicated at the upper left of each image).

Table 2. Tool Life and Tool Wear Rates

Tool Coating	Corner radius, r_c (mm)	Cutting time before failure (sec)	Crater wear		Edge build-up	
			Volume (mm^3)	Wear rate (mm^3/s)	Volume (mm^3)	Build-up rate (mm^3/s)
N/A	0.8	69	$7x10^{-3}$	$1.0x10^{-4}$	$3x10^{-3}$	$0.4x10^{-4}$
TiB_2	0.8	199	$26x10^{-3}$	$1.3x10^{-4}$	$2x10^{-3}$	$0.1x10^{-4}$
TiAlN	0.1	38	-	-	$40x10^{-3}$	$11x10^{-4}$
TiB_2	0.1	115	-	-	$10x10^{-3}$	$0.9x10^{-4}$

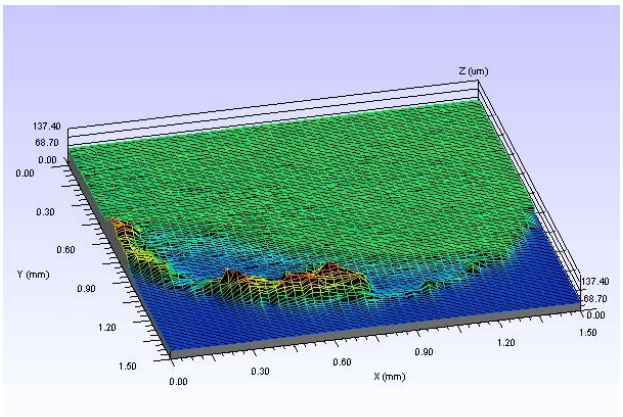

(a) Non-coated WC-Co, 0.8 mm r_c

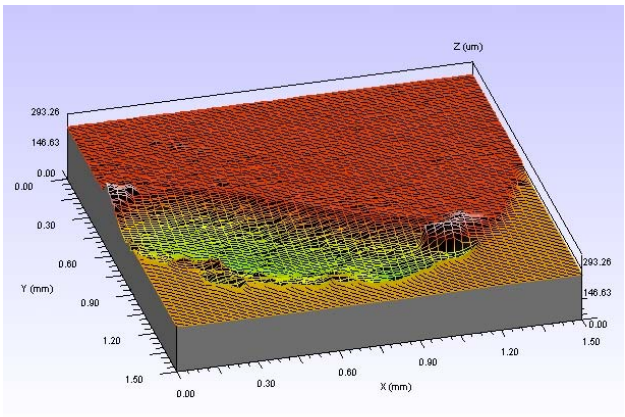

(b) TiB_2 coated, 0.8 mm r_c

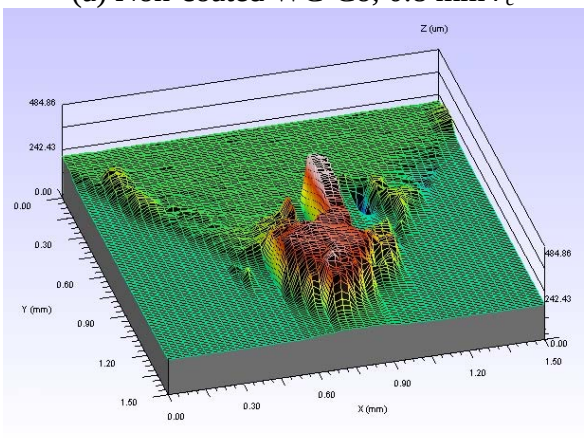

(c) TiAlN coated, 0.1 mm r_c

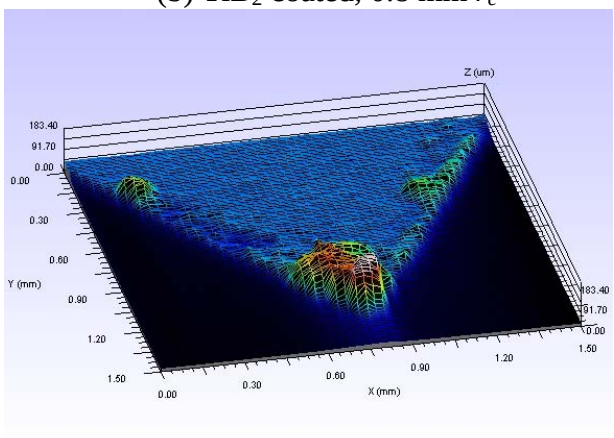

(d) TiB_2 coated, 0.1 mm r_c

Figure 2. 3D profiles of the worn tool tips.

New cutting tool materials. New cutting tool materials are being prepared for testing in high speed machining of Ti alloys. One potential tool material is TiC-Ni_3Al composite invented at ORNL. This composite was initially developed for heavy duty diesel fuel injector plungers and had the composition of 40-50 vol % TiC and 50-60 vol % Ni_3Al. The experimental work at the University of Michigan indicated that this composition is too weak and soft as a cutting tool material. TiC-Ni_3Al with high concentration of TiC (95 vol %) has been processed, and sample tool inserts have been made out of it by wire EDM and hand polishing (Fig. 3). The Vickers' microindentation hardness is about 20.6 GPa (under 200 g-f load), which is harder than a commercial WC-6 vol % Co tool material (18.5 GPa). Preliminary Ti cutting experiments were conducted at University of Michigan (Rui Li and Albert J. Shih). Slightly higher cutting forces were observed on the TiC-Ni_3Al tool compared to the WC-Co tool, probably due to the blunter edge of the hand polished new tool. Unlike the abrasive or adhesive wear on other tool materials, chipping problems, however, significantly limited the TiC-Ni_3Al tool's life. That was probably caused by the porosity (up to 15 μm pore size) in the material (Fig. 4). A composition with a higher concentration (9 vol %) of Ni_3Al is being prepared to eliminate or reduce the porosity and increase the fracture toughness.

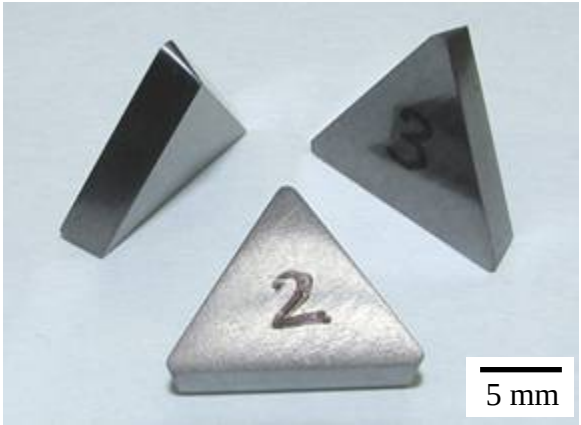

Figure 3. TiC-Ni_3Al (5 vol %) tool inserts.

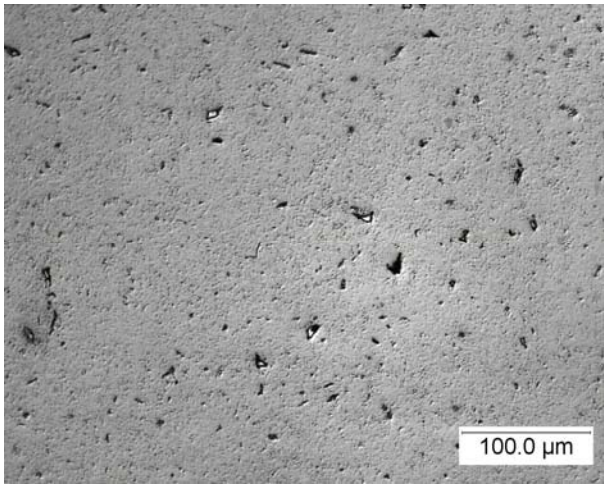

Figure 4. Microstructure of TiC-Ni_3Al (5 vol %).

Machining of Advanced Cermets. Test coupons of a cermet based on nickel aluminide (Ni_3Al) and titanium carbide were prepared for this machining study by T. N. Tiegs and F. C. Montgomery, of the ORNL Metals and Ceramics Division. Two concentrations of hard particles were included: 25 and 50% by volume. The density of the 25% TiC material is 5.41 g/cm^3 and that of the 50% TiC material is 6.21 g/cm^3. Coupons are being pre-machined by T. Jenkins to obtain parallel, flat surfaces on which to conduct the first machining trials. In light of the unexpected delay in obtaining cermet test specimens (sintering furnace problems) it may be necessary to slip the FY 2005 milestone by three months.

Future Plans

(1) Conduct instrumented grinding tests on cermet materials to investigate the effects of hard particle content on grindability and surface quality.

(2) Continue to participate in the development and validation of high-speed machining models for titanium and other materials within the Third Wave Machining Consortium.

(3) Continue to investigate the use of nickel aluminide/titanium carbide cermets as cutting tools.

Travel
None.

FY 2005 Milestone
1) Complete an investigation on the effects of grinding and related abrasive removal processes on surface quality in advanced cermets. **(06/05)**

Presentations and Publications
None.

Cost-Effective Machining of Titanium Alloys

Albert Shih
University of Michigan

Objective/Scope

The objective of this research is to investigate new technologies for cost-effective machining of Ti alloys. Experiments of the drilling of titanium alloys are conducted to study the basic drilling mechanism, the effects of process parameters on drilling performance, and feasibility of high-speed drilling.

Technical Highlights

The experiments of drilling Ti-6Al-4V were conducted. The effects of process parameters, including the spindle speed, application of coolant, drill type, and coatings on the thrust force and torque were studied.

1. Introduction of Ti drilling

Drilling is an important and widely used machining process for automotive engine and transmission component production. The study in this quarter investigates the drilling of titanium experimentally. The finite element modeling research is on-going and will be reported next quarter. In the past decade, new technical advancements in tool material, coating, and tool geometry have make cutting tools more durable and productive. These new cutting tools have not been evaluated for titanium machining. The goal of this study is to investigate the capability of state-of-the-art drills for drilling Ti using an instrumented machine to record the thrust force and torque.

Drilling is a complicated material removal process. The tool geometry and material deformation in drilling are more complicated than in the turning process. In the center of the drill, the cutting speed is close to zero and the work-material is plowed under high negative rake angle using conventional twist drill. The cutting speed and rake angles change along the cutting edges of a twist drill during the chip formation in drilling. The periphery of the cutting edge has the highest cutting speed. The chip, unlike in turning, interacts with hole and tool and needs to be evacuated.

Because of the low thermal conductivity of Ti alloys (6.7 W/m-K for Ti-6Al-4V), the temperature of the chip and tool is high. High temperature softens the tool material and aggravates the rapid drill wear. Previous publications in Ti drilling are very limited [1-5]. None of these study report the detailed of the drilling thrust force and torque, the effect of process parameters (spindle speed and feed rate) on tool wear, chip formation, and hole quality in effective drilling of Ti. In cooperation with Kennametal, a leading cutting tool manufacturer, the drilling of Ti using WC-Co drill is studied and compared with the performance of conventional high speed steel (HSS) twist drill. The feasibility of high-speed drilling is studied in this research.

2. Tool Material and Geometry

Four types of drills, all with 4.0 mm diameter, are studied. The top and side views of each of the drill are shown in Fig. 1.

1. M2 HSS twist drill, denoted as HSS Twist, with 118° point angle is used as the baseline for Ti drilling test. The length of the center web is 0.72 mm diameter.
2. The WC-Co (Kennametal grade K600 with 10% Co) split point drill, denoted as WC-Co Split, is used. This drill also has 118° point angle. This drill does not have the coolant through holes and has simple drill geometry. It can show the benefit of WC-Co tool material when compared to the drilling results with those of HSS Twist.
3. The WC-Co (Kennametal grade K715 with 9.5% Co) spiral point drill, marked as WC-Co Spiral, is tested. This drill has advanced tool geometry design. The center web has the S shape web and near positive rake angle. The web is participating in the cutting, not only indenting like in conventional drill. The point angle is 135°.
4. The same WC-Co Spiral drill with TiAlN coating, marked as WC-Co Spiral+Coating is used to evaluate the coating effect in Ti drilling.

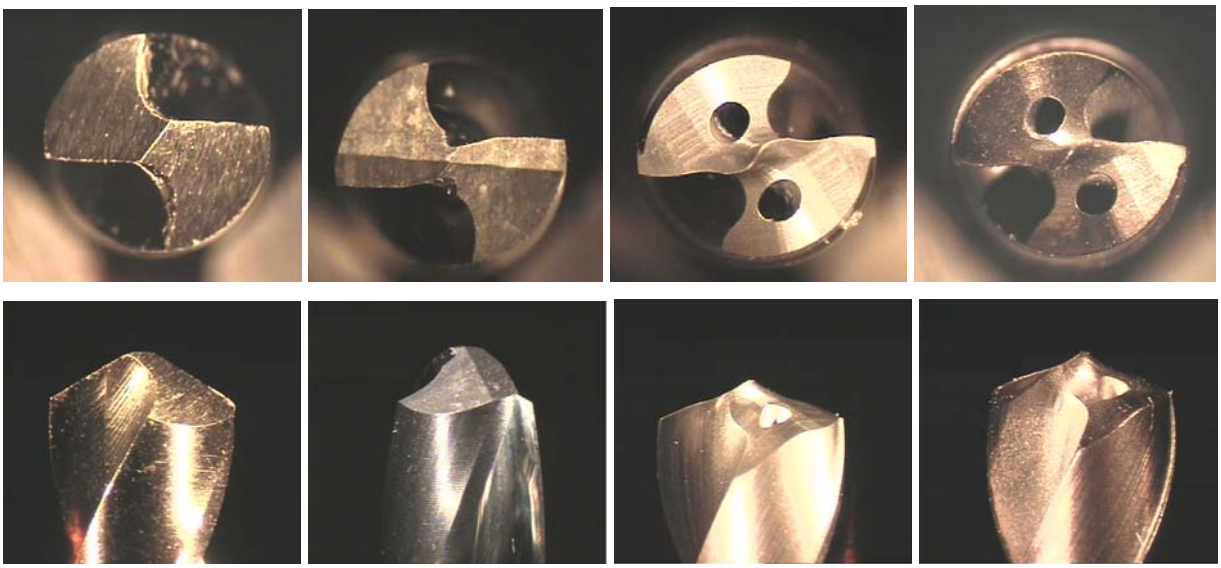

(a) (b) (c) (d)

Fig. 1. Top and side view of four types of drills: (a) HSS Twist(Greenfield Industries Chicago Latrobe 44210), (b) WC-Co Split (Kennametal KWCD00344), (c) WC-Co Spiral (Kennametal K285A01563), and (d) WC-Co Spiral+Coating (Kennametal K285A01563).

3. Experiment Design

The experiment was conducted in computer numerical control machining centers (Mori-Seiki and Fadal). The feed per revolution of all drilling tests was the same: 0.051 mm/rev. By changing the spindle speed, various drill feed rate and peripheral speed could be achieved, as shown in Fig. 2.

Four sets of experiments, marked as Exp. I, II, III and IV, were conducted. Under such drilling condition, high spindle speed will result in fast feed rate and high peripheral cutting speed of the drill.

Exp. I, was conducted using a low-cost conventional HSS Twist drill at three spindle speeds, 730, 1100, and 1470 rpm, without coolant. To study the effect of coolant, Exp. II was conducted with coolant using the HSS Twist drill at the same spindle speed as Exp. I. To study the effect of drill type, Exp. III was conducted using all four types of drill, HSS Twist, WC-Co Split, WC-Co Spiral, and WC-Co Spiral+Coating, at 1470 rpm without coolant. Exp. IV was conducted using both uncoated and TiAlN coated WC-Co Spiral drill at 1470, 2940, 5870, 8800, 11700 and 14700 rpm to study the high-speed drilling of Ti. These drills were tested to their limit and the wear mechanism. Sparks of the high temperature Ti chip can be seen over 5870 rpm. Over 11700 rpm, the drill became red during drilling. Long, continuous chip tangled to the drill was observed in all drilling tests.

The thrust force and torque during drilling were measured using a Kistler 9273 dynamometer.

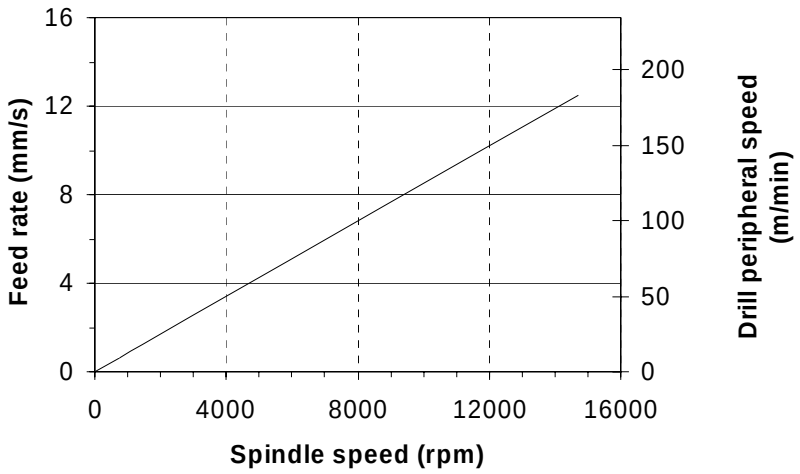

Fig. 2. Feed rate and drill peripheral speed vs. spindle speed.

Table 1. Experiment design for Ti drilling.

Exp.	I	II	III	IV
Drill	HSS Twist	HSS Twist	HSS Twist WC-Co Split WC-Co Spiral WC-Co Spiral+Coating	WC-Co Spiral WC-Co Spiral+Coating
Rotational Speed (rpm)	730 1100 1470	730 1100 1470	1470	1470 2940 5870 8800 11700 14700
Coolant	No	Yes	No	No

4. Results and discussions

Fig. 3 illustrates the three stages, marked as A, B, and C, in drilling after the initial contact (Fig. 3(a)). Stage A occurs when the drill cutting edge fully engaged in the workpiece. The drill has traveled by a distance *d*, which is called the drill point length. The drill point length for all four types of drill is listed in Table 2. When the tip of the drill reaches the back surface of the plate, it is marked as Stage B (Fig. 3(c)). Stage C is defined when the drill cutting edge is theoretically disengaged with the workpiece without considering the deformation of the workpiece and burr formation.

The torque and force changed throughout the drilling process. The thrust force and torque at Stage A is denoted as F_0 and T_0, respectively. The maximum thrust force and torque during drilling are F_m and T_m, respectively. F_0, T_0, F_m and T_m were compared to distinguish different drilling conditions.

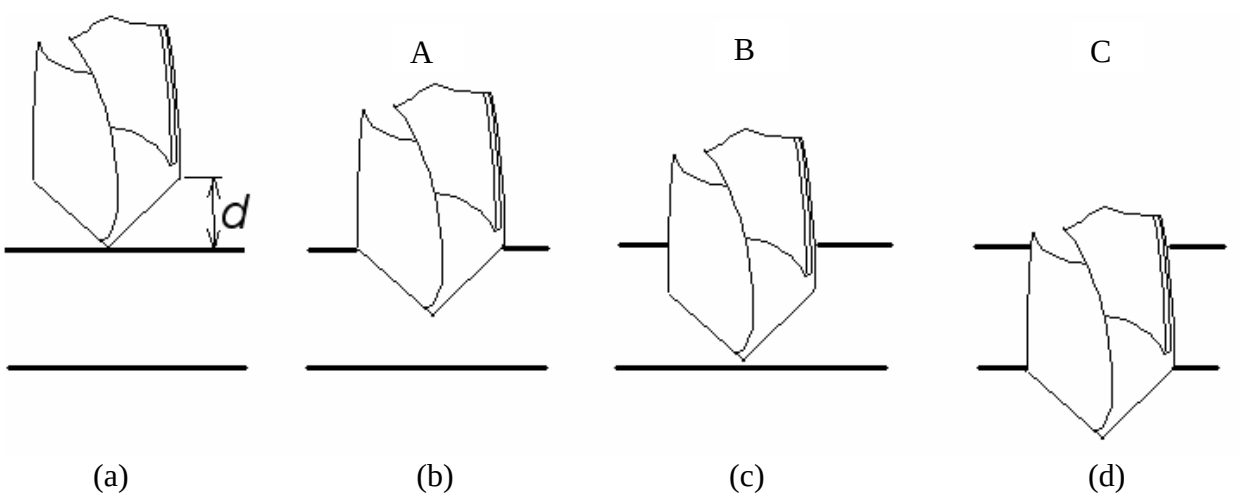

Fig. 3. Illustration of three stages in drilling: (a) initial contact, (b) Stage A, (c) Stage B, and (d) Stage C.

Table 2. Drill point length (*d*) of four drills used in this study.

Drill type	HSS Twist	WC-Co Split	WC-Co Spiral WC-Co Spiral+Coating
Length (mm)	1.24	1.19	0.74

As two parameters used to compare the performance or characteristic of a drill is the energy required to drill a hole from the beginning of contact to Stage C during drilling. The energy E consists of the thrust force and torque terms, E_f and E_t, respectively.

$$E = E_f + E_t \tag{1}$$

$$E_f = \int_l F dl \tag{2}$$

$$E_t = \int_l \frac{2\pi T}{f} dl \tag{3}$$

where F is the thrust force, l is the depth of drilling, T is the torque, and f is the feed. Results of Exp. I – IV are discussed in the following section.

4.1 Exp. IV - effect of cutting speed and tool coating

Exp. IV results are presented first because it is the most intriguing and significant. Ti drilling at high speed has known to be difficult. Using HSS Twist drill, the maximum speed is only 1470 rpm, as will be shown later in Sec.4.3. Using the WC-Co Twist+Coating, we can drill 10 holes on Ti-6Al-4V at 14700 rpm or 183 m/min without using coolant. At such speed, drill through the 6.35 mm thick Ti plate only takes 0.5 s. The thrust force and torque for drilling 10 holes using WC-Co Spiral and WC-Co Spiral+Coating drills are shown in Fig. 4.

The WC-Co Spiral drill, as shown in Fig. 4(a), broke at the 10th hole. During drilling, the thrust force increased slightly. The torque remained at about the same level, except the first hole which is likely to cause by chip interaction with the workpiece.

The WC-Co Spiral+Coating drill can drill 11 holes. As shown in Fig. 4(b), the thrust force increased to about 300 N. Before the failure in the 11th hole, the increase in torque become apparent but the force does not change significantly. It indicates that the peripheral of the cutting edge starts to worn out near the end of drilling.

The drill life is expected to increase with coolant. This study will be reported in the next quarter.

For the uncoated and coated spiral point drills tested at 1470, 2940, 5870, and 8800 spindle speed, the thrust force and torque are shown in Figs. 5 and 6, respectively. The T_0, F_0, T_m, F_m, E_f, E_t, and E are summarized in Table 3.

It is noticed that the difference of torque between uncoated and coated drills are not large, but the coated drill has almost double the thrust force compared with the uncoated drill. The possible reason is the different surface friction properties of the WC-Co substrate material and TiAlN

coating material. Since E_t is much higher than E_f, the difference of the energy needed for drilling is not large for uncoated and coated drills.

4.2 Exp. I -- effect of spindle speed on HSS Twist drill

Fig. 7 shows the thrust force and torque as a function of drilling depth using HSS Twist drill at 730, 1100, and 1470 rpm. The thrust force increased sharply until the drill cutting edge was fully engaged and then decreased slowly with the movement of drill. On the contrary, the torque kept increasing even after the cutting edge was fully engaged. The general trend is that the thrust force and torque decrease with the increase of the spindle speed. The drill performed well at lower spindle speed like 730 and 1100 rpm. But the tool tip melted at the second hole at 1470 rpm. Due to melting, the thrust force and torque lasted longer. It takes longer than 7 s to drill a hole using HSS Twist drill and the drill last for only two holes. It is obvious that HSS Twist drill has limited cutting speed and material removal rate in machining Ti. This limited productivity has hindered to cost and application of Ti in the past.

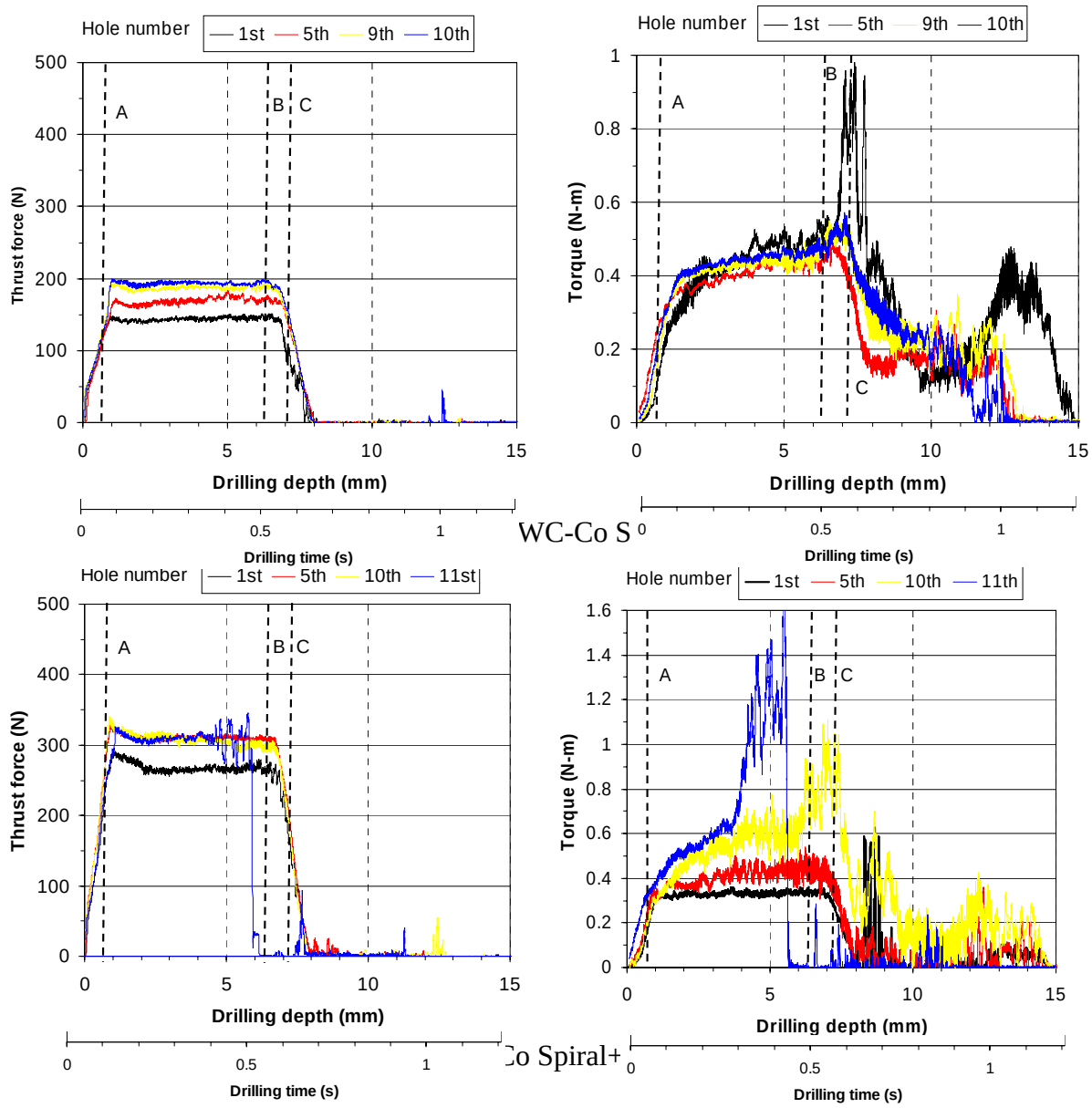

Fig. 4. High speed drilling of Ti-6Al-4V at 14700 rpm (12.5 m/s feed rate and 180 m/min peripheral speed): (a) WC-Co Spiral and (b) WC-Co Spiral+Coating.

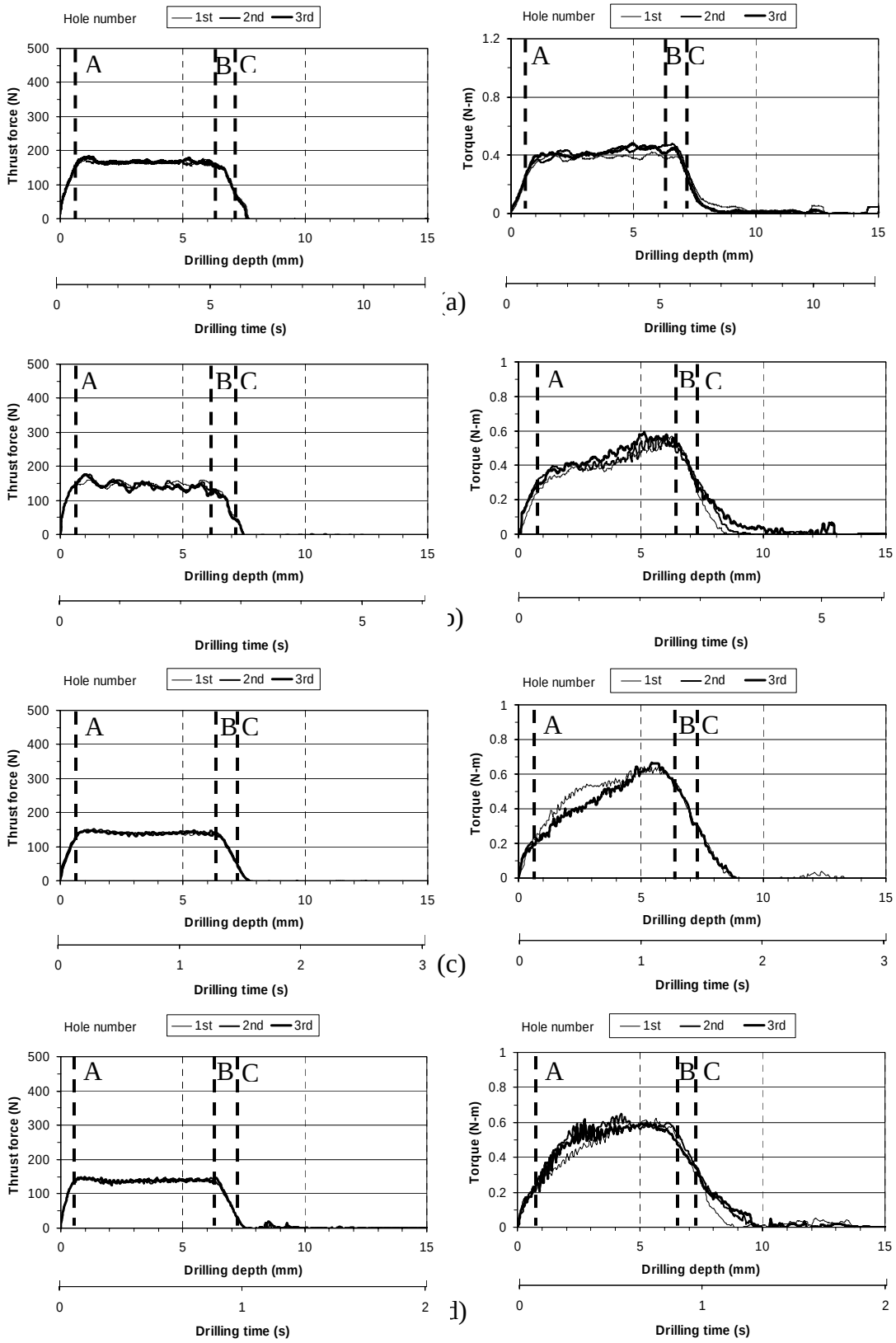

Fig. 5. Thrust force and torque of uncoated WC-Co spiral point drill at four spindle speeds (Exp. IV): (a) 1470, (b) 2940, (c) 5870, and (c) 8800 rpm.

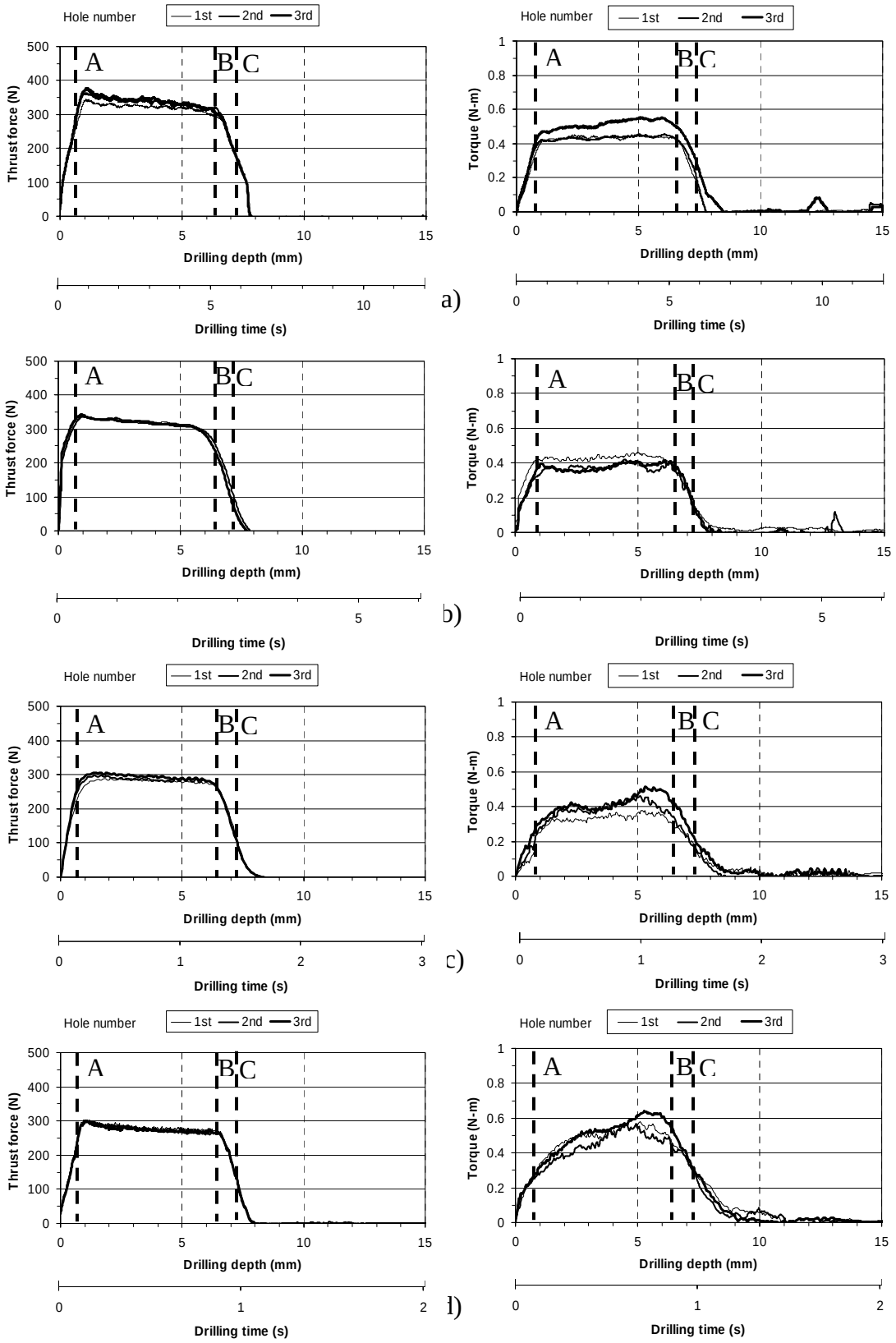

Fig. 6. Thrust force and torque of TiAlN coated WC-Co spiral point drill at different spindle speed: (a) 1470, (b) 2940, (c) 5870, and (c) 8800 rpm.

Table 3. Summary of thrust force and torque of uncoated and coated WC-Co spiral point drill.

Spindle speed (rpm)	Coating	T_0 (N·m)	F_0 (N)	T_m (N·m)	F_m (N)	E_f (J)	E_t (J)	E (J)
1470	Uncoated	0.25-0.27	166-169	0.42-0.48	177-178	1.1	350-394	351-395
	TiAlN	0.30-0.31	321-333	0.45-0.55	337-371	2.3	368-449	370-451
2940	Uncoated	0.33-0.34	145-151	0.61-0.66	159-175	1.0	374-425	375-426
	TiAlN	0.34-0.38	311-324	0.42-0.47	326-333	2.3	336-409	339-411
5870	Uncoated	0.23-0.24	140-144	0.58-0.62	142-146	1.0	411-458	412-459
	TiAlN	0.23-0.31	258-274	0.39-0.55	296-301	2.0	396-392	398-414
8800	Uncoated	0.18-0.21	143-145	0.54-0.56	145-146	1.0	459-529	460-473
	TiAlN	0.28-0.29	269-273	0.55-0.63	297-299	1.9	454-495	456-497

4.3 Exp. II - effect of coolant on HSS Twist drill

Under the dry condition, HSS Twist drill did not perform well in Exp. I. In Exp. II, coolant was used in the same drilling conditions in Exp. I. Fig. 8 shows the thrust force and torque. The drill performed well at higher spindle speed 1470 rpm as well as lower spindle speeds. The use of coolant can elongate the drill life significantly. Table 4 summarizes the T_0, F_0, T_m, F_m, E_f, E_t, and E under these drilling conditions. Compared to dry condition in Exp. I, the thrust force and torque decrease when the coolant was used. Correspondingly, less energy is generated. Combined with the cooling effect of coolant, the drilling temperature can be greatly decreased and drill wear relieved. It is noticeable that the energy generated by torque E_t was much larger than the energy generated by thrust force E_f, for all the conditions. This is a result of the low feed (0.051 mm/rev) allowed for drilling Ti.

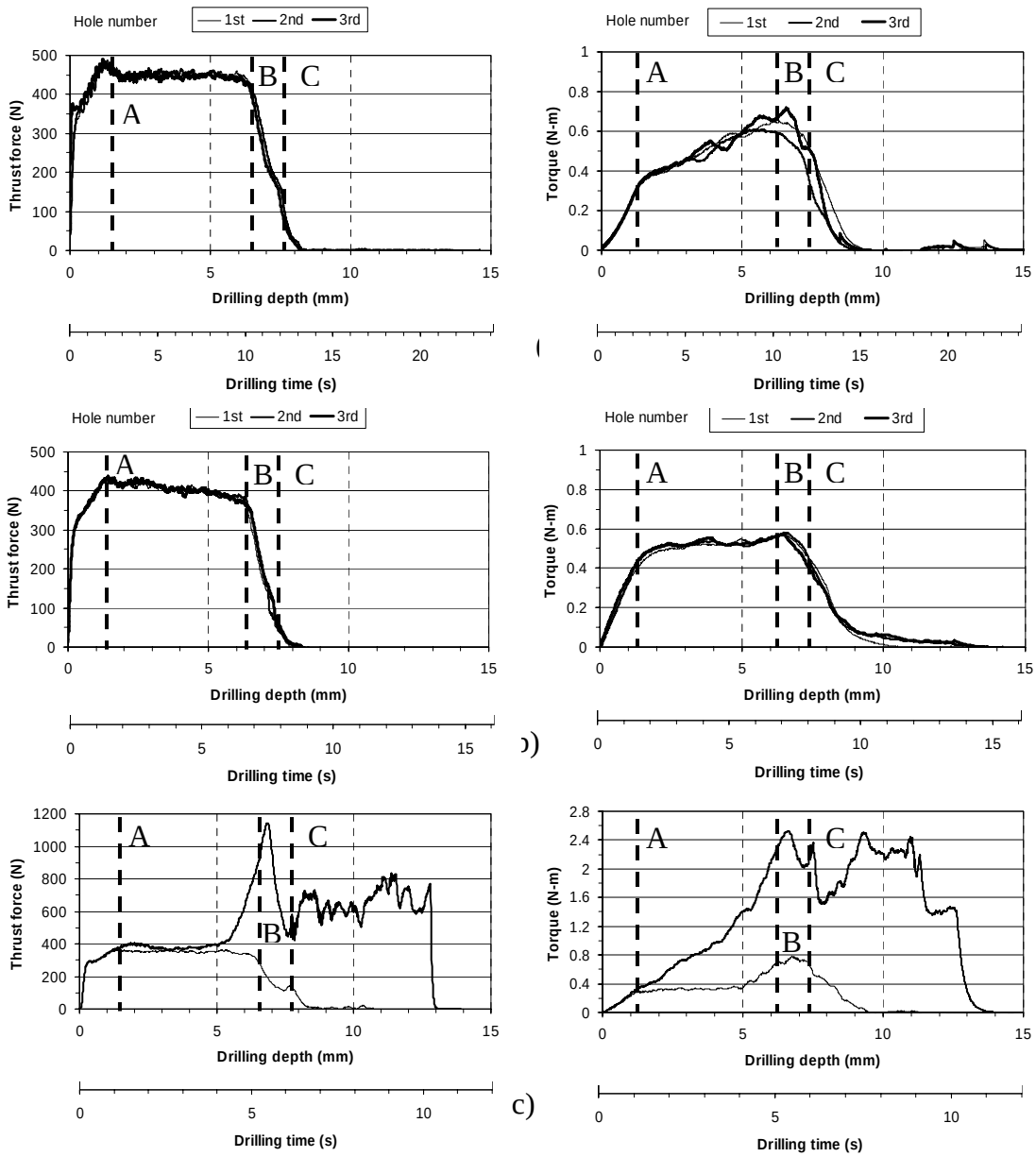

Fig. 7. Exp. 1 thrust force and torque of HSS Twist drill without coolant at different spindle speed: (a) 730, (b) 1100, and (c) 1470 rpm.

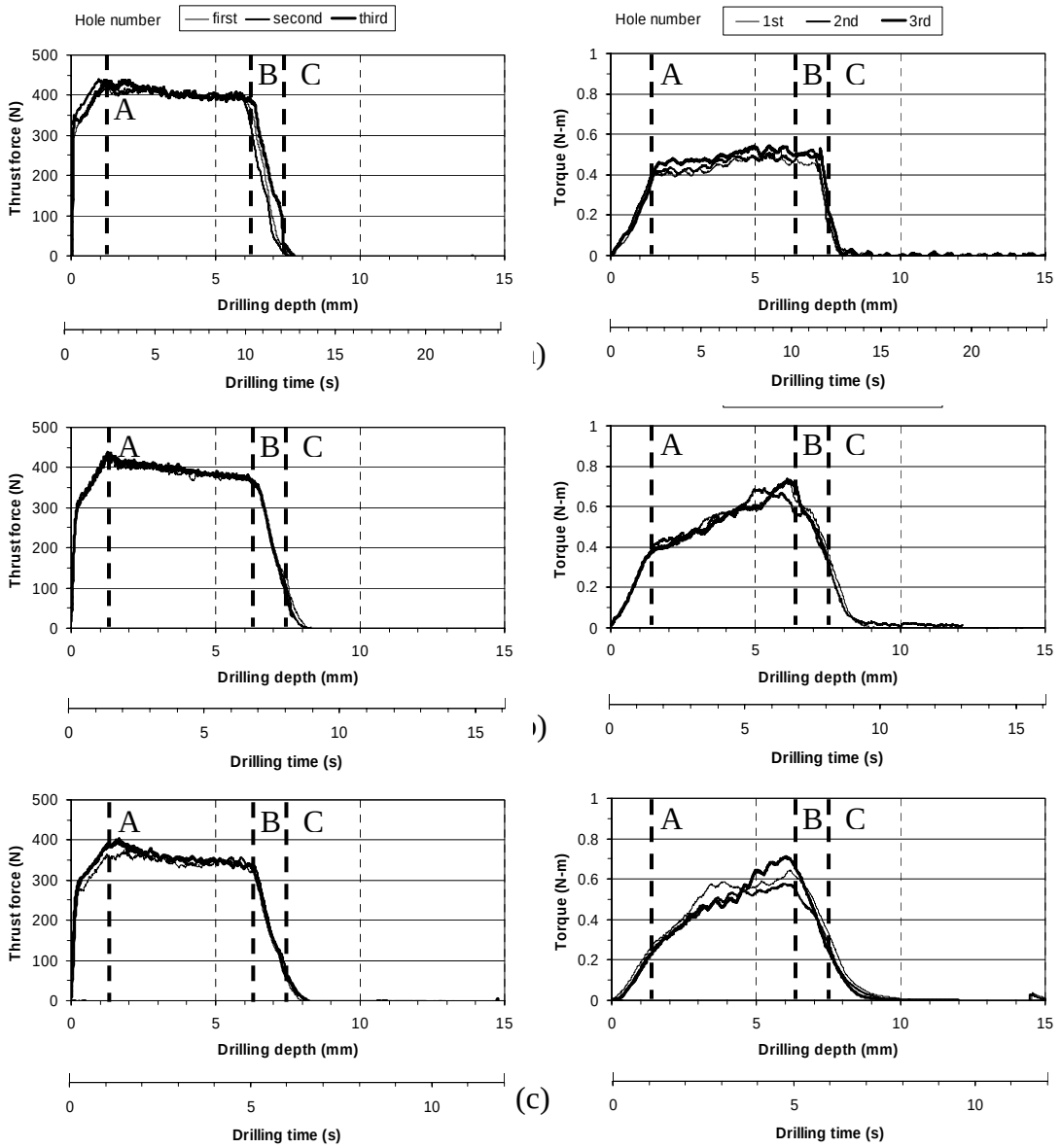

Fig. 8. Thrust force and torque of HSS drill with coolant at different spindle speed: (a) 730, (b) 1100, and (c) 1470 rpm.

Table 4. Summary of thrust force and torque of HSS drill (Exps. I and II).

Spindle speed (rpm)	Coolant	T_0 (N·m)	F_0 (N)	T_m (N·m)	F_m (N)	E_f (J)	E_t (J)	E (J)
730	No	0.33-0.34	471-473	0.65-0.74	484-488	3.1	423-465	426-467
	Yes	0.38-0.40	406-421	0.52-0.54	428-435	2.7	366-403	369-406
1100	No	0.33-0.34	424-426	0.56-0.57	432-435	2.7	452-482	455-485
	Yes	0.35-0.36	417-420	0.65-0.73	424-429	2.7	439-464	442-467
1470	No	0.33 0.33	360 361	0.77 2.51	378 1137	2.5 7.0	425 2280	428 2287
	Yes	0.26-0.28	361-374	0.58-0.74	365-393	2.4	384-425	387-427

4.4 Exp. III - effect of drill type

Fig. 9 and Table 5 show the thrust force and torque when using all four types of drill at 1470 rpm without coolant. Compared with HSS Twist, the WC-Co Split had much lower thrust force, but it generated higher torque, and required much higher energy to finish the drilling operation. In comparison, both uncoated and coated WC-Co spiral point drill generated lower thrust force and torque and required lower energy. It can be concluded that, from the force and torque perspective, WC-Co spiral point drill has better drill geometry design for Ti drilling.

Table 5. Summary of thrust force and torque of different types of drill (Exp. III).

Drill type	T_0 (N·m)	F_0 (N)	T_m (N·m)	F_m (N)	E_f (J)	E_t (J)	E (J)
HSS Twist	0.33 0.33	360 361	0.77 2.51	378 1137	2.5 7.0	425 2280	428 2287
WC-Co Split	0.24-0.32	233-235	0.71-0.91	235-257	1.5	626-712	628-713
WC-Co Spiral	0.25-0.27	166-169	0.42-0.48	177-178	1.1	350-374	351-375
WC-Co Spiral+Coating	0.30-0.31	321-333	0.45-0.55	337-371	2.3	368-439	370-441

5. Conclusions

This study showed the cost-effective, high speed drilling of Ti is possible using the existing advanced drill. For all the drilling conditions, the thrust force and torque showed similar trend. The thrust force increased sharply until the cutting edge is fully engaged with the workpiece, then decreased slowly during the drilling operation, and finally dropped down to zero when the workpiece is penetrated. The torque kept increasing after the cutting edge is fully engaged. With the increase of spindle speed, the thrust force generally decreased slightly and the rate of torque during the drilling operations increases. The energy consumed by torque is two orders higher than the energy generated by thrust force.

HSS twist drill can only work at low spindle speed under dry condition. With the coolant, the performance of it can be improved, but the thrust force and torque are still high. Under the same spindle speed, WC-Co spiral point drill outperforms the HSS twist drill and WC-Co split point drill in terms of thrust force, torque and energy required for drilling. WC-Co spiral point drill can also work at very high spindle speed, a key factor to increase the productivity. Coated with TiAlN coating, the spiral point drill generates much higher thrust force, but the torque does not change significantly.

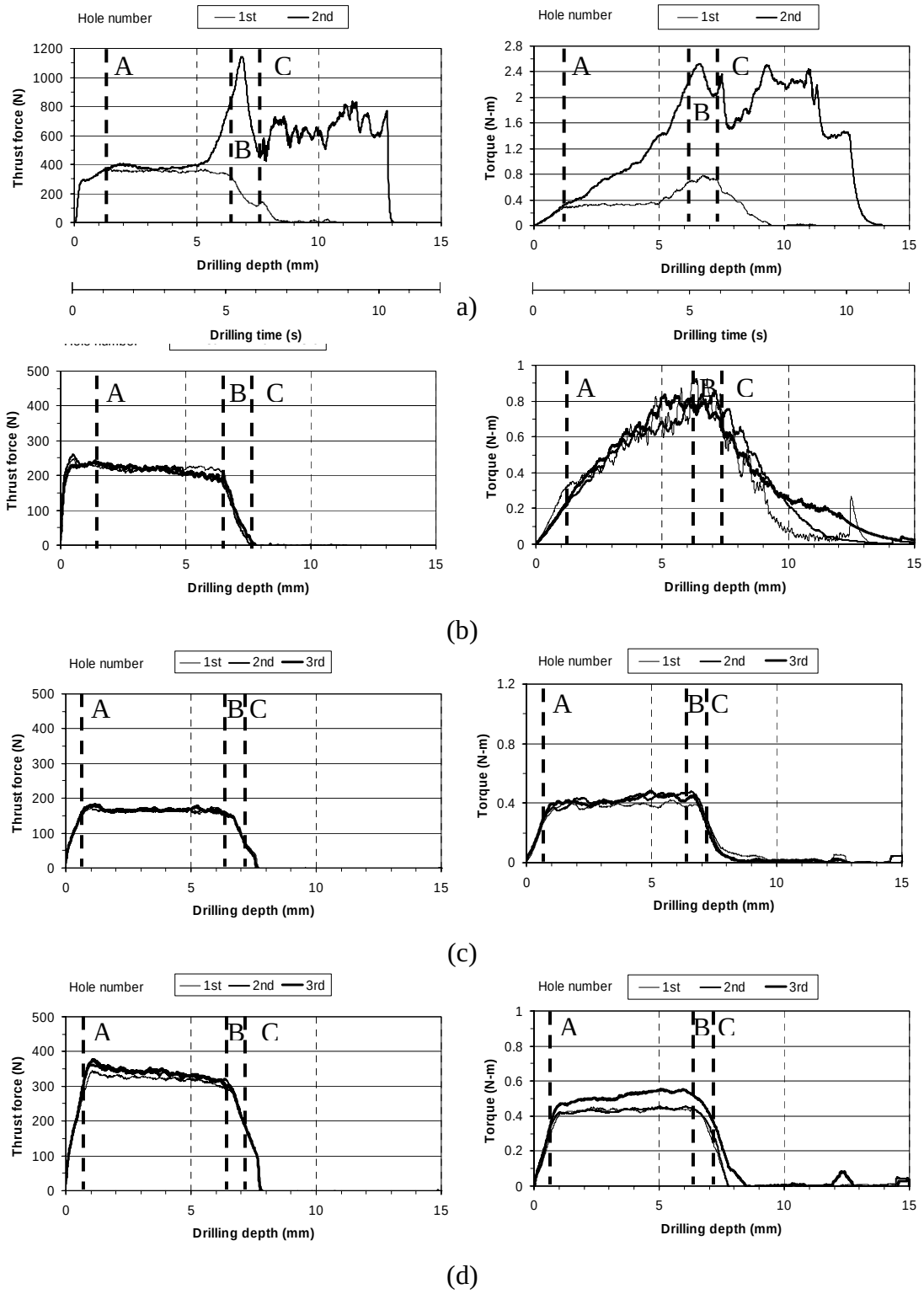

Fig. 9. Thrust force and torque of four types of drill at 1470 rpm: (a) HSS Twist, (b) WC-Co Split, (c) WC-Co Spiral, and (d) WC-Co Spiral+Coating.

Future Work

The drilling test will continue on drill life test of spiral point drill. The Minimum Quantity Lubricant device will be tested in the drilling of Ti alloys. On the finite element modeling, Third Wave Systems is working on improving the drilling simulation efficiency and accuracy.

Status of Milestones

Milestone 1: Experimental study of Ti drilling.
Status: Extensive tests of Ti-6Al-4V drilling have been conducted and reported.

Milestone 2: 3D finite element modeling of titanium drilling process.
Status: This work has just started after a new version of ThirdWave drilling is released.

Milestone 3: Investigation of TiC-based cutting tool material.
Status: Exploratory tests have been conducted. Cutting force have been measured and compared with the results when using WC-Co tool at different cutting speeds and feeds. The material is still too brittle.

Milestone 5: Measure of Ti drilling temperature.
Status: Experiments have been setup to measure the temperature in Ti machining. We are working to develop a mathematical model for inverse calculation of the drill temperature distribution based on the measurement results.

Communications/Visit/Travel

Albert Shih visited ORNL on Feb. 9.

Michael Foos of General Dynamics Land Systems visited UM on March 16 to discuss the Ti machining for Future Combat Systems.

Albert Shih visited BorgWarner Turbo at Asheville, NC on April 15 and toured the Ti compressor wheel manufacturing for International I6 diesel engines.

Publications

R. Li and A. J. Shih, "Finite Element Modeling of 3D Turning of Titanium," *International Journal of Advanced Manufacturing Technology* (accepted).

References

[1] K. Sakurai, K. Adachi, K. Ogawa, 1992, "Low Frequency Vibratory Drilling of Ti-6Al-4V alloy," Keikinzoku/Journal of Japan Institute of Light Metals 42(11) 633-637.

[2] K. Sakurai, K. Adachi, K. Ogawa, R. Niba, 1992, "Drilling of Ti-6Al-4V Alloy," Keikinzoku/Journal of Japan Institute of Light Metals 42(7) 389-394.

[3] K. Sakurai, K. Adachi, T. Kamekawa, K. Ogawa, S. Hanasaki, 1996, "Intermittently Decelerated Feed Drilling of Ti-6%Al-4%V Alloy," Keikinzoku/Journal of Japan Institute of Light Metals 46(3) 138-143.

[4] M. Arai, M. Ogawa, 1997, "Effects of High Pressure Supply of Coolant in Drilling of Titanium Alloy," Keikinzoku/Journal of Japan Institute of Light Metals 47(3) 139-144.

[5] D.A. Dornfeld, J.S Kim, H. Dechow, J. Hewson, L.J. Chen, 1999, “Drilling Burr Formation in Titanium Alloy, Ti-6Al-4V,” CIRP Annals - Manufacturing Technology 48(1) 73-76.

Advanced Cast Austenitic Stainless Steels for High Temperature Components

P.J. Maziasz, John P. Shingledecker, and N.D. Evans
Oak Ridge National Laboratory
and M.J Pollard
Caterpillar, Inc.

Objective/Scope

This is the 2nd CRADA project with Caterpillar, which is focused on commercialization of the new CF8C-Plus cast austenitic stainless steel developed on the first ORNL/CAT CRADA. CF8C-Plus steel is a cost-effective performance upgrade relative to current heavy-duty diesel engine exhaust component materials, including SiMo ductile cast iron. In FY2005, this project will complete the initial properties data base needed for component design or redesign, particularly fatigue, thermal fatigue, and creep, and studies of aged materials, including impact properties. This CRADA (Cooperative Research and Development Agreement) project (ORNL02-0658) began on July 21, 2002, and has been extended for 2 more years beyond the 3 year expiration date of July 21, 2005. More detailed information on this project must be requested directly from Caterpillar, Inc.

Technical Highlights

Background

Current cast iron heavy diesel engine exhaust manifolds and turbocharger housings are being pushed beyond their temperature capabilities as normal duty cycles go to 750°C or higher, and rapid and severe thermal cycling contributes to increased failures. New materials with upgraded temperature capability and reliability for such applications must also be commercially available at a reasonable cost. The new cast CF8C-Plus austenitic stainless steel now being commercialized holds promise of being such a material. Current efforts by Caterpillar, Inc. and ORNL include completing the systematic and thorough properties data base required by designers to optimize component design, and characterizing the properties of trial or prototype commercial components.

Approach

Multiple commercial heats of CF8C-Plus have been cast by several commercial foundries, including static sand and centrifugal casting methods. In FY 2004, new heats of standard CF8C-Plus (Mn+N) and a new modified CF8C-Plus steel (Mn+N+Cu+W) were produced by MetalTek, and are currently being tested and characterized at ORNL. The goal for FY 2005 is to make and characterize prototype or trial components of CF8C-Plus steel for various applications.

Technical Progress

Figure 1 shows yield strength (YS) data as a function of temperature for specimens made from commercial centrifugally-cast heats (typically 500 lb or more, air melted, made by MetalTek) of standard CF8C and two new heats of CF8C-Plus steel. One new heat is the CF8C-Plus with Mn and N additions that improve the YS somewhat compared to standard CF8C steel without those additions. The other new heat is a modified CF8C-Plus steel with further additions of Cu and W

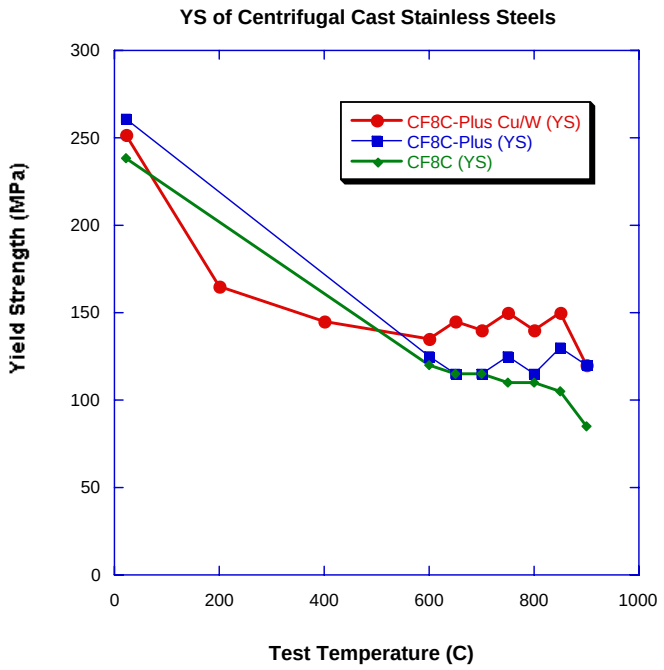

Figure 1 – A plot of yield strength (YS) as a function of test temperature for commercial, centrifugally-cast heats of standard CF8C, two new CF8C-Plus cast stainless steel produced by MetalTek. The original CF8C-Plus steel was improved by Mn and N additions relative to the standard CF8C steel, and a new modified version, with further additions of Cu and W, was made to boost the strength at 800°C and above.

which boost the YS even more at 600-850°C. Work is in progress this extend comparison of these steels to include creep, fatigue, thermal fatigue, and aging (including tensile and charpy impact specimens), and some preliminary results will be reported next quarter.

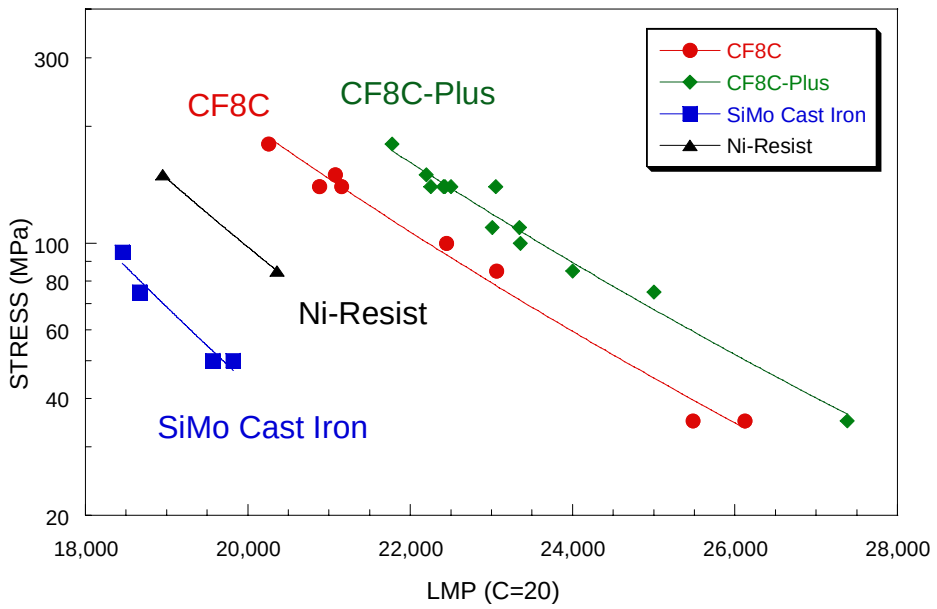

Figure 2 – Creep-rupture stress plotted versus Larson-Miller Parameter (LMP) for various creep-rupture tests run at 500-850°C at ORNL in air of various commercial heats of SiMo ductile and Ni-resist austenitic cast irons, and standard CF8C and new CF8C-Plus austenitic stainless steels. CF8C-Plus shows a significant creep-strength advantage over the standard steel or the cast irons.

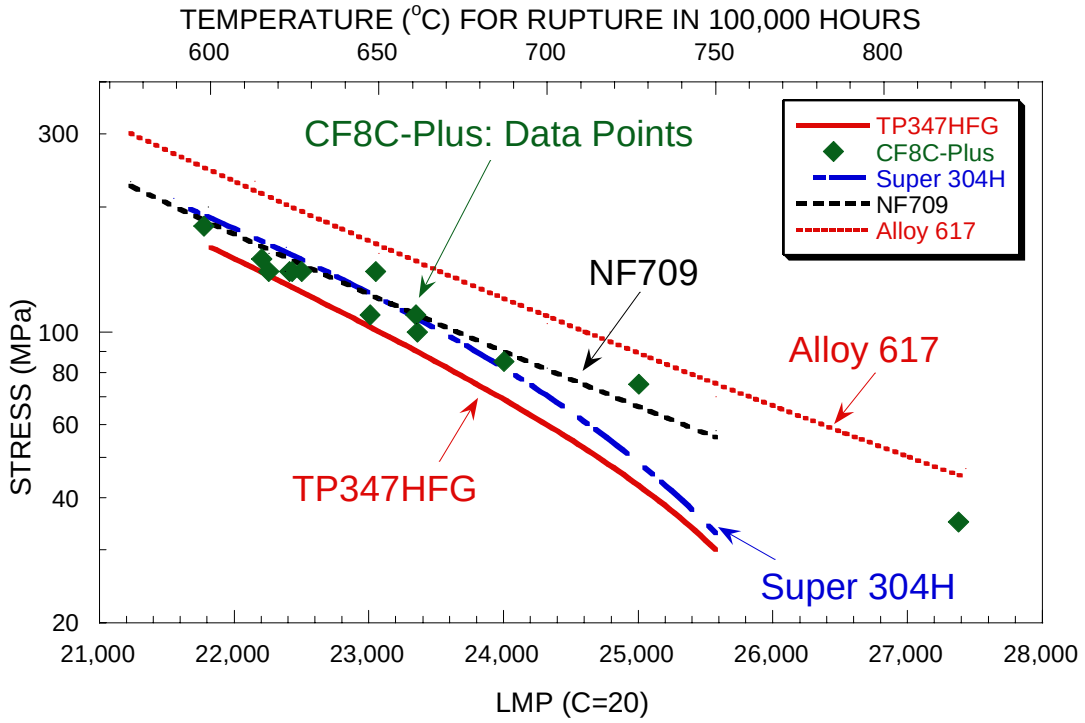

Figure 3 – Comparison of LMP creep data for new cast CF8C-Plus steel and various other high-strength, heat-resistant stainless steel, alloys or superalloys.

Creep rupture testing amplifies the differences seen by high-temperature tensile testing. Clearly, the CF8C-Plus steel has 1.5-2 times more creep-rupture strength than the standard CF8C steel, as shown in Figure 2. There is a far greater creep strength advantage for CF8C-Plus relative to either SiMo ductile or Ni-resist austenitic cast irons. Finally, data from several creep tests of CF8C-Plus steel are used to calculate the Larson-Miller parameter (LMP) that unifies data tested at different temperatures and times, and compared with similar data for some of the strongest wrought heat-resistant stainless steels, alloys and superalloys in Figure 3. CF8C-Plus steel is stronger than 347HFG and Super304H austenitic stainless steels, especially at higher temperatures, and is as strong as NF709, one of strongest stainless alloys available. The creep strength of the CF8C-Plus steel is also close to that of superalloy 617, which is considerably more expensive. Such properties advantages are driving new interest in CF8C-Plus steel for gas-turbine and steam-turbine applications in addition to the diesel exhaust component applications being considered here.

Communications/Visits/Travel

Detailed team communications between ORNL and Caterpillar occur regularly, at least once or twice a week. The new 3 year CRADA began on July 21, 2002, when the previous CRADA ended and is scheduled to end on July 21, 2005. The two-year CRADA extension requested last quarter was agreed to this quarter by ORNL and Caterpillar.

Status of Milestones

FY 2005 Milestones for Subtask 4.10 – 1) Complete properties measurements of new CF8C-Plus heats, including static and centrifugally cast, at 700-850°C (2/05); **complete**, 2) Commercially scale up new CF8C-Plus heats with Cu/W alloying additions for more high-temperature strength, and complete testing (6/05); **on track**, and 3) Extend the current CRADA for another year or more to complete testing and evaluation of prototype components cast from CF8C-Plus (7/05); **complete**.

Publications/Presentations/Awards

In FY 2004, CF8C-Plus steel was awarded ORNL Technology Transfer and Economic Development (TTED) Royalty Funds to enable and accelerate commercial scale-up of the new heats with Cu and W added, which was completed this quarter.

P.J. Maziasz, I.G. Wright, J.P. Shingledecker, T.B. Gibbons, and R.R. Romanosky, "Defining the Materials Issues and Research for Ultra-Supercritical Steam Turbines," paper written, to be published in Proc. 4th International Conference on Advances in Materials Technology for Fossil Power Plants, ASM-International, Materials Park, OH (2005).

P.J. Maziasz, J.P. Shingledecker, N.D. Evans, ORNL and M.J. Pollard, Caterpillar, "Update on ORNL/CAT CRADA on CF8C-Plus Cast Stainless Steel: Progress and Commercial Scale-Up in 2004/2005," talk given at DOE FreedomCAR and Vehicle Technologies Review at ORNL for Sid Diamond, March 2, 2005.

Nucleation and Propagation of Deformation Twin in Polysynthetically Twinned TiAl

L. M. Hsiung[1], Hanchen Huang[2] and L. G. Zhou[2]

Objective and approach

The objective is to reveal mechanisms of how interfacial dislocations influence the twinning process in polysynthetically twinned (or fully lamellar) TiAl. Using molecular dynamics simulations, we have studied the deformation of polysynthetically twinned (PST) TiAl at room temperature with a bicrystal model. The simulation cell was pre-strained and thermodynamically relaxed to a criterion that all stress components of the simulation cell have gone to zeros; in this way no dislocations were pre-existed in γ-α_2 interfaces. A uniaxial compression was then applied along one 1/6<112] direction in the surface. The results show that under the compression, the interfacial dislocation pairs were prolifically generated due to the structural transformation of α_2-lamella. The gliding and agglomerating of these dislocations would finally cause the nucleation of deformation twins from the interface. This is suggested to be a new possible twinning mechanism in the dual phase TiAl alloy. The propagation of this deformation twin, or specifically, its interaction with γ-γ and γ-α_2 interfaces has been discussed. It shows that the α_2 lamella is intent to block the propagation of the deformation twin.

Introduction

TiAl intermetallic compounds and alloys have been a focus of intensive research, due to their supreme properties at elevated temperatures. In particular, they possess high specific strength, high stiffness, and excellent environmental resistance [Appel and Wagner (1998)] at high temperatures. In addition, their density is low. Consequently, TiAl compounds and alloys are primary candidates of the structural materials in the aerospace industry. A major drawback of the compounds is the lack of ductility and toughness at room temperature. Recent efforts have been focused on the development of dual phase alloys with a refined full lamellar microstructure [Hsiung et al. (2002)]. The two phases are γ-TiAl and α_2-Ti_3Al, plus additional alloying elements. Increased fracture toughness and creep resistance result from the refined lamellar structure [Liu et al. (1996, 1998); Morris and Lip (1997)]. A polysynthetically twinned (PST) crystal of TiAl contains only fine lamellae of γ-TiAl and α_2-Ti_3Al [Wegmann et al. (2000); Parthasarathy et al. (2000)]. Such PST crystal is sometimes referred as a single crystal, although it contains twin boundaries. Because of the lamellar structure, PST crystals are highly anisotropic in mechanical properties. When the loading direction is parallel or perpendicular to the lamellar interfaces, the yield strength is high but the ductility is low. In contrast, under other loading directions the yield strength is low but the ductility is high [Inui et al. (1992)]. This anisotropy is related to the preferred glide of dislocations along interfaces. It is, therefore, possible to design materials of controllable strength and ductility by orientational alignment of the lamellae. The optimal design is still a target of on-going efforts [Maruyama et al. (1997)].

One of the controlling factors in the optimization is the deformation twin. According to Farent et al (1993), deformation twins in γ-TiAl form as a result of coordinated glides of a/6<112] partial dislocations. Similar mechanisms have been observed in dual phase TiAl, and the dislocation nucleation at grain boundaries is correlated with the local stress concentration [Jin and Beiler (1995)]. The twins may coarsen when ledges nucleate and migrate along the twin boundaries [Kim and Maruyama (2003)]. Instead of grain boundaries, γ–α_2 interfaces host dislocations due to the mismatch of two phases. These dislocations dissociate into partials at the interface. The glissile partials, either collectively after pileup at the interface [Hsiung et al. (1997, 2002)] or individually [Zhang and Ye (2003)], propagate away from the interface, leading to twin formation in the matrix. These experimental observations have clearly demonstrated the twin formation, and correlated it with pre-existing dislocations at the interface. In terms of twinning mechanism, are pre-existing dislocations necessary for the twin formation? And, how do the twins propagate? In this paper, we address these two issues using molecular dynamics simulations.

[1] Lawrence Livermore National Laboratory, Chemistry and Materials Science Directorate, P.O. Box 808, L-352, Livermore, CA 94551, USA

[2] Department of Mechanical, Aerospace & Nuclear Engineering, Rensselaer Polytechnic Institute, Troy, NY 12180, USA

Methodology

The molecular dynamics simulations involve four crucial components: setup of the simulation cell, interatomic potential, control of thermodynamic variables, and analysis techniques. In the following, we elaborate these four components one by one.

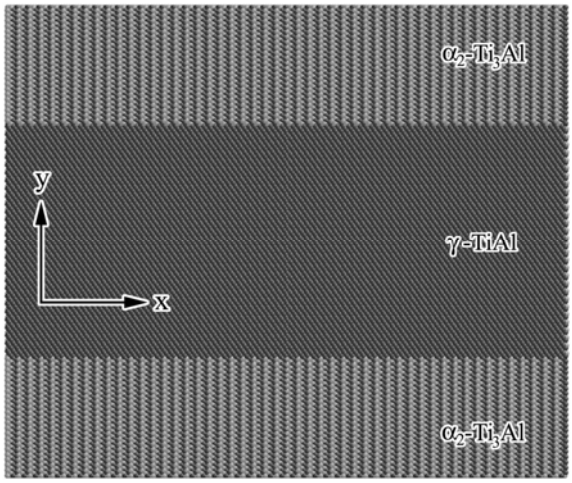

Figure 1: The simulation cell, with Ti atoms in light and Al atoms in dark spheres.

The simulation cell, shown in Figure 1, consists of two slabs, one being the γ-TiAl and the other α_2-Ti_3Al. The two slabs form an interface with both side being close-packed planes, that is $(111)_\gamma//(0001)_{\alpha 2}$. Further, the closed-packed directions on the two sides coincide with each other, that is $<110]_\gamma//<11\bar{2}0>_{\alpha 2}$ [Feng et al. (1989)]. The x-axis is along the $[\bar{1}12]_\gamma//[1\bar{1}00]_{\alpha 2}$, the y-axis the $[1\bar{1}1]_\gamma$ $//[0001]_{\alpha 2}$, and the **z** the $[110]_\gamma/[11\bar{2}0]_{\alpha 2}$. Periodic boundary conditions are applied along all the three directions. The intrinsic mismatches, 2.3% along **x** and 1.5% along **z**, and the corresponding stresses are relaxed through the control of thermodynamic variables; this will be elaborate after the description of interatomic potential. The dimensions of the simulation cell are 50.4 nm along x, 42.5 nm along y, and 2.3 nm along z; the total number of atoms is 288,000.

Atoms in the simulation cell interact with each other according to a prescribed interatomic potential. The Embedded Atom Method (EAM) potential of Ti-Al [Zope and Mishin (2003)] well describes the stability of multiple Ti-Al phases, and is used in this work.

With the prescribed interatomic potentials, atoms move according to the Newton's equation, under given stresses and temperatures. According to the Parrinello-Rahman algorithm [Parrinello and Rahman (1981)], the size and shape of a simulation cell respond to the difference of internal and external stresses, so the internal stresses are kept at desired values. We use this algorithm to control the stress in this work. The temperature of the simulation cell is essentially the kinetic energy. We scale the atomic velocities to control the temperature. In contrast to the use of frictional forces, the scaling scheme minimizes potential artificial impacts to defect activities.

Under given stresses and temperatures, the molecular dynamics simulations provide details of atomic positions as a function of time. These positions must be analyzed to gain physical insights. The bond-pair analysis technique [Clarke and Jonsson (1993)] provides clear distinction between atoms in perfect crystals, interfaces, and near dislocations; and it is used in this study. According to this technique, a bond is considered to be formed between two nearest neighboring atoms. The configuration of others bonds formed by the nearest neighbors of the two atoms forming the bond determines whether the bond is good or bad. For example, each bond in a perfect face-centered-cubic (FCC) crystal has four neighboring bonds. Further, atoms in these four bonds form two other bonds. These two bonds form two non-connect chains, each being one bond in length. This bond configuration is referred to as "421". In the same logic, both 421 and 422 bonds form in hexagonal-close-packed (HCP) crystals. Near a stacking fault two layers of atoms are HCP-like, at a twin only one layer of atoms are HCP-like. In this work, the γ-phase is close to FCC, and the α_2-phase to HCP, and therefore the bond-pair analysis techniques applies.

Results

In this section, we present the mechanisms of twin nucleation and propagation in two-phase lamellar Ti-Al compounds, under mechanical loading. Before applying strains, we prepare an interface that is dislocation free.

Large mismatches exist in the initial simulation cell, shown in Figure 1. Using the Parrinello-Rahman algorithm, we relax the internal stress to zero. As shown in Figure 2a, all stress components of the simulation cell go to zeros beyond 25 ps. At the end of the relaxation, a twin is formed in the γ phase, as shown in Figure 2b. Incidentally, this newly formed twin enables the study of twin interactions, to be presented later.

Subjected to a uniaxial strain along x, applied at the rate of $2x10^8$ s^{-1} (that is $2x10^{-7}$ per molecular dynamics step), the atomic configurations in Figure 2b evolve. At 9.3 ps after the loading starts, pairs of interface dislocations nucleate at the γ-α_2 interface, as shown in Figure 3a. The dislocation nucleation enables interface migration (Figure 3b), which is driven by the strain imbalance. Before the loading, the γ phase is under tension, and the α_2 phase under compression. The compressive loading compensates the tension in the γ phase and reduces the strain energy, and its effect in the α_2

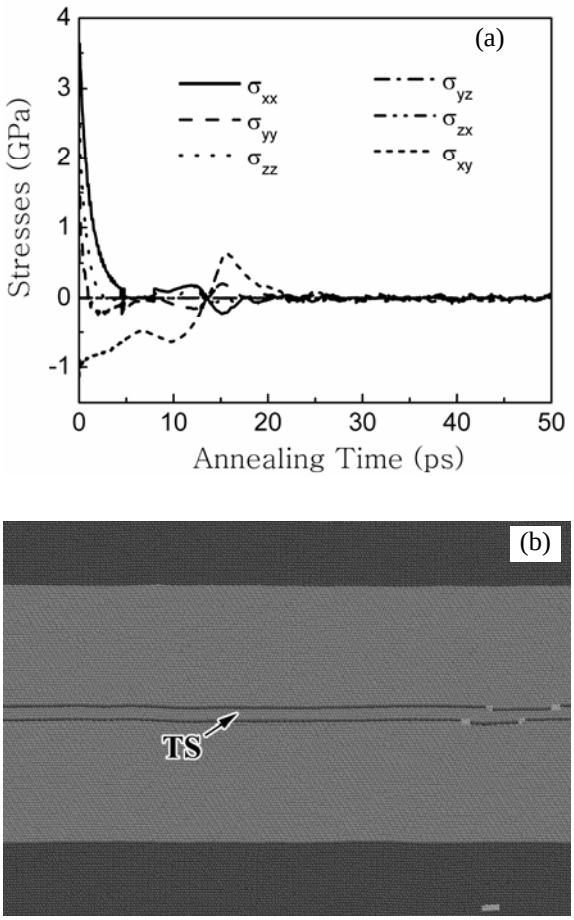

Figure 2: (a) Stresses during relaxation at 300K, and (b) relaxed atomic configuration (projection on x-y plane). The dark, dark gray, and light gray spheres represent HCP atoms, FCC atoms, and other atoms, respectively.

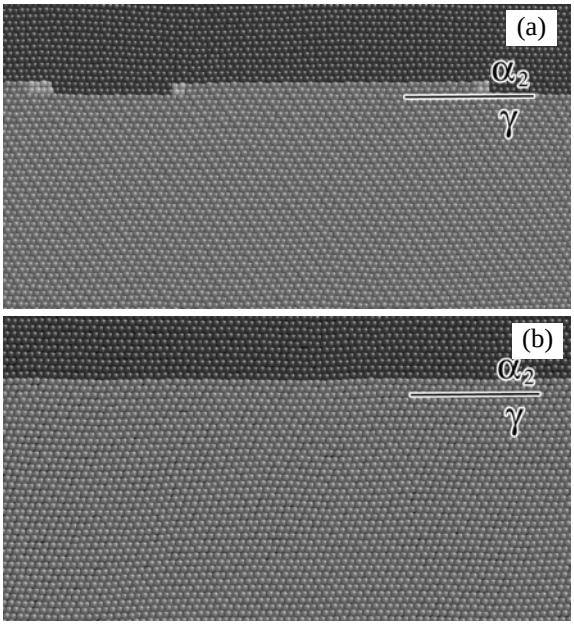

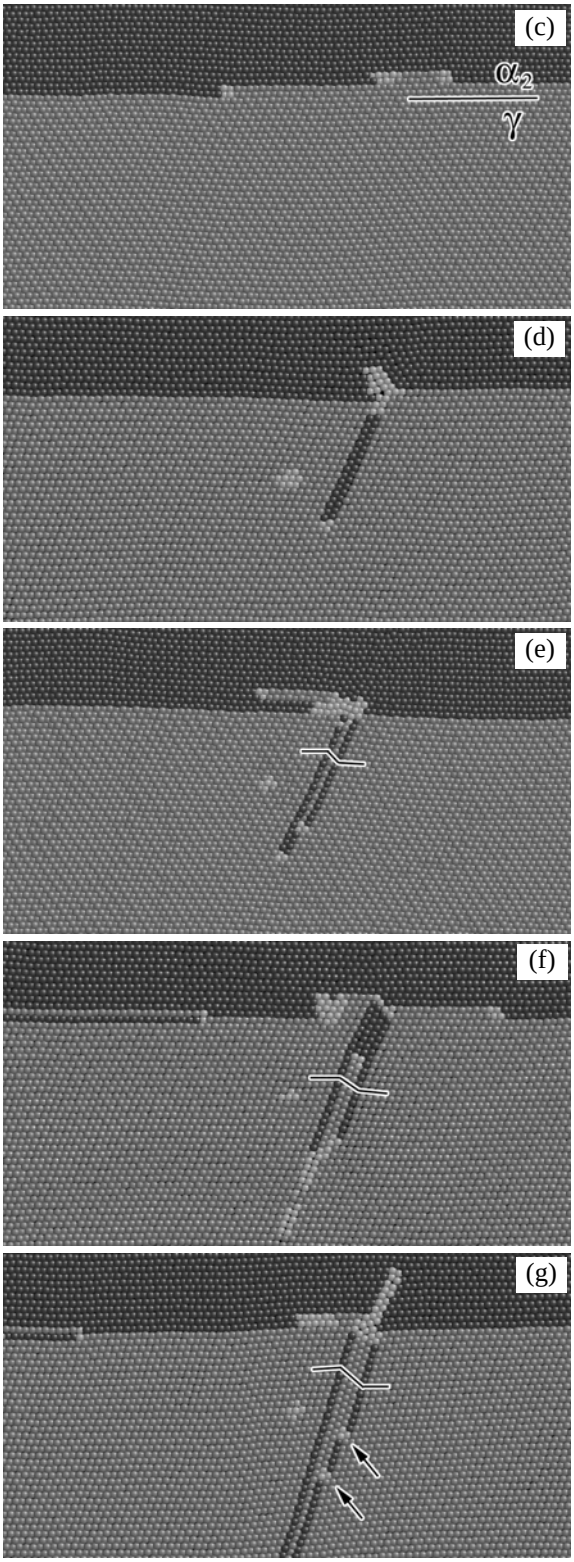

Figure 3: Twin emission from γ-α_2 interface. The dark, dark gray, and light gray spheres represent HCP atoms, FCC atoms, and other atoms, respectively.

phase is the opposite. Consequently, the γ-α_2 interface migrates into the α_2 phase, to reduce the strain energy. The motion of the interface forces the Ti_3Al atoms to arrange in the TiAl structure, and thereby increases the structure energy. The competition of the strain energy reduction and the structure energy increase eventually leads to stabilization of the interface. As shown in Figure 3c, some parts of the interface migrate toward α_2 and others toward γ phase. It is interesting to note that the two neighboring dislocations of the same sign agglomerate. It is worth to point out that, segments advancing into the α_2 lamella have the FCC stacking order and are not the γ phase. The thickness of this dislocation core (the step in the interface) is two atomic layers, consistent with the experimental observation of Hsiung et al (1997). This agglomeration leads to local stress concentration, which in turn triggers dislocation emission into the matrix. Glide systems of large Schmid's factor are readily available on the γ side. Indeed, one part of an interface dislocation emits into the γ phase, as shown in Figure 3d. Taking the γ phase structure as a reference, the interface dislocations have Burgers vectors of $1/6[\bar{1}12]$. The emitted dislocation has a Burgers vector of $1/6[1\bar{1}2]$, which comes from the following dislocation dissociation: $1/6[\bar{1}12]$ → $1/6[1\bar{1}2]$ + $1/3[\bar{1}10]$. As the loading continues, another $1/6[1\bar{1}2]$ dislocation glides on $(1\bar{1}\bar{1})$ with the same mechanism, forming a nucleus of twin (Figure 3e). Once the twin has nucleated, the dislocation component left at the grain boundary is hard to move, as such it blocks the gliding of the other $1/6[\bar{1}12]$ (or $1/6[1\bar{1}\bar{2}]$) interfacial dislocations (Figure 3f). This causes a larger localized stress, and therefore, the twin keeps growing by the successive emission of $1/6[1\bar{1}2]$, as pointed by arrows in Figure 3g.

So far our results have shown that a dislocation free γ-α_2 interface may emit twins. The emission happens by nucleation of dislocation pairs at the interface, and subsequent emission of partial dislocations from interface to the matrix. Continuation of the dynamic loading leads to propagation of the twin across another twin and a γ-α_2 interface.

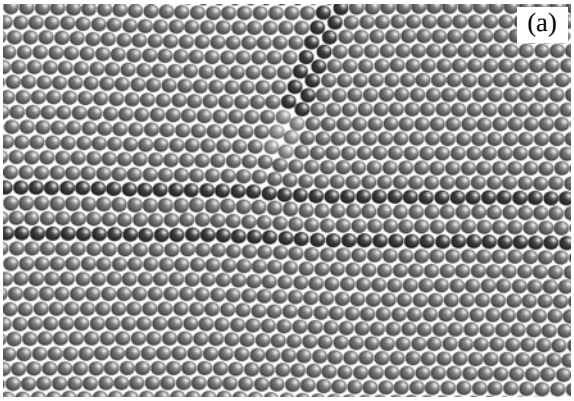

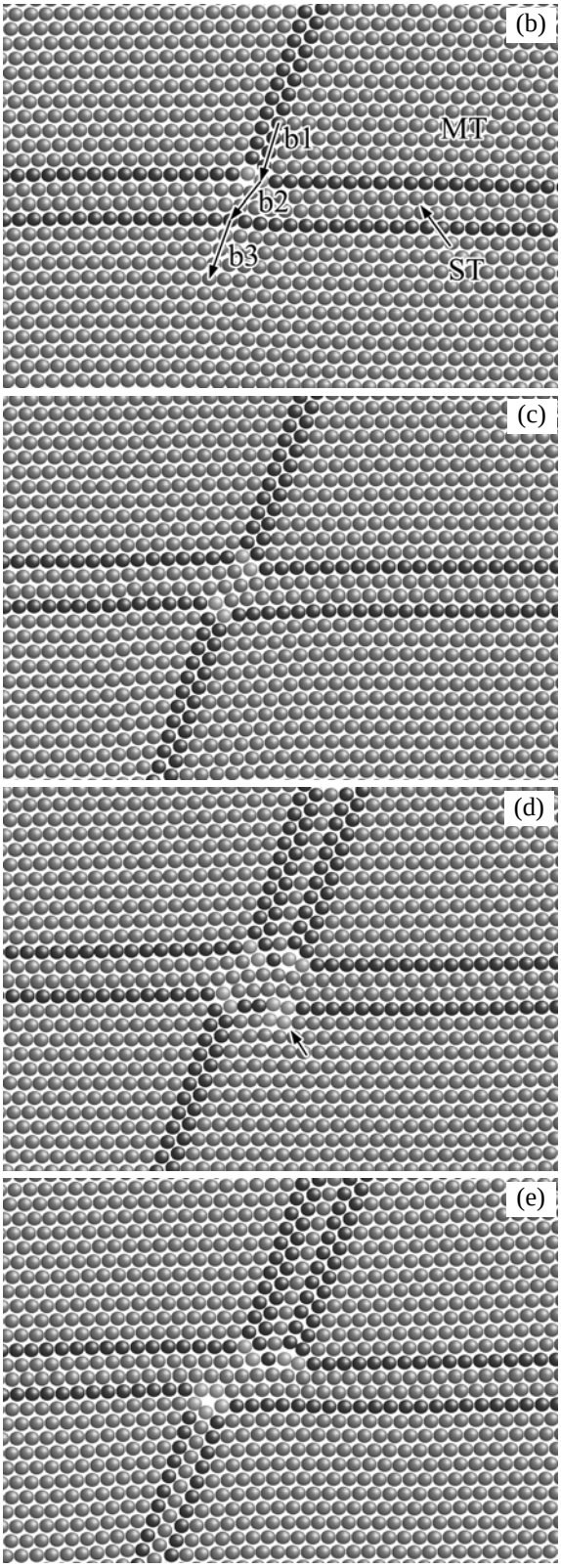

Figure 4: Twin (and partial dislocations) propagation cross a pre-existing twin.

As the load reaches 3.3% compressive strain, the emitted twin propagates toward a pre-existing twin, as shown in Figure 4a. A $1/6[1\bar{1}2]$ partial dislocation leads the propagation of the twin, and it glides on the $(1\bar{1}\bar{1})$ plane. An expanded view of the leading dislocation is shown in Figure 4b. The pre-existing twin ST forms during the initial structure relaxation, and now serves to interact with the newly emitted twin (and the leading partial dislocation). At the twin boundary, the partial dislocation $1/6[1\bar{1}2]$ dissociates into two dislocations $1/6[1\bar{1}4]$ + $1/3[00\bar{1}]$. The second dislocation, with Burgers vector **b2**=$1/6[1\bar{1}4]$, or $1/2[1\bar{1}0]$ in terms of the matrix ST, propagates across the twin (Figure 4b). At the following twin boundary, this dislocation **b2** =$1/6[1\bar{1}4]$ dissociates into two other dislocations, reversely: $1/6[1\bar{1}2]$ +$1/3[001]$. The dislocation, with Burgers vector **b3** = $1/6[1\bar{1}2]$, continues propagating. Crossing the twin, the leading partial dislocation has left behind two dislocations with Burgers vectors $1/3[00\bar{1}]$ and $1/3[001]$ (Figure 4c).

Following the leading partial dislocation is another one that borders the emitted twin. The second partial follows the footstep of the first, and forms a new twin, after passing through the pre-existing twin (Figure 4d). It is cautioned that the quantitative behavior of the second dislocation depends on the thickness of the pre-existing twins, in particular when two $1/6[1\bar{1}2]$ dislocations approach instead of repelling each other (Figure 4e). Therefore, we emphasize the mechanism of first dislocation passing through the pre-existing twin.

n contrast to the easy penetration of a twin boundary, a γ-α_2 interface is more difficult for the twin (and partial dislocations) to propagate across. As the strain reaches 3.5% compression, the partial propagating twin reaches the γ-α_2 interface, shown in Figure 5a. An expanded view near the interface is shown in Figure 5b. The twin is unable to propagate all together across the γ-α_2 interface. Instead, one partial dislocation is bounced back, while another one propagates through. At the interface, the propagating dislocation dissociates into two others according to the following Burgers vector balance: $1/6[1\bar{1}2] \rightarrow 1/24[5\bar{5}14]$ + $1/24[\bar{1}1\bar{6}]$. The dislocation $1/24[5\bar{5}14]$, or $[1\bar{1}02]/4$ in terms of the α_2 matrix, continues propagating into the α_2 phase, while the other dislocation $1/24[\bar{1}1\bar{6}]$ remains at the interface (Figure 5c). Upon the propagation of the leading partial dislocation, the other partial dislocation in the propagating twin also returns to the interface (Figure 5d). However, the front of the leading partial dislocation stops propagating forward into the α_2 phase. Instead, the front dislocation dissociates into two other dislocations, one going back toward the interface, and another parallel to the interface. This branching of the propagation ends the forward propagation of the leading partial dislocation and thereby the propagating twin.

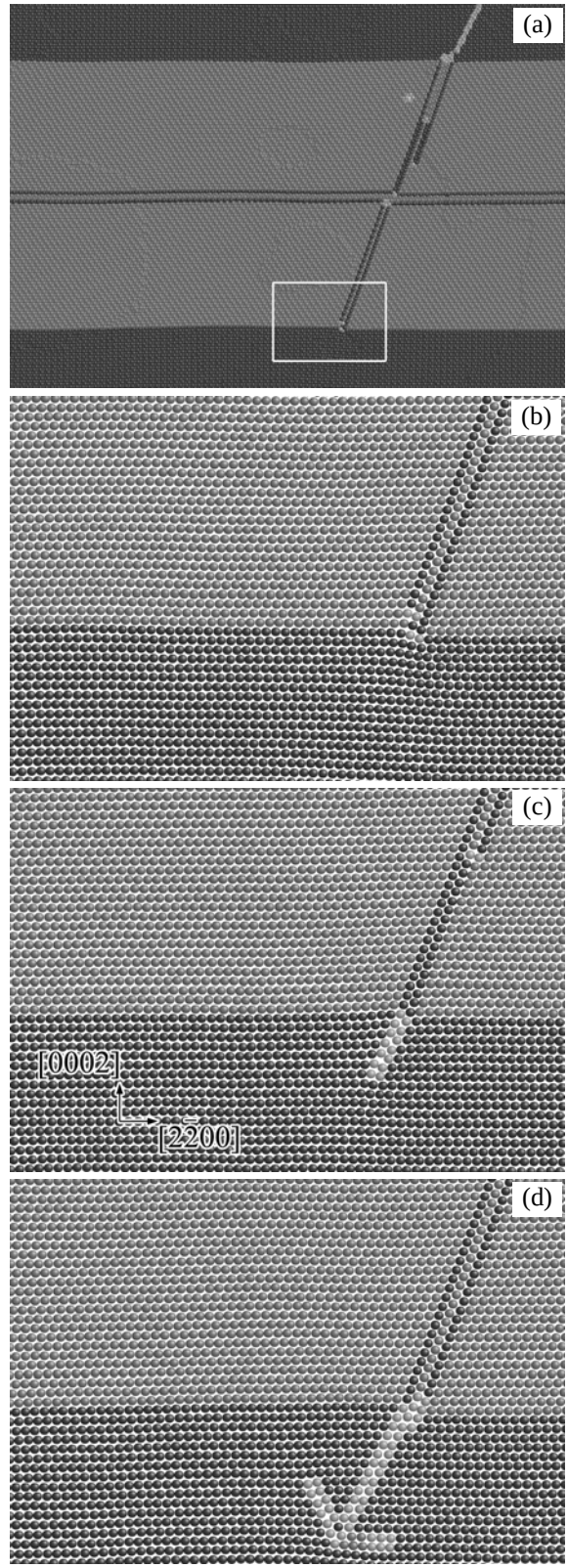

Figure 5: Interaction of the twin with γ/α_2 interface

The results of twin propagation show that it can easily go through another twin in the γ phase, leaving a $1/3[00\bar{1}]$ dislocation at each twin boundary. In contrast, the twin propagation across γ phase is more difficult. This difficulty could lead to potential hardening effects.

Summary

Molecular dynamics simulations have been performed to study the interface deformation of PST TiAl. The results show that:

(1) The structural transformation taken place in the γ/α_2 interface, and therefore the generation of interface dislocations is the another factor except from the dislocation mismatch, that can cause the nucleation and propagation of the deformation twin from the γ/α_2 interface;

(2) Pioneered by a stacking fault crossing over the twin, the type I twin-twin interaction can be happened by the procedures of getting incident 1/6<112] dislocations from one side, then nucleating and growing a twin on the other side.

(3) The incident dislocation from the γ lamella is hard to propagate in the α_2 lamellas. Therefore the α_2 lamellas maybe lead to potential hardening effects.

References:

Appel, F.; **Wagner, R.** (1998): Microstructure and deformation of two-phase gamma-titanium aluminides. *Mater Sci Eng R*, vol.22, pp. 187-268.

Clarke, A. S., Jonsson, H. (1993): Structural-changes accompanying densification of random hard-sphere packings. *Phys Rev E*, vol. 47, pp. 3975-3984.

Farenc, S.; Coujou, A.; Couret, A. (1993): An in-situ study of twin propagation in TiAl. *Philo Mag A*, vol. 67, pp. 127-142

Feng, C. R.; Michel, D. J.; Crowe, C. R. (1989): Twinning in TiAl. *Script Metal*, vol. 23, pp.1135-1140.

Hsiung, L. M.; Nieh, T. G. (1997): The evolution of deformation substructure in a creep deformed full-lamellar TiAl alloy. *Mater Sci Eng A*, vol. 239-240, pp. 438-444.

Hsiung, L. M.; Nieh, T. G.; Choi, B.W.; Wadsworth, J. (2002): Interfacial dislocations and deformation twinning in fully lamellar TiAl. *Mater Sci Eng A*, vol.329, pp.637-643.

Inui, H.; Oh, M. H.; Nakamura, A.; Yamaguchi, M. (1992)**:** Room-temperature tensile deformation of polysynthetically twinned (PST) crystals of TiAl. *Acta Metal Mater*, vol. 40, pp. 3095-3104.

JIN, Z.; BIELER, T. R. (1995): An in-situ observation of mechanical twin nucleation and propagation in TiAl. *Philo Mag A*, vol. 71, pp. 925-947.

Kim, H. Y.; Maruyama, K. (2003): Stability of lamellar microstructure of hard orientated PST crystal of TiAl alloy. *Acta Mater*, Vol. 51, pp. 2191-2204.

Liu, C. T.; Maziasz, P. J. (1998): Microstructural control and mechanical properties of dual-phase TiAl alloys. *Intermetallics*, vol. 6, pp. 653-661.

Liu, C. T.; Schneibel, J. H.; Maziasz, P. J.; Wright, J. L.; Easton, D. S. (1996): Tensile properties and fracture toughness of TiAl alloys with controlled microstructures. *Intermetallics*, vol. 4, pp. 429-440.

Maruyama, K.; Yamamoto, R.; Nakakuki, H.; Fujitsuna, N. (1997): Effects of lamellar spacing, volume fraction and grain size on creep strength of fully lamellar TiAl alloys. *Mater Sci Eng A*, vol. 240, pp. 419-428.

Morris, M. A.; Lipe, T. (1997): Creep deformation of duplex and lamellar TiAl alloys. *Intermetallics*, vol. 5, pp. 329-337.

Parrinello, M.; Rahman, A. (1981): Polymorphic transitions in single-crystals - a new molecular-dynamics method. *J Appl Phys*, vol. 52, pp. 7182-7190.

Parthasarathy, T. A.; Subramanian, P. R.; Mendiratta, M. G.; Dimiduk, D. M. (2000): Phenomenological observations of lamellar orientation effects on the creep behavior of Ti-48at. %Al PST crystals. *Acta Mater*, vol. 48, pp. 541-551.

Wegmann, G.; Suda, T; Maruyama, K. (2000): Deformation characteristics of polysynthetically twinned (PST) crystals during creep at 1150 K. *Intermetallics*, vol. 8, pp. 165-177.

Zhang, J. X.; Ye, H. Q. (2003): The deformation twin in lamellar Ti_3Al/TiAl structure. *Soli Stat Comm*, vol. 126, pp217-221.

Zhang, J.X.; Ye, H. Q. (2001): Twin intersection in a deformed TiAl alloy. *Script Mater*, vol. 45, pp. 133-138.

Zope, R. R.; Mishin, Y. (2003) Interatomic potentials for atomistic simulations of the Ti-Al system. *Phys Rev B*, vol. 68, pp. 024102.

Status of FY 2005 Milestones

Milestone: Investigation of the effects of shock waves on the microstructure and potential delamination of ultrafine TiAl-Ti_3Al laminate materials is on schedule and will be completed and reported in September 2005

Travel

2005 MRS Spring Meeting, San Francisco, CA (3/29 – 4/1, 2005).

Publication

L.M. Hsiung and T.G. Nieh "In-Situ TEM Study of Interface Sliding and Migration in an Ultrafine Lamellar Structure," presented in 2005 MRS Spring Meeting, to be published in MRS conference proceedings.

High Density Infrared Surface Treatment of Materials for Heavy-Duty Vehicles

T. N. Tiegs, D. C. Harper, F. C. Montgomery, and C. A. Blue
Oak Ridge National Laboratory

Objective/Scope

High Density Infrared (HDI) technology is relatively new to the materials processing area and is gradually being exploited in materials processing. For many applications in heavy-duty vehicles, superior properties, such as corrosion and wear resistance, are only required at the material surface. The project using HDI technology will be exploratory and will examine the application of wear-resistant coatings based on hard-metal type compositions.

Technical Highlights

Earlier work had shown that adherent coatings of hardmetal compositions could be applied to a variety of metal substrates (D-2 tool steel, 4140 alloy steel, and cast iron). However, a problem with the earlier coatings was that a preheat step was required to minimize sintering of the slurry coating prior to bonding with the substrate. When the slurry coating was heated too fast, it tended to peel off from the substrate and crack. The preheating step allowed the substrate to get hot enough so bonding occurred.

Samples have been fabricated that use WC and TiC particles only for the coating. The sintering temperature for these plain carbides is significantly higher than the melting point of the substrates. Consequently, because no binder additions (i.e. Ni or Ni_3Al) are present, sintering and cracking will be inhibited. This will allow the coating to heat up to a sufficiently high temperature so that the underlying substrate will melt and be wicked into the coating by capillary action. Previous work has shown that WC-cast iron composites have excellent wear behavior, so these are the initial compositions.

The variables that are being investigated include: coating thickness (50 and 100 µm); WC particle size (2 and 8 µm), and substrate type (cast iron or 4140 steel). The samples have been fabricated and will be IR treated during the next reporting period.

Status of Milestones

On schedule.

Communications/Visits/Travel

None.

Problems Encountered

None.

Publications

None.

High Temperature Aluminum Alloys

Yong-Ching Chen
Cummins Inc.

Objective/Scope

Work at Cummins has identified three potential paths to improve the high temperature strength and fatigue resistance of aluminum casting alloys. These paths have been partially investigated under cooperative agreement DE-FC05-97OR22582. Each path showed some promise and further work is needed to determine the useful applications.

Task 1, Ternary Phase Diagrams

This task involves a ternary phase aluminum alloy utilizing rare earth metals to provide precipitate size control and stability. Limited information on these alloys indicates high temperature strength and stability, however, the predicted cost of the alloy is high. Additional work shall be performed to determine if additional rare earth (or other metal) elements which produce beneficial properties at a reasonable cost. Cummins shall develop ternary phase compositions by means of modeling of the equilibrium phase diagram, castings and evaluating the properties of alloys identified.

Task 2, NASA-Developed Process

This task involves a conventional aluminum alloy, which has been chemically modified by a process developed at NASA-Huntsville. The elevated temperature properties reported by NASA are attractive, but it is preferred for Cummins to use alloy with lower silicon content. Eck Industries purchased the license for the NASA-developed technology on high silicon casting alloy and has expanded the range to include conventional low silicon casting alloys. Limited testing of these modified conventional low silicon alloys at Cummins has not shown the property improvement anticipated. Physical and mechanical property measurements shall be performed on specimens provided by NASA and by Eck to characterize the material and determine the optimal properties possible by this method.

Task 3, Particulate-Reinforced Alloy

This task involves a particulate loaded aluminum alloy patented by Chesapeake Composites Inc. The nano-phase particulate at 50 volume percent provides adequate high-temperature strength in early experiments, however, the particulate loaded alloy could only be forged or squeeze cast so complex shape capability is limited. Cummins shall fully characterize the specimens previously made to determine the mechanical behavior of the alloy. Casting modifications shall also be investigated to determine shape capability for the alloy.

Task 4, Reporting Requirements

Quarterly reports and final reports

Task 5, Quality Assurance Requirements

Technical Highlights

Task 1. Ternary Phase Diagram

Task Summary

The main objective of this task is the employment of ThermoCalc in the prediction of the Al-rich portion of the ternary phase diagram of Al-Y-Yb alloy system. The versatility of the ThermoCalc software had been demonstrated previously with the well-known Al-Fe-Mn ternary system. The binary phase diagram of Al-Yb had also been assessed. In general, a good agreement was found between the model and the standard phase diagram published in the literature.

In the absence of literature data, efforts will be undertaken to carry out several assessment experiments of the following two alloy systems, namely Al-Y and Y-Yb. Upon the completion of the assessment, we will embark on the evaluation of the thermodynamic properties of the alloy systems, which will serve as input to our Thermo-Calc data bank. The master schedule of the program is presented in Table 1. This shows that upon the purchase of the master alloys, the first four months of the study will be used for an intensive assessment of the two alloy systems. The extent of the assessment required may influence the time of completion of the program.

Table 1. Program Master Schedule and Deliverables

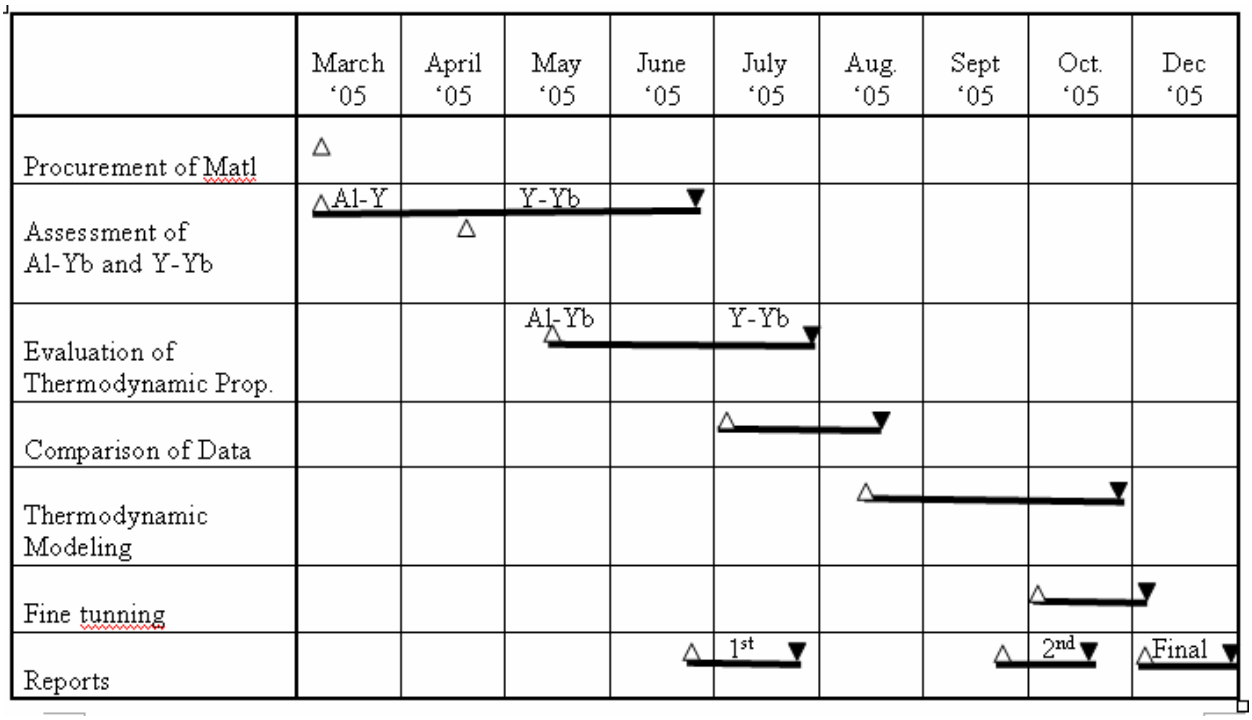

Task 2. NASA-Developed Process

Task Summary

Extensive mechanical tests were conducted on the NASA 388-T5 and T6 alloys. Tests included elevated temperature tensile tests and rotating beam fatigue tests of samples with or without long-term thermal soaking. Test results were compared to those of the current production materials. Slight improvement in the tensile strength was only realized at test temperatures above 300ºC for the NASA 388-T5 alloy as compared to the current materials. The degree of improvement was deemed to be insignificant as compared to the further development needed for the new casting process and prototype trials. The decision was made to discontinue the evaluation work for the NASA 388-T5 alloy for intended application.

The NASA 388-T5 alloy was originally developed for automotive engine components such as pistons to utilize less material, which can lead to reducing part weights, material cost, as well as improving gas mileage and engine durability. The potential application of the NASA 388-T5 alloy in diesel engine pistons was communicated to the piston suppliers. One of the piston suppliers conducted fatigue tests of the NASA 388-T5 alloy and their production aluminum alloy at 350ºC. The NASA 388-T5 alloy exhibited slightly better fatigue strength at 350ºC than the production aluminum alloy. However, the NASA 388-T5 alloy was found to be difficult to cast in diesel piston size without defects. The piston supplier also decided not to pursue the development of NASA 388-T5 alloy in the piston application.

Task 3. Particulate-Reinforced Alloy

Task Summary

This task involves a nano-phase particulate loaded aluminum alloy patented by Chesapeake Composites Inc. A patented, low cost, liquid metal infiltration process is utilized to produce a billet form ready for secondary operations. This composite material combines the enhanced elevated temperature strength, toughness, and ductility of dispersion strengthened (DS) alloys with the stiffness and low CTE of metal matrix composites (MMCs). It was claimed that this composite can be readily turned using WC tooling and drilled and tapped using high-speed steel tools. Potential applications include pistons, compressor wheel, and engine components.

Initial tensile and fatigue tests of 1090 Al and 2024 Al alloy reinforced with nanoscale Al_2O_3 particles (DSC) at elevated temperatures showed impressive results. Almost 100% improvement in tensile strength and yield strength was obtained on the DSC material as compared to those of the current production materials. No degradation in the tensile strength and fatigue strength was observed in the DSC material after 500 hours of thermal soaking at 400ºC.

A potential increase in pressure ratio from turbochargers has been requested by diesel engine manufacturers. To increase pressure ratio means to increase operation temperature of compressor wheels (impellers). Current aluminum alloys used for impellers are being used at their critical temperatures and little chance to further increase their operating temperatures. Titanium alloys are the current solution for higher temperature application, but they extremely expensive for this application. The proposed nano-particle dispersion strengthened aluminum matrix composites show a promise to meet the requirements.

Holset carried out risk assessment in evaluating potential risks associated with the use of DSC material as turbocharger impellers. The following is the list of the potential risks. Figure 1 shows the risk assessment matrix that includes the probability of occurrence of each risk and its impact to customer. The code red risk is that the DSC material may not be able to be machined cost effectively. The counter measure is to conduct machining trials as early as possible in the project.

1. Not machinable cost effectively
2. Production supplier of preform
3. Production supplier of infiltration process
4. Quality of product – defects
5. Cost prohibitive relative to Ti
6. Inadequate mechanical properties at operation temperatures
7. Inadequate fatigue properties at operation temperatures
8. Unacceptable increase in inertia relative to Ti
9. Unacceptable increase in inertia relative to Al

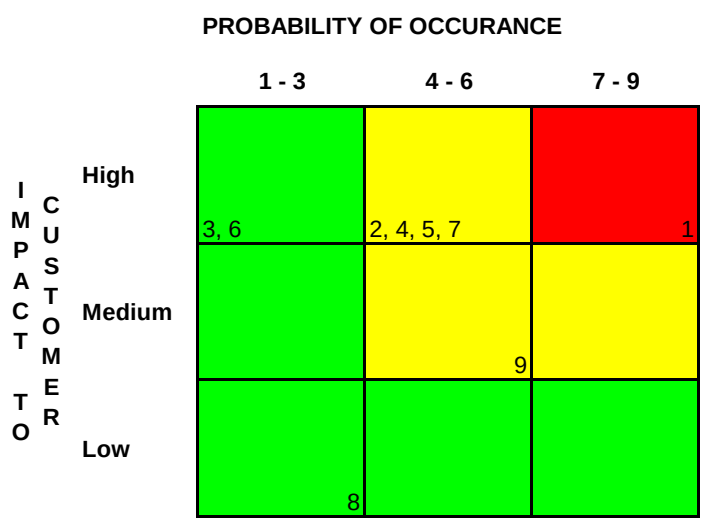

Figure 1. Risk assessment matrix of using DSC as impeller material

In order to further verify that the DSC material exhibit adequate mechanical strength to meet the operation requirements, mechanical and physical properties of DSC materials will be measured. Chesapeake Composites Corporations and PCC-AFT manufactured billets of DSC material with 1.7-in. diameter and 7.0-in. long. The DSC billets contain 40 volume percent of Al_2O_3 nona-particles were infiltrated with 1090 aluminum alloy. Figure 2 shows one of the as-infiltrated DSC billets. Samples will be taken from the billets for testing. The following lists the test plan for this year.

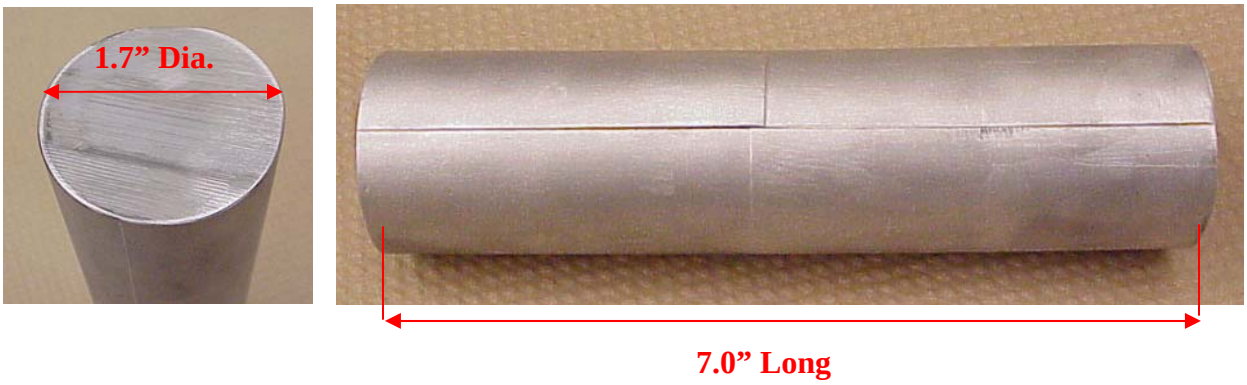

Figure 2. As-infiltrated DSC billets for material property testing

Test plan

Test Type	Responsible	Estimated Completion Date
Residual stress measurements	CTC	2Q
Physical property measurements	CTC	3Q
Notch sensitivity tests	CTC	3Q
Creep tests	CTC	4Q
Machinability study	Holset	3Q
Strain-controlled axial fatigue	Holset	4Q

Overall Summary

1. ThermoCalc is being used to generate the Al-Y-Yb ternary system and to identify optimal compositions for casting trial and material property characterization.
2. NASA 388-T5 alloy did not exhibited significant enough improvement in elevated temperature strength. Decision was made not to continue evaluating this alloy.
3. DSC material exhibited excellent high temperature tensile and fatigue strengths, excellent thermal stability, and good machinability. There is a good potential to be machined into impellers from bar stocks as a half way house to the temperature capability of titanium impeller.
4. Project will move forward in completing material property evaluation on DSC material.

Applications of Titanium Alloys for Heavy-Duty Vehicles

Paul C. Becker
Oak Ridge National Laboratory

In this quarter, the following tasks will be reported on:

1) Ti-6-4 alloy as a replacement for cast iron in diesel engine heads and blocks.
2) Slurry cast process (SLP) for Al alloys for improved fatigue resistance.

Task 1: Explore the use of Ti-6-4 alloy as a replacement for cast iron in diesel engine heads and blocks.

1. An invited presentation was made by Paul C. Becker in Orlando, FL at the Advanced Materials Conference for Military Ship and Ground Vehicles that outlined all of the DOE projects that are concerned with low cost Ti. Among the nine projects described, the project on determining the feasibility of replacing cast iron in diesel heads and blocks with Ti was detailed.

Task 2: Determine if there are fatigue benefits by casting Al parts using the Sub-Liquidus Casting (SLC) process instead the permanent mold process.

1. The cast bars have been made by THT Presses and delivered to Metcut Technology for machining and testing. All of the testing at room temperature has been completed. There appears to be some improvement in fatigue life, about 16%, compared to permanent mold castings at very high cycles, $5x10^7$, compared to permanent mold cast material. However, there was a high degree of scatter in the data. Metallography has shown that the SLC castings are not as porosity-free as expected. This would explain the scatter. The supplier of the castings, THT Presses, has been asked to replace the castings with more sound castings so that the process can be further evaluated.

Mechanical Behavior of Ceramic Materials for Heavy Duty Diesel Engines (Q2-FY05)

A. A. Wereszczak, H. Wang, M. K. Ferber, and M. Lance
Ceramic Science and Technology (CerSaT)
Oak Ridge National Laboratory

Objective/Scope

The application of more ceramic components in engines and transportation systems would be enabled if they could be confidently manufactured and machined faster (i.e., more cost-effectively) and if mechanisms that limit their mechanical performance were understood, predictable, and controlled. This project quantifies "quasi-plasticity/fracture thresholds" in ceramics (e.g., cubic oxides and non-oxides, nanoceramics and nanocermets, piezoelectric ceramics, micaceous ceramics, and traditional structural ceramics) and examines the competing mechanisms that dictate when and how quasi-plasticity or fracture dominates the other during controlled and instrumented static and dynamic indentation and scratch testings. The thorough understanding of the competition of fracture and quasi-plasticity in ceramics will enable improved and faster means of ceramic component manufacturing and surface engineering (e.g., ductile regime machining) and maximize mechanical performance when surface condition (e.g., bending) or when surface-located events (e.g., wear, impact) are service-life-limiters in engine and transportation system components.

Technical Highlights

Static and dynamic indentation hardnesses of Ceralloy 147-31N, NBD200, SN101C, TSN-03NH, and NC132 silicon nitrides were measured as a function of load and their results are respectively shown in Figs. 1-5. An indentation size effect (ISE) and a rate effect are exhibited by all (increased H and greater ISE with rate).

A good fit to the experimental data is often obtained using a formula that Frohlich, *et al* [1] and Li and Bradt [2] attribute to Bernhardt [3]

$$P = a_1 d + a_2 d^2 \qquad (1)$$

where P is indentation load, d is indent diagonal size, and a_1 and a_2 are constants. The a_1 term is relatable to the energy consumed in creating new surfaces [1-2] whereas the a_2 term is relatable to the volume energy of deformation [4]. The determination of those terms for each of the silicon nitrides as a function of rate is shown in Fig. 6. Additionally, a new brittleness parameter is being advocated in this project that involves the ratio of a_2/a_1 because it can provide insight into the competition of those two mechanisms and is under exploration. The brittleness of the five silicon nitrides is shown in Fig. 7, and the relation shows that all five silicon nitrides respond in a less brittle fashion when they were dynamically indented. The machinability of these ceramics as well as other mechanical properties will be examined in reference to this brittleness.

The exploration of the effect of indentation on residual stress generation was initiated using optical fluorescence. An illustration of this is shown in Fig. 8 for a 99.9% alumina that was Knoop indented at 2 kg. A maximum tensile stress of ~100 MPa is observed at the tip of the

cracks that come from the Knoop indent diagonals. Quantification of these effects will enable engineering control of ceramic machining or allowable wear conditions to inhibit or avoid deleterious effects that may be more strongly linked to fracture or quasi-plastic processes or both.

The Hertzian indentation model is continuing to undergo refinements. A 3D model is being explored using "concrete-like" elements that will enable the prescription of strength asymmetry. A tensile strength values will be imputable that will be associated with fracture processes whereas a compressive strength value will be imputable that will be associated with contact-induced quasi-plastic deformation mechanisms.

Instrumented (pendulum) scratch testing continued during the present reporting period. It was observed that scratch indenter life was insufficient using an inexpensive diamond conical dressing tool, so higher quality 90 and 120° tools were purchased from Gilmore Diamond Tool (E. Providence, RI) and their usage is now under evaluation. Familiarity with the operation of the AFM in the Surface Processing and Mechanics Group was gained and is now being used to quantify the scratch sizes. An example of a typical generated scratch in Ceralloy 147-31N is shown in Fig. 9 with the normal and tangential load histories associated with its formation. The energies associated with the scratch formation are undergoing interpretation and scratch performances of the five silicon nitrides will be compared, and ultimately linked to machining performance.

Status of FY 2005 Milestones

Establish dynamic indentation and instrumented scratch testing facilities. Completed.

Communications/Visits/Travel

A. Wereszczak and H. Wang attended the 299th International Conference on Advanced Ceramics and Composites, 23-28 January 2005 in Cocoa Beach, FL. H. Wang gave a presentation entitled "Mechanical Responses of Silicon Nitride Under Dynamic Indentation," and submitted a companion proceedings paper for publication.

A. Wereszczak visited Advanced Engineering Technologies, Atlanta, GA, on 22 Feb 2005 to discuss ANSYS modeling of strength asymmetry in ceramics and its effects during indentation.

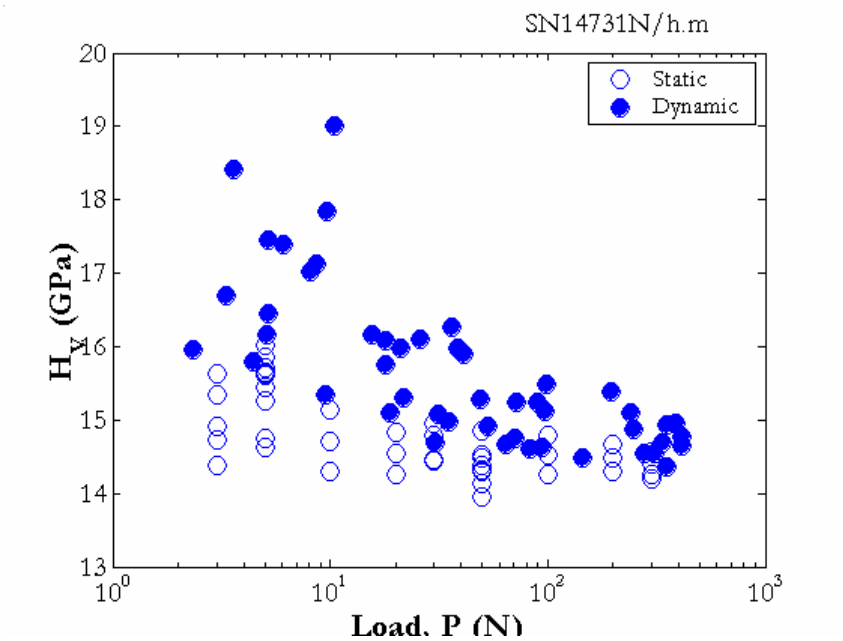

Figure 1. Vickers Hardness for Ceralloy 147-31N Si_3N_4 as a function of load for quasi-static and dynamic indentation.

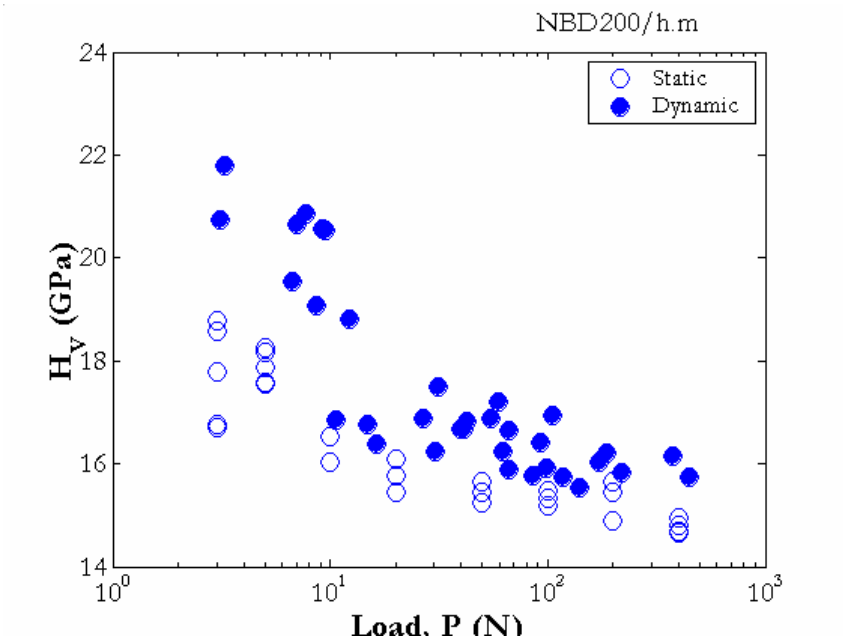

Figure 2. Vickers Hardness for NBD200 Si_3N_4 as a function of load for quasi-static and dynamic indentation.

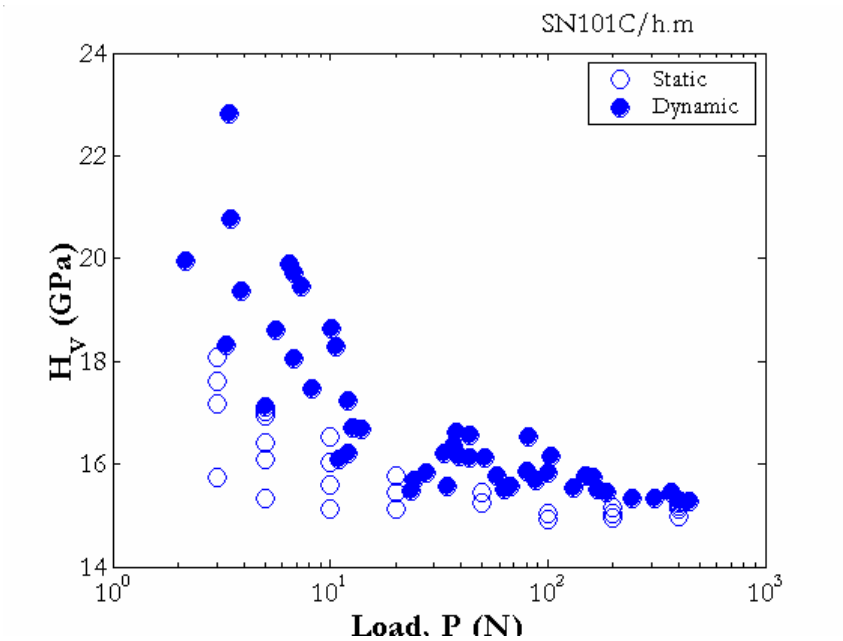

Figure 3. Vickers Hardness for SN101C Si_3N_4 as a function of load for quasi-static and dynamic indentation.

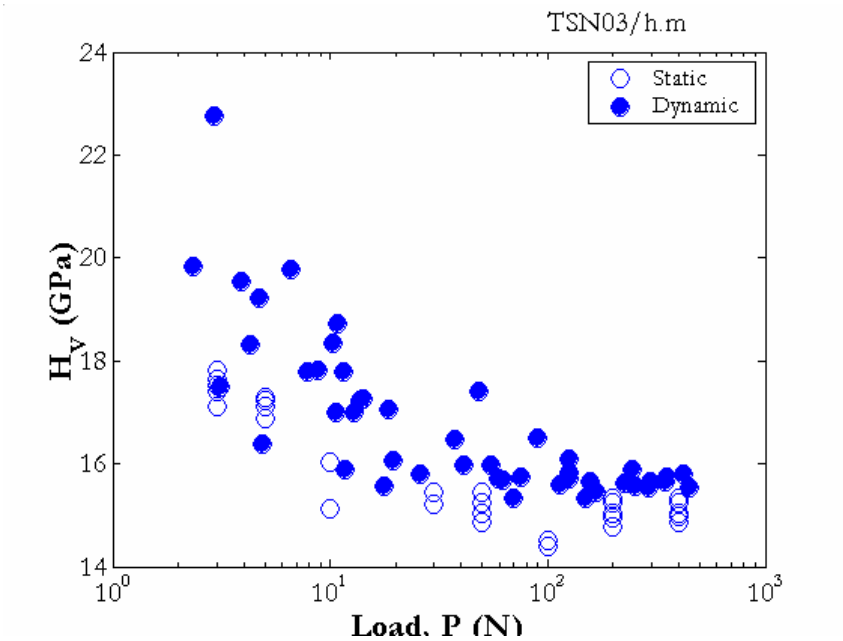

Figure 4. Vickers Hardness for TSN-03NH Si_3N_4 as a function of load for quasi-static and dynamic indentation.

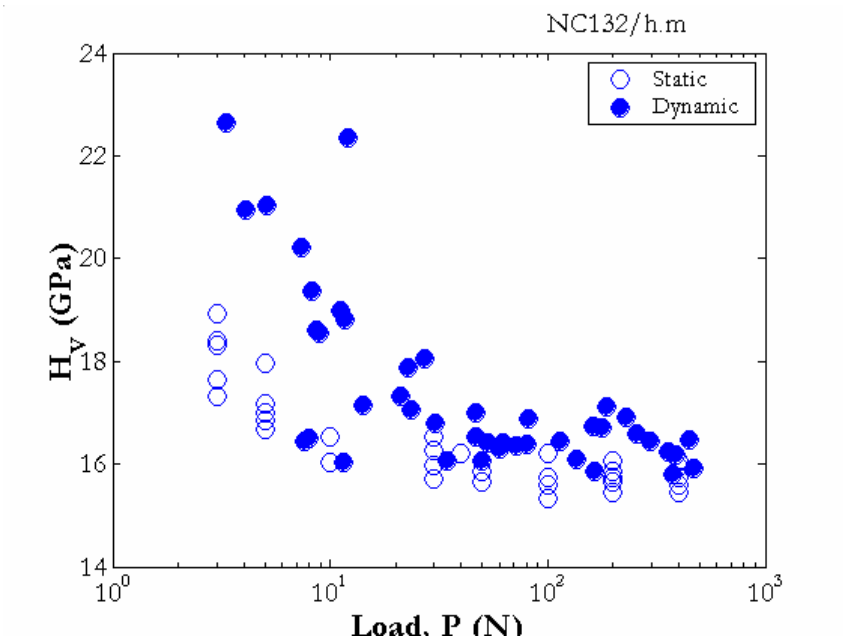

Figure 5. Vickers Hardness for NC132 Si_3N_4 as a function of load for quasi-static and dynamic indentation.

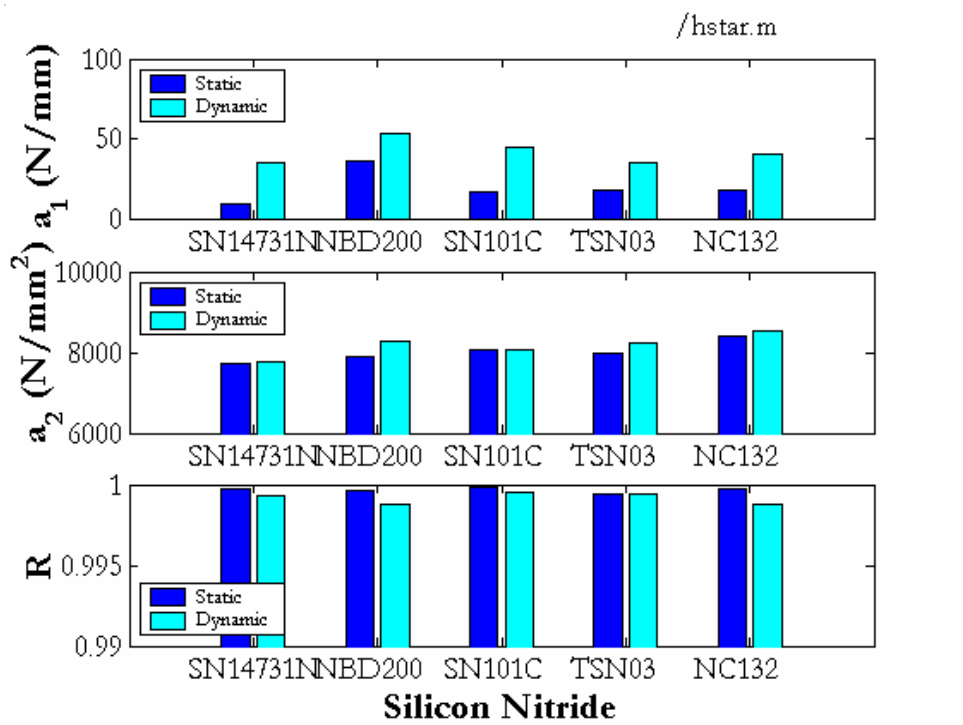

Figure 6. Comparison of a_1 and a_2 terms (see Eq. 1) for the five silicon nitrides when indentation was performed statically and dynamically.

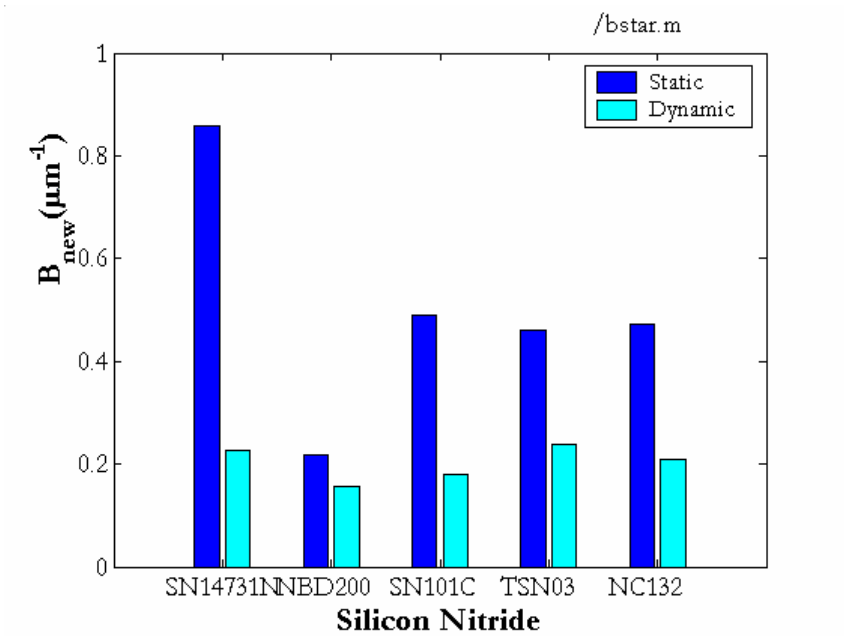

Figure 7. Comparison of a new Brittleness parameter (a_2/a_1) for the five evaluated silicon nitrides for static and dynamic loadings. The trends show that all the grades act less brittle when they were dynamically loaded.

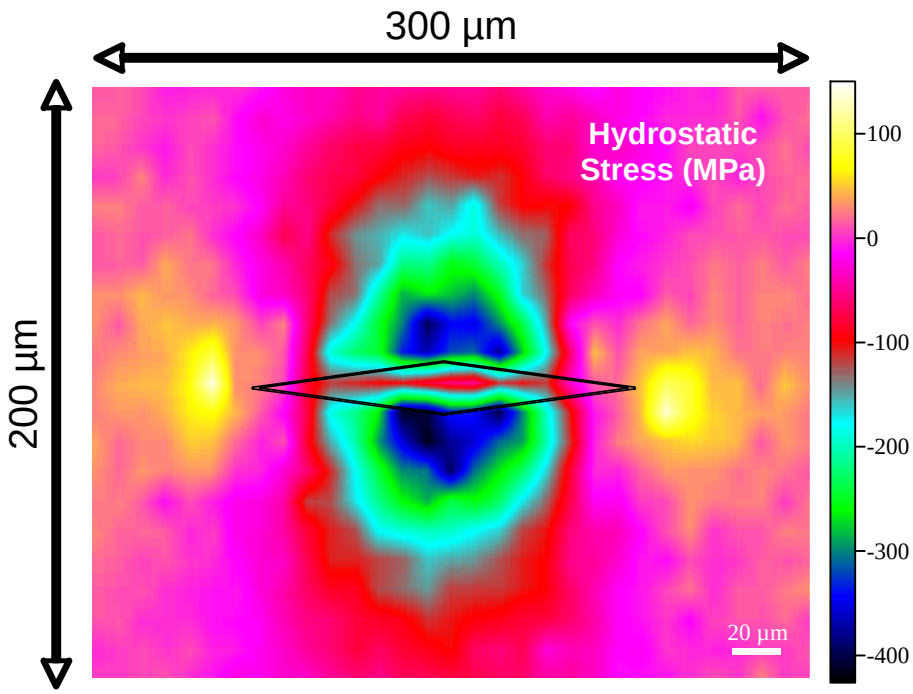

Figure 8. Hydrostatic stress map generated with optical fluorescence about a 2kg Knoop indent in a 99.9% alumina having a ~2-3 µm average grain size.

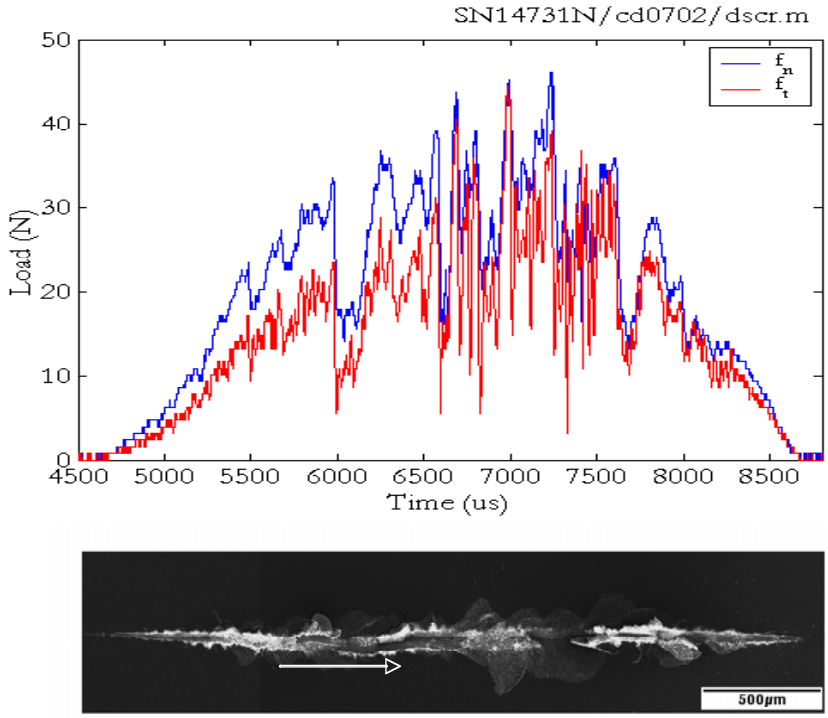

Figure 9. Histories of normal (blue) and tangential (red) forces associated with the scratch test on Ceralloy 147-31N.

Publications

H. Wang and A. A. Wereszczak, "Mechanical Responses of Silicon Nitride Under Dynamic Indentation, to be published in *Ceramic Science and Engineering Science Proceedings*, 2005.

G. Subhash, M. A. Marszalek, A. A. Wereszczak, M. J. Lance, "Scratch Resistance and Residual Stresses in Longitudinally and Transversely Ground Silicon Nitride," to be published in *Ceramic Science and Engineering Science Proceedings*, 2005.

A. A. Wereszczak and T. P. Kirkland, "Exclusivity of Strength-Limiting Intrinsic and Hybrid Flaws," to be published in *Ceramic Science and Engineering Science Proceedings*, 2005.

H. Wang, A. A. Wereszczak, and M. K. Ferber, "Characterization of Dynamic Indentation of Silicon Nitrides by Using Vickers Indentation, in preparation.

References

[1] F. Fröhlich, P. Grau, and W. Grellmann, *Phys. Stat. Sol. (a)*, **42** 79-89 (1977).
[2] H. Li and R. C. Bradt, *J. Non-Crystalline Solids*, **146** 197-212 (1992).
[3] V. E. O. Bernhardt, *Z. Metallkde*, **33** 135-144 (1941).
[4] H. Li, A. Ghosh, Y. H. Han, and R. C. Bradt, J. Mat. Res., **8** 1028-1032 (1993).

Deformation Processes for the Next Generation Ceramics

Paul F. Becher
Oak Ridge National Laboratory

Objective/Scope

This project seeks to determine how to exploit the deformation response of ceramics to enhance mechanical properties and develop novel shape forming with particular emphasis on the impact of nano-scale microstructures. This project involves two major thrusts. The first is a collaborative effort with researchers in the Synthesis of Nanocrystalline Ceramics task at Pennsylvania State University in the processing and sintering of nanocrystalline ceramics. The goal being to develop the technology to form "green" (unfired) bodies of nanocrystalline particles with densities well in excess of 50% of the theoretical density to allow one to devise pressureless sintering profiles to produce dense monolithic bodies with grain sizes < 100 nm [1]. This is aimed at finding approaches to produce sizeable monolithic bodies for subsequent evaluation. The second thrust focuses on the mechanical and wear behavior of nanocrystalline ceramics and the influence of external parameters (e.g., stressing rate, temperature, environment (e.g., air, vacuum), and electric fields (in collaboration with researchers at North Carolina State University) on the plastic deformation behavior.

Technical Highlight

In order to shape forming by plastic deformation in nanocrystalline ceramics, the yield stress of zirconia ceramics as a function of temperature and stressing rates is being evaluated for two different yttria solute contents and grain sizes. This data will serve as the baseline for assessing enhanced deformation that can be achieved in sub-100 nm grain size ceramics. As expected, a strong reduction in yield stress occurs as the temperature increases and/or the stressing rate decreases, Figure 1a. Based on the data in Figure 1b, the effects of increased yttria content and increased grain size are minimal in this temperature range; however, additional data are needed to confirm this.

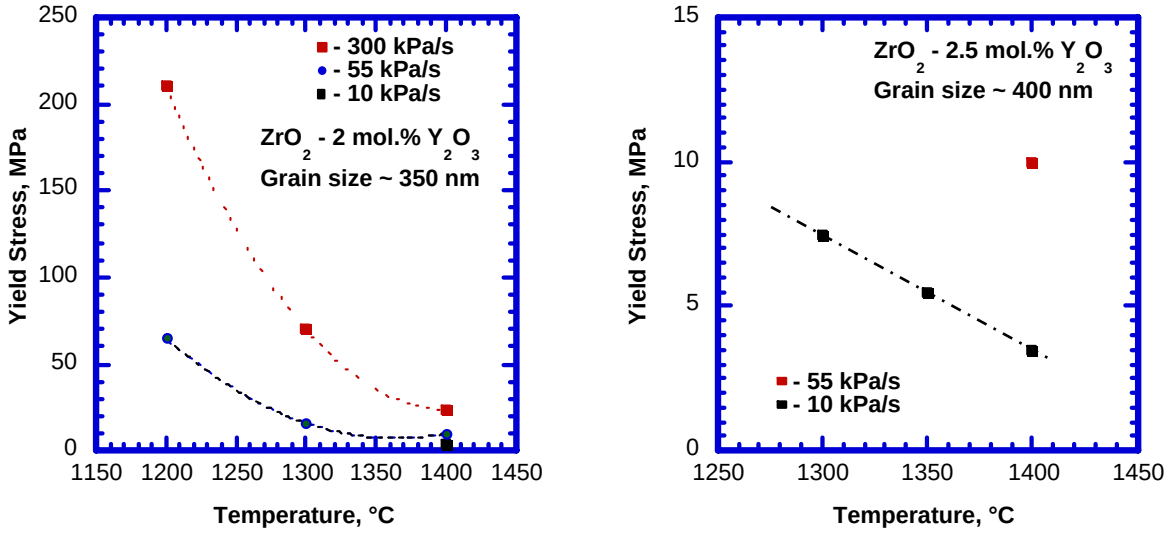

(a) (b)

Figure 1. Temperature and stressing rate dependence of yield stress of nanocrystalline zirconia ceramics.

Status of Milestones
New project

Communications/Visits/Travel
Discussions held with (1) Prof. Adair, Pennsylvania State University, on processing of nanocrystalline zirconia and with Dr. Richard Schorr (MetaMateria) on evaluating nanocrystalline oxides during the American Ceramic Society meeting in April. Prof. Adair also presented results on processing and sintering of nanocrystalline zirconia ceramics at the American Ceramic Society meeting.

Subtask with Prof. Hans Conrad, North Carolina State University, on electric field effects was extended through CY 2005.

Publications
*C. H. Hsueh and P. F. Becher, "Effects of Dopant Segregation on Lattice-Diffusional Creep of Nanocrystalline Ceramics," Phys. Rev. B, 71, 014115–1 to –7 (2005).

_____
* Study was jointly sponsored with U. S. Department of Energy, Office of Basic Energy Sciences, Division of Materials Science and Engineering.

High Speed Machining of Titanium Project

Rahul Aphale
Third Wave Systems, Inc.

Objective/Scope

Develop Drilling Model for Solid Tools-

Development of Drilling modeling capability continued for the months of January 05 through March 05. Specifications were defined for the developing steady state and exit state stage modeling. Development activity also continued in drilling modeling with modifications to adaptive meshing and contact algorithms for overall performance and robustness improvements. Benchmark simulations were performed at Third Wave Systems.

Technical Highlights

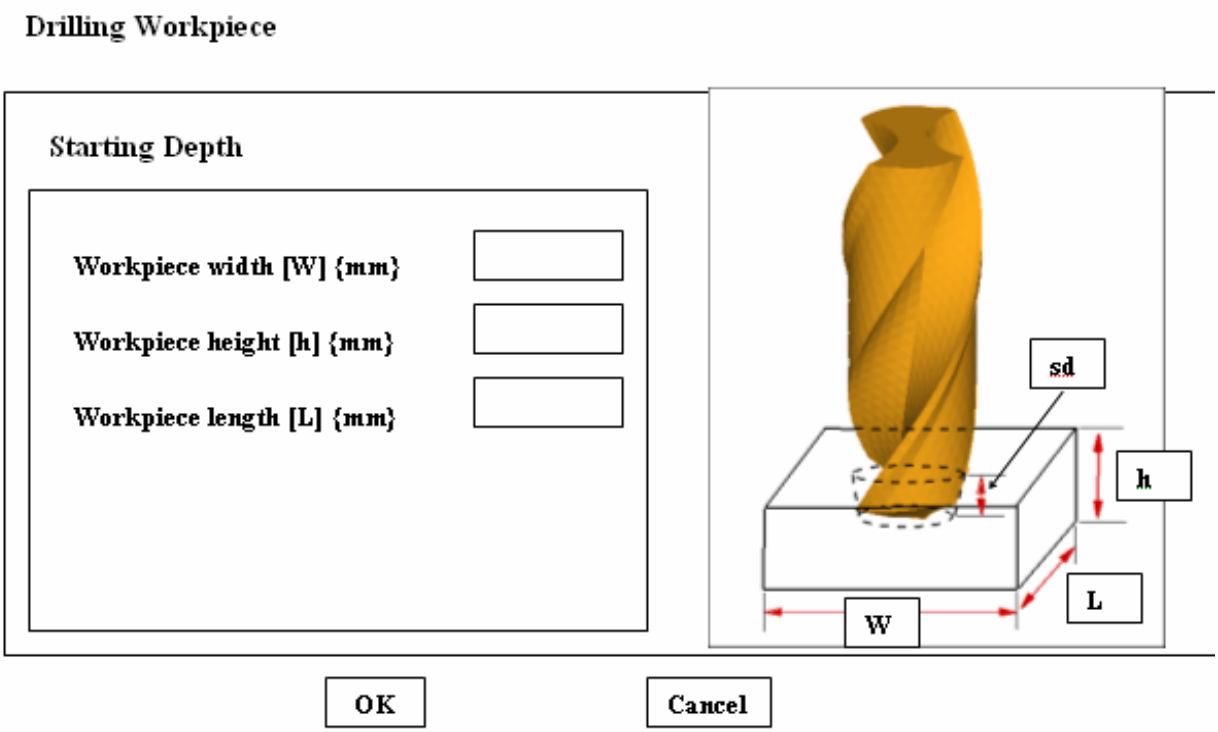

Figure 1. User interface for modeling steady state stage drilling

In order to develop steady state stage and exit state stage modeling cabalilities, specifications were defined. Figure 1 shows user interface to be developed for the steady state state modeling. User needs to specify the starting position of the drill into the workpiece and model will generate a workpiece with a predrilled hole and place the drill at the bottom of the hole as its starting position. Primary benefit from steady state modeling is an ability to get force and torque results quickly as the drill starts from the predrilled hole. This also helps in reducing computational time. Figure 2 shows user interface to be developed for the exit state stage modeling. In this scenario, user would provide distance from the bottom of the workpiece where drill would be

placed. Main objective of this feature would be the analyze drill exit from the workpiece and burr formation during the exit.

Development of the drilling model continued with with modifications to adaptive meshing, contact algorithms for overall performance and robustness improvements. Various simulations were setup and performed for comparing computational times between previous release and new release. Figure 3 shows corresponding performance improvement in AdvantEdge 4.6 Beta.

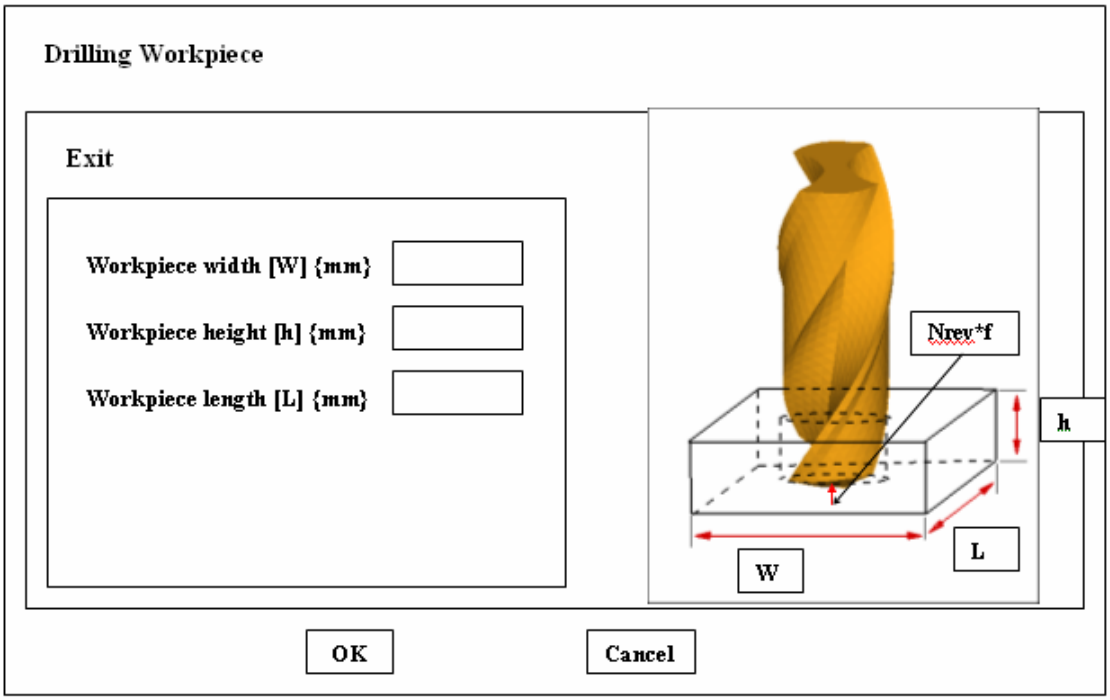

Figure 2. User interface for modeling exit state stage drilling

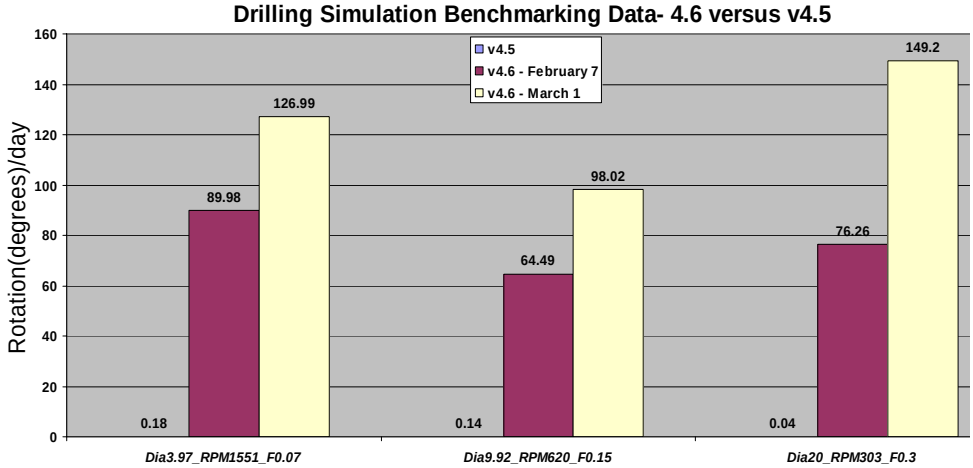

Figure 3. Performance improvement in drilling between previous release and 4.6 Beta

Status of FY 2005 Milestones
Development of Drilling Model is in process on schedule as per Milestone for FY 2005.

Communications/Visits/Travel
Project status updates were provided to Dr.Jun Qu via email and telephone conference. Group meeting for project particants is scheduled on May 6th in Dearborn, Michigan.

Publications
None.

References
None.

Synthesis of Nanocrystalline Ceramics

James H. Adair
Pennsylvania State University

Objective

Advanced particle processing will be used to produce dense, bulk nanocrystalline oxide ceramics. Two routes to obtaining well-dispersed powders (i.e., comminution and colloidal processing) will be emphasized. The large surface areas of such powders lead to large quantities of adsorbates, which must be removed both to enhance particle packing and subsequent sintering. Both reactive atmosphere and microwave thermolysis have merit and will be evaluated to eliminate adsorbates at low temperatures. This project will scale-up the processes to be able to produce dense YSZ ceramics with grain sizes less than 100 nm having sample dimensions ≥ 25mm in diameter by ≥3 mm in thickness to be delivered to ORNL for further testing. Additional effort will focus on fabrication of said samples with grain sizes < 50 nm for testing by ORNL staff.

Background

Particle processing has the potential to produce dense, bulk nanocrystalline materials with a variety of chemical compositions and architectures including composite materials. Outstanding challenges in particle processing to form bulk, dense nanograin sized materials include the dispersion of the nanosize particles and control of gas evolution from the very high surface area compacts during sintering. Typically, nanometer size particulates suffer from a high degree of agglomeration, which results in poor particle packing (green densities < 40% of theoretical) and inhibits sintering and promotes undesirable grain growth. Two routes to obtaining well-dispersed powders include comminution and colloidal processing. Recent advances in colloidal processing have obtained high green densities (>50% of theoretical) with 8 nm YSZ particulates, which preliminary sintering efforts resulted in a translucent, fully dense 45 nm grain sized ceramic. Finally, gas evolution during sintering can occur due to the very high surface areas of nanoparticulate green bodies and disrupt sintering processes. While the thermodynamics and kinetics in the gas phase evolution reactions are reasonably well established, the fundamental science and engineering aspects must be addressed for each nanoparticulate system. Recent considerations indicate that innovative gas phase treatments (e.g., injection of reactive gases during the sintering cycle) can be used to overcome the undesirable effects of evolution gases from the nanoparticulate bodies during sintering.

Status

The focus of research during the past quarter has been the preparation and drying of filter-pressed and dry-pressed zirconia pellets. Drying of pellets filter-pressed from aqueous suspension has proven to be difficult. To date, all pellets have cracked during or before drying, most likely due to differential drying during handling or humidity-controlled drying. In order to correct this issue, several attempts have been made to filter-press nano-zirconia suspended in ethanol. The pellets recovered from these experiments dry quickly and are fragile; however, several whole pellets have been recovered. More samples will be made using this protocol and used in sintering studies.

Several experiments have been conducted to evaluate the alternative of dry-pressing nano-zirconia synthesized with the current protocol. It has been found that, when oxalate-washed zirconia is pan-dried from aqueous suspension, excess oxalic acid from solution crystallizes between particles, forming hard aggregates that do not easily deform under load. Pellets pressed from oxalate-washed zirconia were brittle and had low green strength. It was proposed that bicine may act as a binder if left in the dry powder. It has also been proposed that, during drying from aqueous suspension, compressive capillary forces between nano-particles form very strong aggregates. Therefore, several suspensions were washed with an aqueous bicine solution, instead of oxalic acid, and transferred into ethanol, which produces much weaker capillary forces during drying. Compaction curves of powders washed with bicine and dried from ethanol show a more typical behavior, with aggregate breakdown occurring at around 5000-10,000 psi. Bicine-washed pellets pressed as high as 50,000 psi retained its green shape, whereas oxalate-washed pellets cracked upon die removal.

Efforts are now being made to produce samples, both by filter-pressing and dry-pressing, using these new protocols for sintering studies.

Patents

None to report.

Publications/Presentations

None to report.

Development of Titanium Alloys for Heavy-Duty Diesel Engines

Nan Yang, Jeremy S. Trethewey, Mike J. Pollard, Jesus Chapa-Cabrera, John A. Grassi
Caterpillar Inc.

Introduction

The present cost of producing titanium has significantly decreased, and the forecast is for the decreasing trend to continue, making titanium alloys an attractive alternative to other strong, lightweight materials. Turbochargers on diesel engines play an integral role in meeting emission regulations and controlling fuel economy. Caterpillar Inc. has introduced the use of two turbocharger systems on some on-highway diesel engines in order to meet current and future emission regulations. The presence of two turbocharger systems challenges the already limited under-hood space for on-highway truck applications. Therefore, the development of an alternative turbocharger system that is smaller and lightweight is of great interest.

Project Objectives

The purpose of this program is to develop one or more heavy-duty diesel engine components using titanium alloys. The chosen engine components must demonstrate an improvement in fuel efficiency while reducing emissions. Caterpillar has selected the turbocharger wheel as an engine component to be fabricated from titanium aluminide (TiAl). In addition, Caterpillar has patented a new compact design for the turbocharger known as the HEAT™ (High Efficiency Advanced Turbocharger) that will utilize the TiAl turbo wheel. The HEAT™ consists of two compressor wheels and one turbine wheel attached to the same driveshaft. One compressor wheel is made from an aluminum alloy while the second compressor wheel is made of Ti-6V-4Al.

In order for the HEAT™ to meet the performance specifications of two turbocharger systems, a high strength, lightweight turbo wheel must be developed, which is the primary objective of this project. Thus, lightweight titanium materials (e.g. TiAl) are among the critical technologies for the successful development of this new turbocharger design that will meet transient emission regulations while improving the engine's fuel efficiency and responsiveness in various applications.

Approach

An interdisciplinary team has been organized at Caterpillar to develop the TiAl turbine wheel. Staff members from the Advanced Materials Technology (AMT) lead and manage the project development efforts. Experts from the Large Engine Center (LEC) Air Systems division work with Engine Research to design and bench test the turbo wheel. Manufacturing and process engineers from the Mossville Engine Center (MEC) work with machining experts at the Advanced Production Technologies to develop a cost competitive manufacturing implementation plan.

Quarter Summary

Supplier Readiness

The Advanced Materials Technology (AMT) team continues meeting frequently with suppliers to ensure manufacturing readiness for providing the TiAl turbine wheels with required quality. A batch of gas stand quality turbine wheels (TCT500) for the C175 engine has been received from Supplier A. Also, a second order consisting of full sized wheels and two different sized specimen bars have been cast and are currently being heat treated. These samples are due by the end of this reporting period. The AMT team is also working with Supplier B for the casting trials of larger size turbine wheels.

Materials Characterization

Mechanical tensile testing at room and elevated temperatures have been completed for the materials from Supplier B. The results are currently being analyzed. The materials from Supplier A will be tested at the same test house once they are received. A summary of the tensile testing results of the materials from Suppliers A and B will then be incorporated into the next quarterly report. A creep testing matrix has been developed along with a plan to measure the creep activation energy and establish the creep mechanism map. A proposal for this work has been submitted to HTML. Specimens for physical properties measurement are currently being machined. Thermomechanical fatigue (TMF) testing conditions are currently being established based on field data from the turbocharger supplier.

Foreign Object Damage (FOD) Testing

A primary concern for designing turbine wheels from materials with limited ductility is the susceptibility to foreign object damage (FOD). To address this concern, a FOD test plan has been established and a test house has been selected. This testing will provide data on the FOD resilience of various designs of turbine wheels. Eight wheel categories will be tested; they will vary with respect to material (TiAl, Inconel 713C), model type (“300”, “500”) and geometry (blade thickness). An investigation of the change in the fatigue response of the material after FOD is out of scope for this round of the testing. As such, particular attention will be paid to the failure mode of catastrophic damage (e.g., blow-out, penetration, reverse-side damage). The results of this test will be in the format of a deformation map as seen in Figure 1. Results on the eight variations of turbine wheels will be obtained by 3Q05.

Joining

The initiation of cracks during joining has been one of the main technical challenges in the project. The team has identified the critical process parameters that cause thermal stresses leading to cracking. Through intensive finite element analysis (FEA) and simulation, we have also acquired a general understanding of the correlation between the critical parameters and the thermal stresses during the joining process.

The simulations are carried out using FEA software based on a thermal mechanical model. Temperature profile, stress components and strain components (deformation) are output from the simulation (an example is shown in Figure.2). These outputs are then correlated with the inputs including the critical factors. Based on these results, we determined that the geometry effect on the thermal stress needs to be optimized. Minimization of thermal stresses will be completed

through experimental trials on full-sized wheels. The optimization will be realized as the process controls are incorporated. Optimizing the control of other critical factors to minimize the thermal stresses needs to be completed through experimental trials defined by the output obtained from the simulations.

A modification of the joining apparatus that incorporates the necessary process controls has been designed to minimize thermal stresses. The parts for this design have been ordered and will be assembled before the next iteration of joining trials in the next reporting quarter. Titanium bars have been purchased together with TiAl wheels currently being machined for the next iteration of welding trials.

A design of experiments (DOE) for the next iteration of welding trials will use metallurgical information obtained from previous welding trials. The microstructures of previously welded joints are currently being documented. The investigation results will be correlated with the local cooling rate/temperature gradient obtained through the FEA simulations. This correlation will represent an additional parameter for the DOE besides the considerations for minimizing thermal stresses.

Brazing

Preliminary trials have been performed to determine the feasibility of brazing TiAl to 4140 steel using Ni-based brazing alloys. Current commercially available processes use alloys that tend to form brittle intermetallics within the bond thus limiting the strength. This includes the formation of borides, which are found when high boron braze metals are used. Preliminary trials were performed using a boron-free Ni-Cr-Si alloy (BNi-5) to bond TiAl to steel. Tensile specimens (half dog bone) of TiAl and steel were brazed together using an Instron unit to hold the joint tight in compression. Brazing trials were conducted within an environmental chamber used to create a vacuum and using induction heating to the joint only. Immediately upon cooling, the joint was pulled in tension in the same setup. The use of BNi-5 has shown a minor improvement in strength compared to BNi-2 foil based on a limited number of trials. The BNi-5 is not available in foil form, so braze tape with a binder was used. It has been observed that the binder cannot be completely removed, leaving a significant amount of carbon at the interface to potentially form carbides. Future trials will focus on using a binder-free form of BNi-5 to achieve bond strength at or above the base metal (TiAl) strength.

Outline of Future Work

Modification of the welding facilities to incorporate process control will be assembled and tested in the beginning of next quarter (Apr-Jun). A design of experiments (DOE) of the next iteration of welding trials will be completed with the objective of completing the development of a robust joint. Upon receiving the materials from Supplier A, TMF and creep testing will start in the next quarter. Physical properties measurement will be completed in the next reporting period.

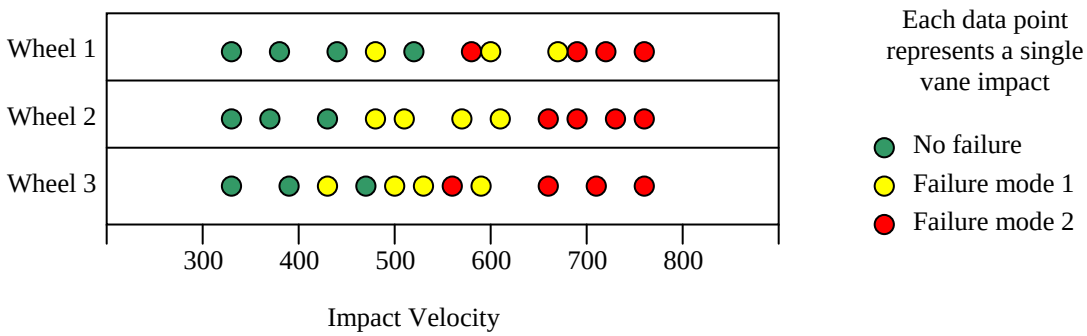

Figure 1. Hypothetical deformation map of FOD damage on three different turbine wheel designs.

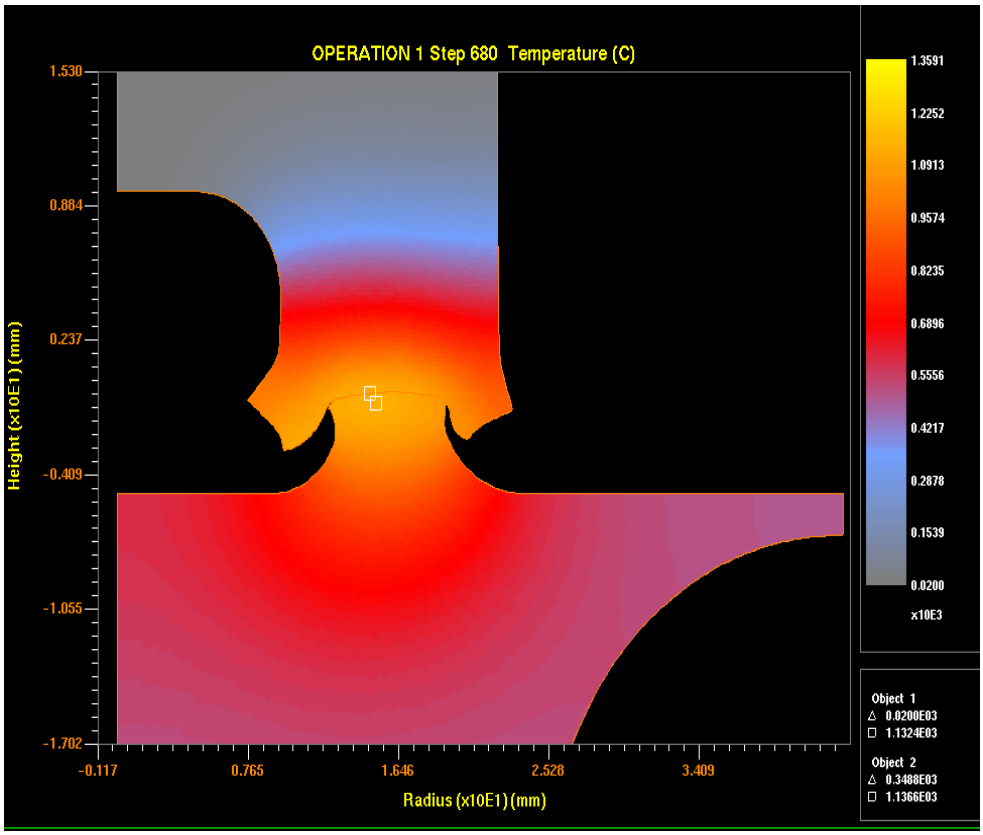

Figure 2. A temperature profile at the beginning of the forging stage obtained through simulation using a thermal mechanical model. The simulation was carried out for the friction and forging stages of the joining process.

Rolling Contact Fatigue

A. A. Wereszczak and T. P. Kirkland
Ceramic Science and Technology (CerSAT)
Oak Ridge National Laboratory

Objective/Scope

The understanding and control of contact damage behavior of ceramics under rolling and sliding conditions are enablers to more widespread utilization of ceramics as cam followers, valves, valve seats, and other important transportation-related components. International interest exists to understand the fundamentals of rolling contact fatigue (RCF) of ceramics because greater control (or minimization) of RCF will result in longer life of such components. Rolling contact fatigue is internationally studied through a variety of test methods and analytical approaches; interest exists in the present project to link their measured performances. Toward that, RCF studies (primarily of Si_3N_4) involving both international and domestic interactions are being pursued as Annex III of the International Energy Agency (IEA) agreement.

Technical Highlights

Perhaps the most important goal of this project is to link RCF performance to ceramic microstructure and any machining-induced sub-surface damage that resulted from the finished ball manufacturing. Quinn, *et al.*, [1] did this for flexure strength tested cylinders and it is desirable to attempt to understand the same relationship for ceramic spheres used (or under consideration for use) in roller elements and hybrid bearings. Fractography of the Ceralloy 147-31N Si_3N_4 RCF, rotary bend strength (RBS), half-RBS, and ASTM C1161B test specimens will certainly aid that endeavor; however, because none of those geometries are spheres, uncertainty will always exist that the resulting sub-surface damage that resulted from their production is not exactly the same that exists in machined spheres. As a consequence, there is strong desire to be able to "strength test" existing finished ceramic balls in a manner that high tensile stresses are produced at the sphere surface and cause fracture of the sphere.

A primary reason why such "sphere strength" testing has not been routinely conducted before is the fact that causing the fracture of a whole ceramic sphere and quantifying a strength value associated with that is not a trivial endeavor. It is tempting to diametrally compress a whole a sphere with parallel, flat platens or even using two other ceramic spheres; however, in these cases, the generated Hertzian stress field can be high enough to cause localized cracking or localized spalling or even crushing, but fracture of the whole sphere will not be the result. Attempting to study any machining-induced sub-surface damage is greatly hindered (if not impossible outright) by the contact-induced damage and the relatively complicated and highly compressive stress state that existed when that damage was produced.

In attempt to circumvent these meddlesome problems, a new specimen geometry is undergoing development in this project whose fracture will be the result of a high tensile stress being generated at the outer surface of a ceramic sphere (and in the absence of complicating high compressive stresses) and whose fracture will readily facilitate the characterization of machining-induced sub-surface damage. This is an intriguing prospect because that will in turn facilitate the study and interpretation of how that sub-surface damage affects RCF performance. The new specimen geometry is being called a "C-sphere" because of its analogousness to the

used “C-ring” specimen geometry. A schematic of a C-sphere undergoing compressive loading is shown in Fig. 1. If the specimen geometry is designed properly, then the produced fracture will initiate at the sphere’s outer surface at a maximum tensile stress that is linkable to the sub-surface damage located there.

Different C-sphere geometries were considered for a 12.7-mm diameter ceramic sphere. An acceptable geometry was one that would produce a very high likelihood of fracture being initiated at the outer-fiber location shown in Fig. 1. Slot thickness (3.175 and 6.35 mm) and slot depth (designated as no offset, a 0.25-mm offset, and a 0.635-mm offset) were considered. The 6.35-mm-thick slot produced ~5x higher outer fiber tensile stress than a 3.175-mm-thick slot for the same slot depth and compressive load, so further consideration of the 3.175-mm-thick slot did not occur. Slot depth was then examined using a 6.35-mm-thick slot and the three considered cases are shown in Fig. 2. The “no offset” case is when the origin of the slot’s 3.175-mm radius is coincident with the center of the sphere. The two other cases (0.25 and 0.635 mm) shown in Fig. 2 represent additional slot depths beyond that “no offset” case. For the same compressive load, the outer fiber tensile stress is larger as the slot depth is increased, see Fig. 3. As an example, if a stress of 1000 MPa was needed to initiate fracture in the sphere, then ~1600N, ~1200, and ~700N of compressive loads would be needed with the “no-offset”, 0.25-mm offset, and 0.635-mm offset specimen, respectively. Though fracture would indeed be caused in each case, causing fracture at the lowest load is more desirable because there will be less stored energy in the specimen at fracture and there is a lower propensity for secondary fractures and a consequential lower likelihood of problems created from collateral damage from impacting fragments. An oblique view of the ¼ model geometry and the outer fiber stress field are shown in Fig. 4

As a consequence of this analysis, a 0.635-mm offset, 6.35-thick slotted C-sphere specimen was selected from the evaluated C-sphere candidate geometries. NBD200 and SN101C balls were sent to a commercial ceramic machine shop to fabricate the C-sphere geometry. They will be fractured afterward and fractography will be performed to link measured strength to flaw size and sub-surface damage. Additionally, the effective area and effective volume (both as a function of Weibull modulus) of the C-sphere geometry will be determined using CARES.

The first of four-machined ball sets were received (second listing in Table I & see Fig. 5) from PremaTech Chand, and receipt of the other three sets are expected early in Q3. This larger diameter will be used by Bournemouth University to reduced to a 12.7-mm diameter using an internally developed lapping procedure that will essentially yield a fourth finish condition. The 13.2-mm balls were forwarded to Prof. Mark Hadfield at Bournemouth University.

Table I. Grinding Conditions for Silicon Nitride Spheres.

Diameter & Finish	Step	Wheel	Removal	Removal per pass
12.7 mm / 0.500" Coarse	1 (roughing) 2 (induce damage) 3 (finishing)	accepted practice 100 grit 600 grit	 0.004” 0.0005”	0.001” 0.001” 0.0001”
13.2 mm / 0.520" Coarse	1 (roughing) 2 (induce damage) 3 (finishing)	accepted practice 100 grit 600 grit	 0.004” 0.0005”	0.001” 0.001” 0.0001”
12.7 mm / 0.500" Fine	1 (roughing) 2 (induce damage) 3 (finishing)	accepted practice 180 grit 600 grit	 0.004” 0.0005”	0.001” 0.001” 0.0001”
12.7 mm / 0.500" RCF-Conventional	“Accepted” practice for RCF test bar finishing			

Wei Wang, a PhD candidate co-advised by Prof. Mark Hadfield at Bournemouth University and ORNL’s Wereszczak, will commence his 6-month research visit at ORNL in early May. Mr. Wang will perform three-ball-on-rod testing while at ORNL and assist in the C-sphere strength and material characterization.

The Air Force Research Laboratory’s H. Trivedi forwarded several ceramic balls that were damaged from their RCF testing for our characterization of that damage. Resonant ultrasound spectroscopy will be used to see if the presence of damage can be readily detected. Other microscopy techniques will also be used to study that damage in an effort to better understand the relationship between RCF performance and ceramic microstructure and microstructural damage.

Japan’s AIST will start a three-year standardization project of RCF testing funded by Japan’s METI, Japan. AIST’s W. Kanematsu invited this project participation for the purpose of performing three-ball-on-rod RCF testing, and the invitation was accepted. The UK and Germany will also participate. AIST will provide materials for the testing.

Status of FY 2005 Milestones

Characterize the effect of sub-surface machining damage on Si_3N_4 rolling contact fatigue performance and submit paper to the open literature on the results and interpretations. [09/05]
On schedule.

Communications/Visits/Travel

- Hitesh Trivedi of UES/USAFRL (Dayton, OH) was visited on 06 January 2005 to discuss RCF testing and material characterization.
- Discussions with Vimal Pujari (Saint-Gobain Advanced Ceramics, Northboro, MA) occurred regarding the RCF testing and characterization of their bearing grade Si_3N_4's.
- Discussions with Biljana Mikjelj (Ceradyne, Costa Mesa, CA) occurred regarding the RCF testing and characterization of their bearing grade Si_3N_4's.
- Several communications occurred with W. Mandler of Enceratec regarding the testing of Toshiba TSN 03-NH Si_3N_4 spheres.

- Professors C. Rubin and G. Hahn of Vanderbilt University were visited on 31 March 2005 to discuss possible RCF interactions/collaborations.

Publications

Y. Wang, M. Hadfield, W. Wang, and A. A. Wereszczak, "Rolling Contact Fatigue of Ceramics," in internal review, to be published as a DOE/ORNL Technical Memorandum.

References

[1] G. D. Quinn, L. K. Ives, and S. Jahanmar, "On the Fractographic Analysis of Machining Cracks in Ground Ceramics: A Case Study on Silicon Nitride," NIST Special Publication 996, National Institute of Standards and Technology, US Department of Commerce, May 2003.

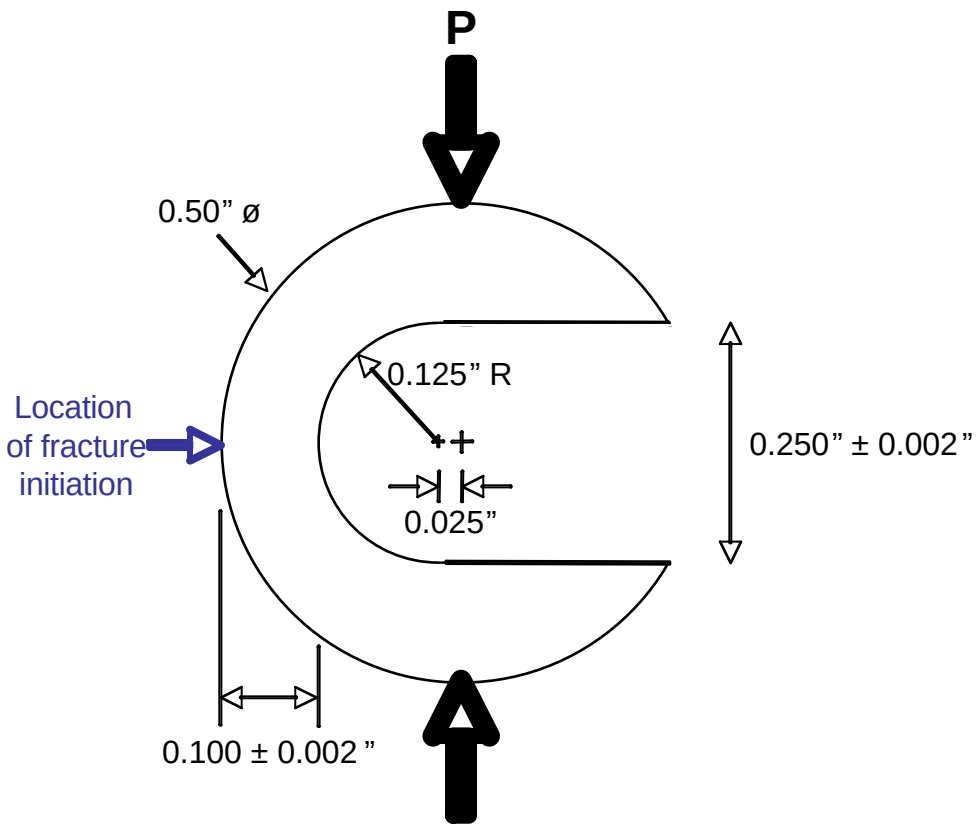

Figure 1. Schematic of the "C-Sphere" test specimen and its diametral compressive loading. Fracture will initiate at the outer surface and propagate radially inward.

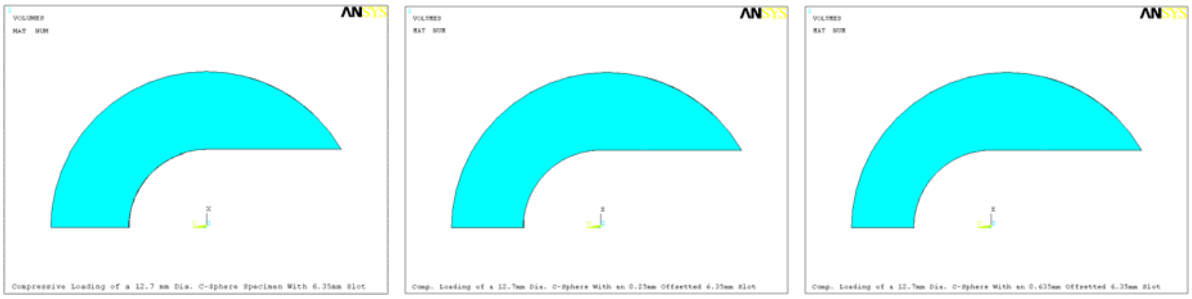

Figure 2. Side views of considered C-sphere specimen geometries. The sphere in all three cases has a 12.7-mm diameter and a through-slot thickness of 6.35 mm. Symmetry about the horizontal plane and the plane of the page enabled the analysis using a 1/4 model. The centerline of the slot's radius of curvature and that of the sphere are coincident in the left image. The slot is shown 0.25 mm deeper in the center image, and is 0.635 mm deeper in the right image.

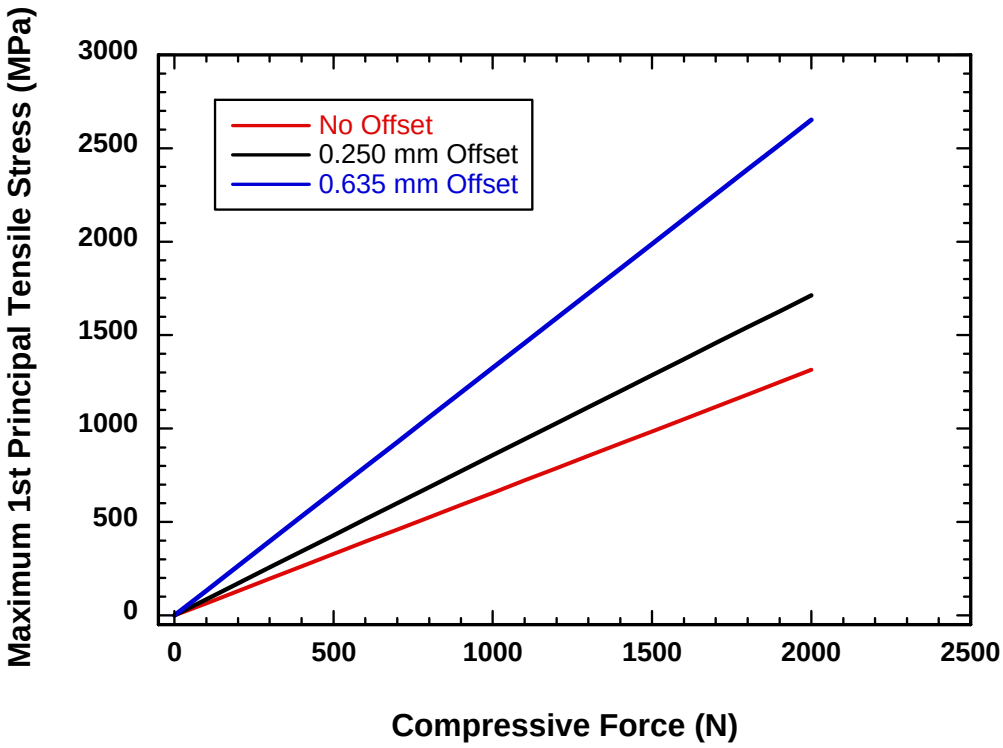

Figure 3. Comparison of generated maximum 1st Principal tensile stress as a function of compressive force for a 12.7-mm-diameter silicon nitride C-sphere with the three geometries shown in Fig. 2. For a given load, the generated out fiber stress is higher when the slot is machined deeper into the sphere.

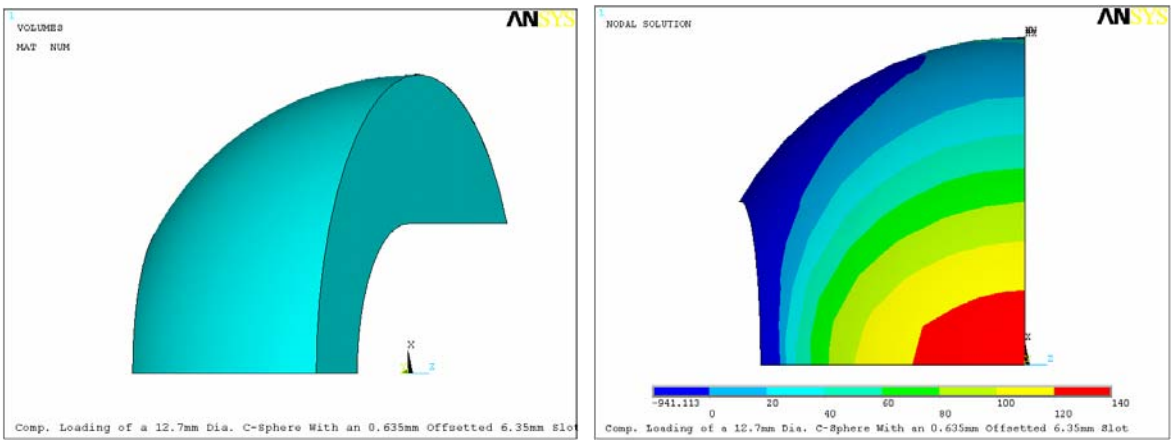

Figure 4. Oblique view (left) of the C-sphere specimen (1/4 model) having a 0.635-mm offset. First Principal Stress field (right) at the specimen's outer fiber for a silicon nitride specimen subjected to 100 N of compressive loading applied on the outer diameter (and perpendicular to the slot).

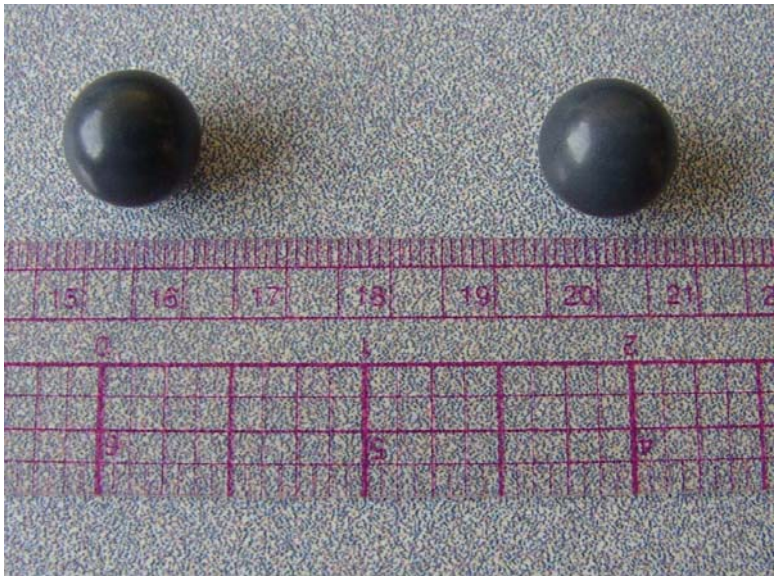

Figure 5. 13.2-mm diameter balls from matrix listed in Table I.

Implementing Agreement For A Programme Of Research And Development On Advanced Materials For Transportation Applications

M. K. Ferber
Oak Ridge National Laboratory

Objective/Scope

The current mission of the IA-AMT is to investigate promising new technologies for evaluating and ultimately improving the performance of materials for transportation systems. The primary motivation for this activity is the fact that new material technologies are required to increase efficiency and reduce harmful emissions in these systems. Examples of these technologies include (1) light weighting to improve fuel efficiency, (2) surface engineering to improve the resistance to wear and contact damage, (3) development of durable coating systems for thermal, wear, and environmental management, and (4) development of revolutionary materials (structural ceramics and ceramic matrix composites) for operation at much higher temperatures and pressures. As discussed below, the research activities within the IA-AMT focus specifically on (1) the identification of promising new technologies for improving materials performance and (2) the development of specialized characterization techniques for validating the applicability of this technology to improve material properties while maintaining acceptable life-cycle costs.

Technical Highlights

This reporting period the laser spallation test for the measurement of coating adherence [1, 2] was evaluated further. In this test, the tensile forces required for coating debonding are generated by a pulsed laser focused on the back of the substrate. This initial impingement generates a compressive wave, which on reflection becomes tensile. Specific tests utilized commercial hardware for Laser Shock Peening (LSP), which is a relatively new surface treatment for generating compressive stress fields in the near surface regions of metallic materials. When applied to selected regions of engineering component such as gas turbine airfoils, these stress fields can greatly improve resistance to fatigue and increase tolerance to foreign object damage. The depth of the compressive residual stresses are typically much greater than those induced by conventional shot peening. As illustrated in Figure 1, the technique involves the production of mechanical shock waves by using a laser to generate a plasma over a small spot on the surface. This plasma is formed by the vaporization and subsequent ionization of a sacrificial material such as black tape or paint, which is first applied to the region to be treated. An over-layer of water, which is transparent to laser radiation, is used to confine the expansion plasma such that a shock wave is driven into the component. The surface and near surface regions are subject to plastic deformation if the pressure of the shock wave is greater than the yield strength of the material under shock conditions. In plane compressive stresses arise as the undeformed material attempts to restore the original shape of the surface.

The compressive pulse that is generated on the front face will be reflected as tensile pulse from the rear surface. If the tensile stresses are of sufficient magnitude they can lead to spallation of material located at the rear surface [3]. If a thin coating is present along the rear surface, these same tensile stresses can cause coating spallation [4].

The present study evaluated the adherence of a thermal barrier coating (TBC) system consisting of (a) bond coats of either vacuum plasma-sprayed (VPS) Ni-22Cr-10Al-1Y or VPS Ni-23Co-

18Cr-12Al-0.3Y, (b) air plasma sprayed (APS) yttria stabilized zirconia (YSZ), and (c) substrates of either single-crystal (SX) Rene N5 or Mar M. In all cases the substrates were in form of 25 mm diameter disks approximately 6 mm in thickness. Typical bond coat and top coat thicknesses were 100 and 250 µm, respectively.

Figure 2, which illustrates a plot of incident power density versus specimen number, was discussed in the previous quarterly report. The samples shown in this figure were subsequently sectioned into two halves and the surface of one the sections polished using conventional ceramographic techniques. As shown in Figure 3, the primary crack in the sample subjected to the lowest power density formed totally within the top coat. Secondary cracks were also observed at the bond coat/substrate interface. In the case of the sample subjected to the highest power density (Figure 4), the primary crack formed at the bond coat/top coat interface and was responsible for coating spallation. Secondary cracking was also observed at the bond coat/substrate interface.

Status of Milestones

(1) Develop draft plan (Annex IV proposal) for implementation of lightweight materials activity. **(Completed: 09/04)**.

(2) Complete Annex II-Subtask 13 effort and issue report. **(Draft prepared-12/04).**

Communications/Visits/Travel

None.

Publications

[1] "Implementing Agreement For A Programme Of Research And Development On Advanced Materials For Transportation Applications (IA-AMT), Strategic Plan," March 2004, available on web site IA-AMT.ornl.gov.

References

[1] P. A. Steinmann and H. E. Hintermann, "A review of the mechanical tests for thin-film adhesion." Journal of Vacuum Science Technology A, Vol. 7, No. 3, 1989, pp. 2267-2272.

[2] J. Valli, U. Makela, and A. Matthews, "Assessment of Coating Adhesion." Surface Engineering, Vol. 2, No. 1, 1986, pp. 49-53.

[3] M. Boustie, F. Cottet, Y. Chauveau, and S. A. Marta, "Spalling of Aluminum and Copper Targets by Laser Shocks," pp. 741-50 in Shock-Wave and High-Strain-Rate Phenomena in Materials, edited by M. A. Meyers, L. E. Murr, and K. P. Stadhammer, Marcel Dekker, Inc., New York, 1992.

[4] M. Boustie, E. Auroux, and J. P. Romain, "Application of the Laser Spallation Technique to the Measurement of the Adhesion Strength of Tungsten Carbide Coatings on Superalloy Substrates," Eur. Phys. J. AP, 12, 47-53 (2000).

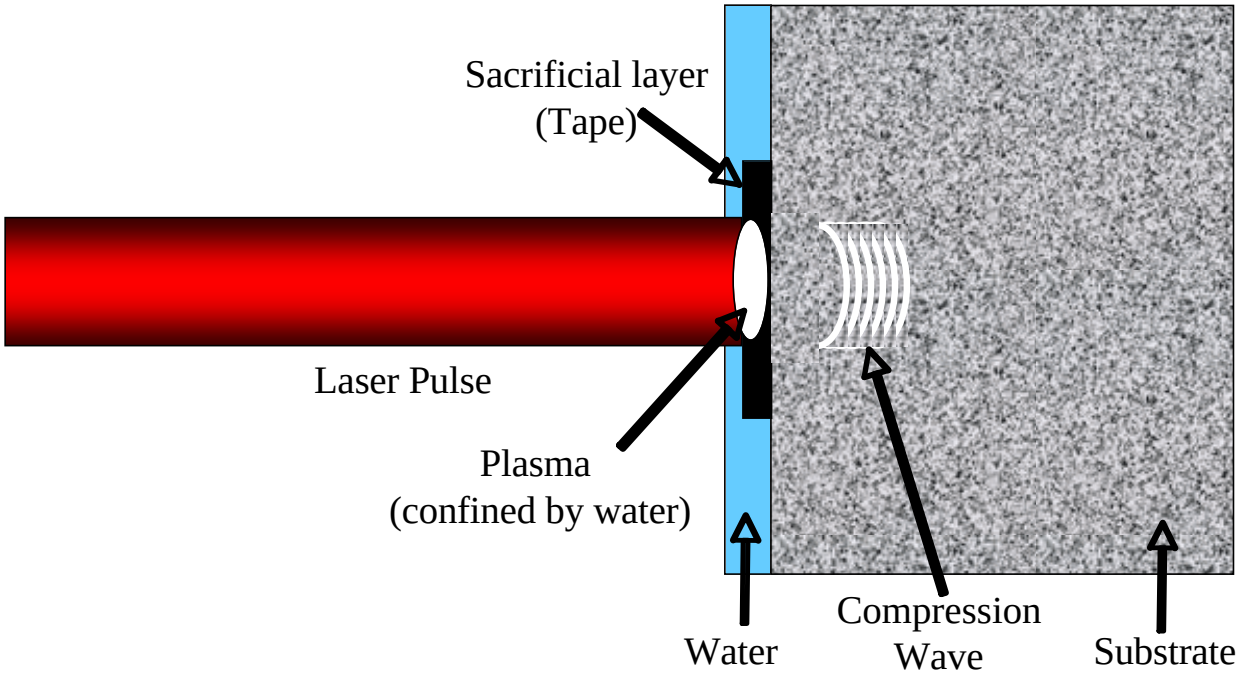

Figure 1: Schematic representation of the LSP process.

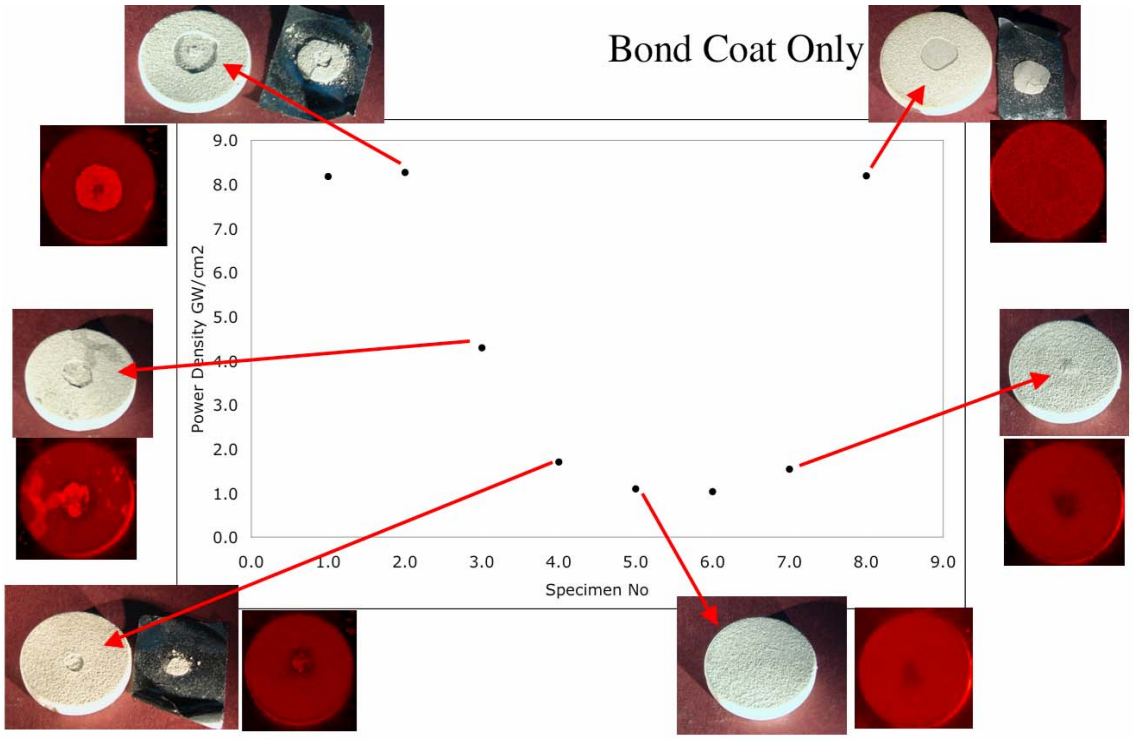

Figure 2: Graph of incident power density versus specimen number.

Specimen 6

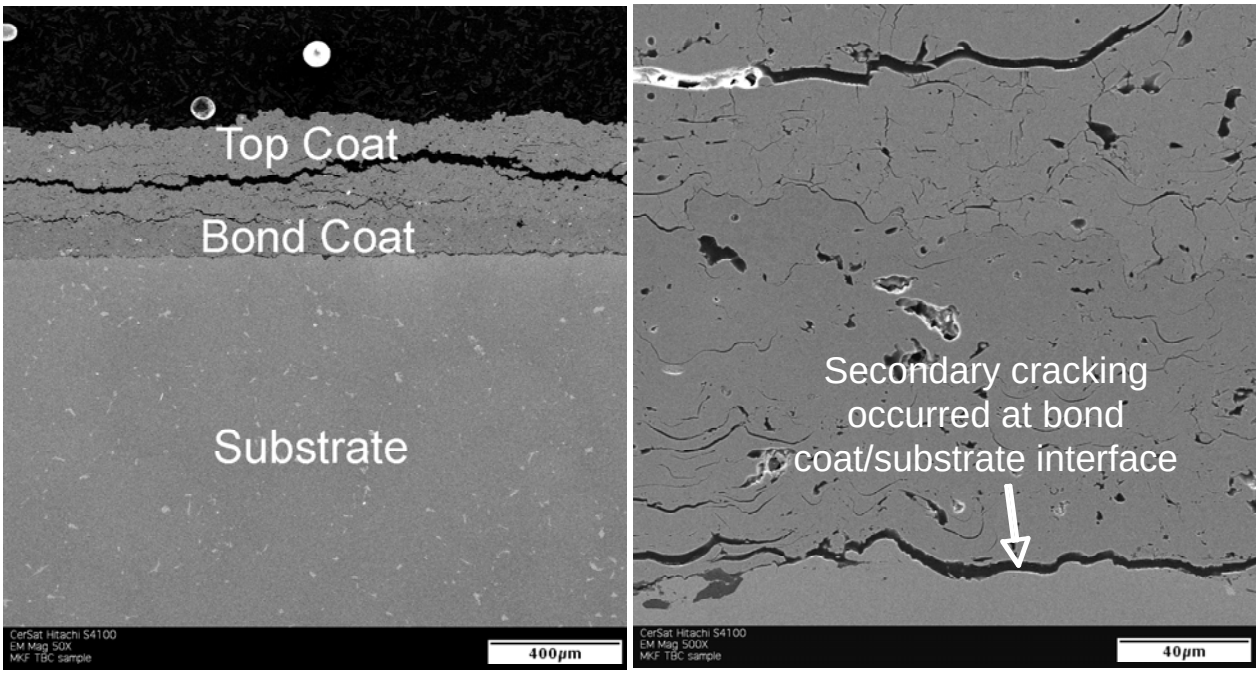

Figure 3: Polished cross-section of Sample 6 (subjected to lowest power density).

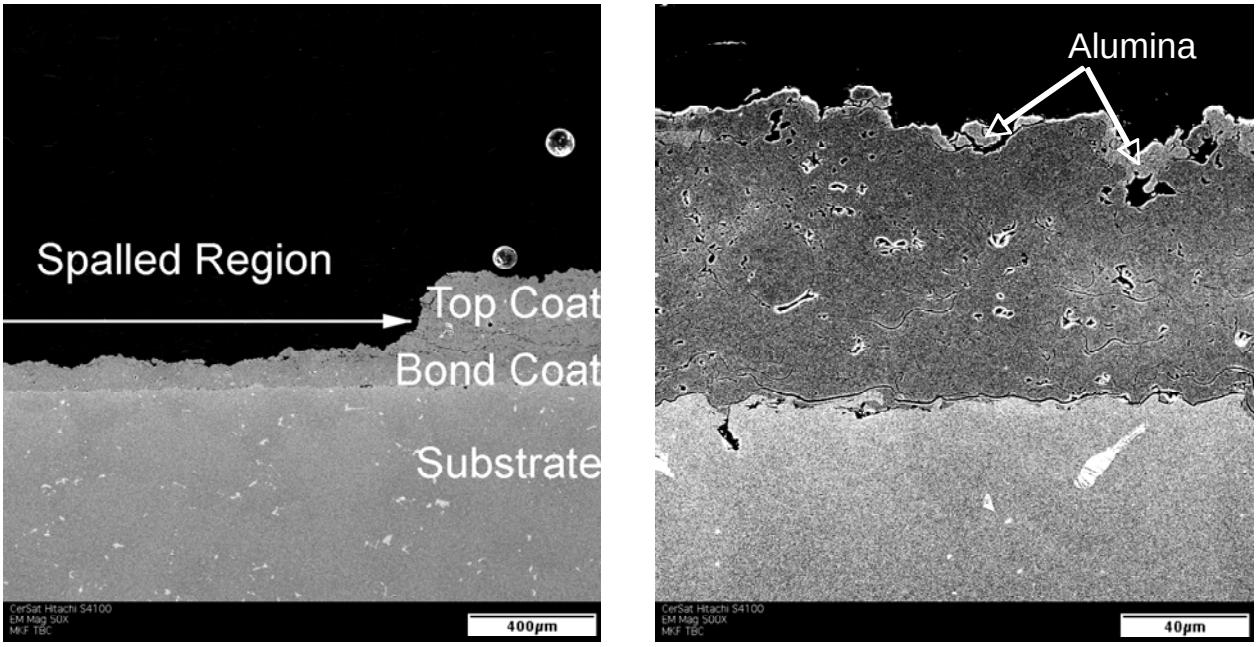

Figure 4: Polished cross-section of Sample 1 (subjected to highest power density).

Mechanical Property Test Development

George Quinn
National Institute of Standards and Technology

Objective/Scope

This task is to develop mechanical test method standards in support of the Propulsion Systems Materials Program. Test method development should meet the needs of the DOE engine community but should also consider the general USA structural ceramics community as well as foreign laboratories and companies. Draft recommendations for practices or procedures shall be developed based upon the needs identified above and circulated within the DOE engine community for review and modification. Round robins will be conducted as necessary. Procedures will be standardized by ASTM and/or ISO.

Technical Highlights.

1. General

A review paper: "Design and Reliability of Ceramics, Do Modelers, Designers, and Fractographers See the Same World?" was presented at the American Ceramic Society conference in January. One of the case studies cited in the paper was the excellent work done by the Ford Motor Company in the early 1980's on a model silicon nitride gas turbine rotor that was spun to failure in a hot test rig (Figure 1).

A status report on the flexural strength test method for round rods was prepared for ASTM Committee C-28. Work continues on a Guide to Practice for Fractography. A compromise solution was found for the scaling of flexural strength numbers in ASTM standard F 2094 for silicon nitride ball bearings. Several ASTM Committee C-28 draft standards were reviewed. New fracture resistance experiments were started using the Vickers indentation crack length method on NIST standard reference materials 2100. Work on split cylinder flexure testing resumed.

Figure 1. A Ford model rotor that was spun to failure and fractographicly analyzed. The origin was either inside bore grinding damage (on right) or grinding damage on a curvic coupling gear tooth (not shown).

2. Fracture Toughness

Despite the fact that a high quality ASTM standard for fracture toughness evaluation has been on the books for 8 years, and the fact that NIST has a Standard Reference Material 2100 to support it, people are still using the defective Vickers indentation crack length method to evaluate fracture toughness. This is despite years of confusion and wildly contradictory data. A sign of the confusion is that there has been an unbridled proliferation of alternative "refined" equations. Some of these are even making their way into material specifications.

Even more alarming is that some users are using the NIST Standard Reference Material 2100, which is a commercial silicon nitride with meticulously measured fracture toughness, to lend credence to the indentation method and are even adjusting the equations to get better agreement with the NIST certified values. This may be acceptable in the short run, but it is clear that fine tuning an equation for one particular silicon nitride will not guarantee that the equation is appropriate for other silicon nitrides, much less other ceramics like alumina or zirconia.

We therefore have begun some Vickers indentation crack length measurements to estimate the "indentation fracture resistance" of the NIST SRM 2100, in order to demonstrate the shortcomings of the method and the errors that can result. Our goal is to get these findings into the literature as soon as possible before the adoption of indentation crack length methodologies gets codified too far. We advocate the use of genuine fracture mechanics tests for evaluating fracture toughness. The Vickers indentation crack length method evaluates a particular measure of fracture resistance, which crudely approximates fracture toughness. The indentation crack length method may have some utility, but data from it ought to be deemed "indentation fracture resistance" and not "fracture toughness."

3. Fractography

Work continued on a NIST user-friendly "Guide to Best Practice" for fractographic analysis. Several case studies were written up and illustrations prepared as examples of applied fractographic analysis. The November 2004 ballot responses for 13 proposed definition changes to standard C 1322 Standard Practice for Fractography were reviewed at the C-28 meeting in Cocoa Beach. Some of the revisions were accepted, but five had to be revised and sent out for further ballot review in March 2005. Two other proposed revisions in November 2004 were accepted. Two proofs of the revised standard C 1322 were reviewed and errors noted and reported to ASTM for correction.

4. Flexural Strength Testing of Cylindrical Ceramic Specimens

We are planning to resume activity on this in May. A new student is on board who will pick up where some of the work left off. Strain gage data will be collected on a steel rod in a new test fixture for round

rods. Some of this work had been done previously, but only at low loads. We are getting inquiries about this and spent some time preparing a summary brief report on the status of this work with some suggestions. This brief package will be sent to future inquirers upon request. A good summary of the status of the project with some preliminary data was prepared for distribution

5. Split Cylinder Flexural Strength Testing

We have resumed activity on this topic this quarter. New zirconia fuel injector pin specimens have been received from Cummins. Some of these will be split and tested in flexure, and the results compared to Cummins' own 3-point flexure data. A new student is on board who will work on this project nearly full time. The technical literature for strength and fracture toughness of zirconia was reviewed in preparation for this work.

6. Hardness

No activity.

7. Diametral Compression

No progress this quarter.

8. Other

Revisions to ASTM Standard F 2094, Specification for Silicon Nitride Ball Bearings and new ISO Proposals

Following up work started last quarter, we continued to work on the revision to this standard. It was adopted in 2001 by ASTM Committee F-34. Over the years we have contributed a lot to the development of this standard, which has aided the commercialization of silicon nitride ball bearings. One of the loose ends in the document was a questionable table on required flexural strengths for the three grades (materials class) of silicon nitride specified in the standard. The standard specifies average flexural strengths, which could be measured by either 3-point or 4-point flexure, and either by the USA-ASTM-European methods or by the Japanese Industrial Standard method. Unfortunately, these methods all have different effective volumes and effective surfaces so the numbers should vary with the test procedure.

After one formal ASTM ballot was taken, and some subsequent back and forth with Bill Mandler of Enceratec, a new table was prepared by Bill that satisfies Ceradyne and other USA interests. A revision to F 2094 will the new conversion table is currently being balloted in ASTM. The compromise solution uses some 3-point values for the baseline strength and some 4-point values in other instances. The timing is important since we have subsequently learned that the Japanese delegation will formally submit a New Work Item proposal to ISO Technical Committee TC 206 very soon on this matter. We have also learned that in September 2004, European interests submitted yet another proposal for a silicon nitride bearing ball specification to ISO committee 4, Rolling Bearings. The latter draft is almost an exact clone of the ASTM F

2094. This intensive specifications activity is a sign that commercialization of silicon nitride bearings is progressing very well.

ASTM Committee C-28, Advanced Ceramics support

G. Quinn reviewed the new static fatigue test method draft standard that is being balloted in C-28. Kristin Breder is doing a good job with this draft standard.

G. Quinn also reviewed the entire history of Committee C-28's awards and furnished a summary report to Kristin Breder, the current award committee leader. Quinn also reviewed the history of the development of two ASTM powder characterization standards C 1282 and C 1274 and sent a summary to Steve Gonczy, the C-28 chairman. Gonczy wanted to know the background so that plans could be made to upgrade or refine or drop these two standards as appropriate. Similarly, G. Quinn compiled a history of the development of the two C-28 nondestructive standards C 1212 and C 1336, on seeded inclusions and seeded voids.

Status of Milestones

412149 Prepare ballot-ready first ASTM draft of cylindrical rod flexure strength test.

Overdue

412151 Prepare review paper on flexural testing of cylindrical rods.

Overdue, Ongoing work on error analysis

Communications/Visits/Travel

1. Andy Wereszczak visited in April to discuss new hardness and indentation fracture toughness results for silicon nitride material. G. Quinn searched for and copied some relevant indentation size effect data from the University of Cambridge in the 1980's as well as several dynamic fracture toughness references.
2. A letter was sent to Theo Fett in Germany regarding his proposed new method for testing disks in biaxial loading. Fett proposes loading with three balls while also supporting the disk with three balls. This is one way to deal with warped or as-fired disks, but the Weibull effective volumes or Weibull effective surfaces will be puny.
3. Ted Lilley inquired about the status of the flexure strength of round rod standards and a progress report was sent to him.
4. G. Quinn attended the ASTM Committee C-28 meeting in Cocoa Beach.
5. Zirconia pins were received from Randy Stafford at Cummins for evaluation.

Publications and Presentations

1. G. D. Quinn, "Design and Reliability of Ceramics, Do Modelers, Designers and Fractographers See the Same World?" presented at Jan. 2005 Cocoa Beach Ceramic Society Conference, to be publ. Ceram. Eng. and Sci. Proc., 2005.

Surface Modification of Engineering Materials for Heavy Vehicle Applications

Stephen Hsu
National Institute of Standards and Technology

Objectives

- Organize an international cooperative research program on an integrated surface modification technology under the auspice of the International Energy Agency (IEA)
- Design and identify surface features and patterns that can achieve friction reduction and enhanced durability for heavy duty diesel engine components.
- Develop understanding and appropriate models to explain the texturing effects on frictional characteristics. Develop appropriate thin films and coatings to achieve synergistic and complementary relationship with texturing to enhance performance.
- Discover and develop surface chemistry for protecting the films and coatings which work in synergy with the coatings.

Approach

- Determine the effect of size, shape, pitch, and patterns of surface textural features on friction under 1) high speed, low load regime; 2) high load, high speed regime; 3) high load, low speed regime.
- Develop cost effective fabrication technologies for creating surface textural features on various surfaces including metals, ceramics, and coatings.
- Develop test methodology to measure the effects of the textures on friction
- Conduct research to develop an integrated system approach to combine the best practices in thin films, coating, and surface chemistry for performances unrealizable by individual approach alone.
- Concurrently, organize an international cooperative research program under the auspice of the International Energy Agency (IEA) to pool resources and share this energy conservation technology worldwide.

Accomplishments this quarter

- Planned a joint Symposium with COST 532 (European Cooperative Research consortium on Triboscience and Tribotechnology) on surface texturing on Oct. 12, 2005, in Porto, Portugal.
- Visited various Chinese Organizations in Beijing and made contacts with the Ministry of Science and Technology regarding IEA activity. Lanzhou Institute of Chemical Physics of the Chinese Academy of Sciences has agreed to participate in IEA surface texturing research.
- Developed a cost-effective chemical etching technique on steel surfaces that gave comparable friction reduction results as those from nanomechanical scratching techniques under boundary lubricated conditions.

Introduction

Frictional losses are inherent in most practical mechanical systems. The ability to control friction offers many opportunities to achieve energy conservation. Over the years, materials, lubricants, and surface modifications have been used to reduce friction in automotive and diesel engine applications to promote energy efficiency. However, in recent years, progress in friction

reduction technology has been slow since much inefficiency has been eliminated already. A new avenue is needed.

Recently, laser ablated dimples on surfaces have shown friction reduction properties and have been demonstrated successfully in conformal contacts such as seals where the speed is high and load is low. The effect of dimples on friction reduction appears to depend on dimple size, pattern of dimples, and density of dimples on the contacting surfaces. However, this friction reduction property has not been shown to be effective under high load, low speed conditions. Nevertheless, the use of surface texture has opened a new avenue to explore friction reduction in engine applications.

The objective of this project, therefore, is to explore the possibility of surface texture designs to achieve friction reduction in energy transmission devices in conjunction with thin films and coatings under a broad range of contact conditions and develop design guidelines for technology implementation world wide.

To achieve world wide energy conservation, a concomitant international cooperative research under the auspice of the International Energy Agency will be launched to pool resources from various countries to accelerate this technology development. Towards this end, UK, Germany, Finland, Sweden, Israel, and Japan have agreed to participate under the IEA annex IV on this activity.

Approach

Previously, experiments were conducted to examine various surface textures on steel surfaces using photolithography and chemical etching. Using the same area coverage (% of area occupied by the surface textural features), surface features such as grooves, triangles, ellipses, circles were compared under high speed low load conditions similar to those used by surface seals. Results indicated that 1) surface feature shape had great influence on friction reduction; 2) friction reduction also depended strongly on the orientation of the surface features with respect to the direction of sliding. This suggested that conventional theory of hydrodynamic lift was not adequate to explain these observations. A new theory is needed. Therefore, an in situ video camera was set up to observe the lubricant flow pattern in a single dimple under different operating conditions. The magnification, however was inadequate to clearly define the detailed flow patterns to deduce the friction reduction mechanism, this quarter with improved technique and instrument, we observed cavitation for the first time based on model fluids.

For high load low speed conditions, the same surface textural features yielded higher friction than untextured surfaces due to increased surface roughness. A collaborative effort with Northwestern University using a sophisticated elastohydrodynamic friction model confirmed our experimental observations. Basically, under boundary lubricated conditions (high load low speed), the edge stresses around the dimple increase friction rather than decrease friction. A new surface textural feature with an inclined plane at the bottom of the feature was developed using a mechanical scribing technique by a triboindenter. Because of the triboindenter had limited load range, soft metals such as aluminum, copper, and brass were used. Since the pin-on-disk apparatus was limited by load, a four-ball wear tester with the configuration of ball-on-three-flat was used to generate high contact pressures. Using this kind of features, elongated dimples on soft metals

were successful in achieving significant friction reduction under high contact pressures exceeding one GPa. Last quarter, the triboindenter was upgraded to have a high load head so we were able to fabricate features on 52100 steel surfaces. We achieved significant friction reductions under boundary lubricated conditions. This quarter, we focus on developing a low cost chemical etching technique and test the samples to see whether we can achieve the same friction reduction capability.

Technical highlight

When we used hard metals such as 52100 steel, the initial high contact pressure caused severe wear damaging the surface textures and the friction reduction results were erratic. To overcome this issue, we developed a wear-in procedure to create a smooth crater surface of approximately 0.5 mm diameter and the texture was then carved onto the surface inside the crater with a diamond tip on the triboindenter. This way, a controlled interface was created to avoid severe wear-in. Last quarter, we demonstrated that friction in a 52100 steel/52100 steel contact could be reduced significantly from 0.09 to 0.06. Increasing feature density helps but the optimum may be in the shallow textural depths.

This quarter, we focus on developing a low cost and rapid fabrication method and conduct tests to verify the friction reduction characteristics of the new fabrication technique. We have used microlithography/chemical etching process previously to fabricate dimples with depth ranging from 3 to 10 μm. For shallow dimples, we need to control the etching process precisely.

Numerous factors can affect the electrochemical etching, including electrolyte properties, voltage, and composition of the material. Since electricity always passes the way with high conductivity, the inhomogeneous oxidant on the work piece will make etching selective. This is critical when shallow depth is needed. A special electrolyte composed with acids was used for this purpose. Acid is effective to remove the oxidant on the surface so that etching can start uniformly.

Conducted a series experiments to verify if etched patterns also have the effect of friction reduction at boundary lubrication regime. In order to compare to the results with the texture fabricated by the nanoindenter, all conditions except the fabrication method were kept the same as in the experiments reported last quarter. The texture was fabricated on the pre-worn scar on the disk of 52100 hardened steel. The surface textural features were circle in shape with etched depth ranging from 0.25 to 1.00 micrometer. All features have the same fractional area density of 7%. Table 1 illustrates the experimental design and Figure 1 shows the appearance of the textured surfaces.

Table 1 Experimental design

		Depth (μm)		
		0.25	0.50	1.00
Diameter (μm)	20	Texture 11		Texture 13
	40		Texture 22	
	60	Texture 31		Texture 33

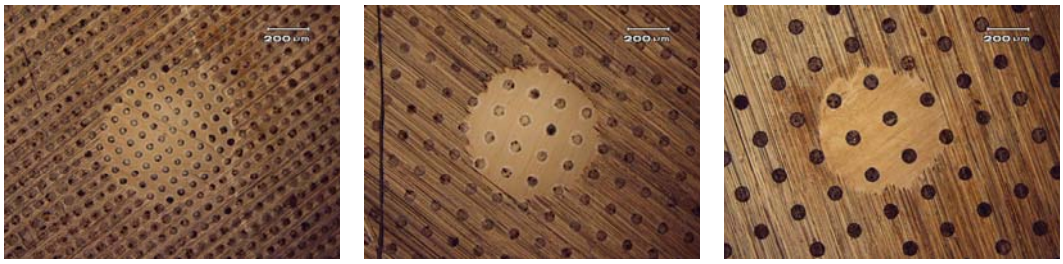

Fig. 1 Appearance of textured surfaces

A four-ball wear tester was used to carry out the friction tests using a ball-on-three flat configuration. The load was varied from 10 kg to 30 kg, corresponding to the average contact pressure ranging from 300 MPa to 450 MPa. The rotational speed was increased from 500 rpm (0.19 m/s) to 3500 rpm (1.34 m/s). All the initial friction coefficients for the untextured surface were from 0.08 to 0.1 signifying that the test condition was in the boundary lubricated condition.

Figures 2 and 3 present the friction coefficient obtained at 10 kg and 30 kg respectively. The results show that up to 32% friction reduction has been achieved by Texture 11. Thus, the etched dimples may still be effective at boundary lubrication regime. The results of different texture patterns indicate that the pattern with small and shallow dimples is more effective than that with large and deep dimples.

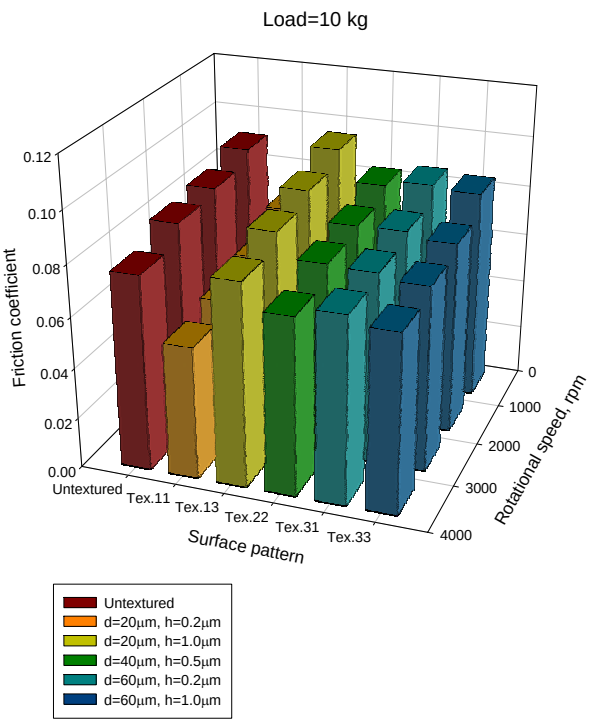

Fig. 2 Friction coefficient of untextured and textured surface at the load of 10 kg

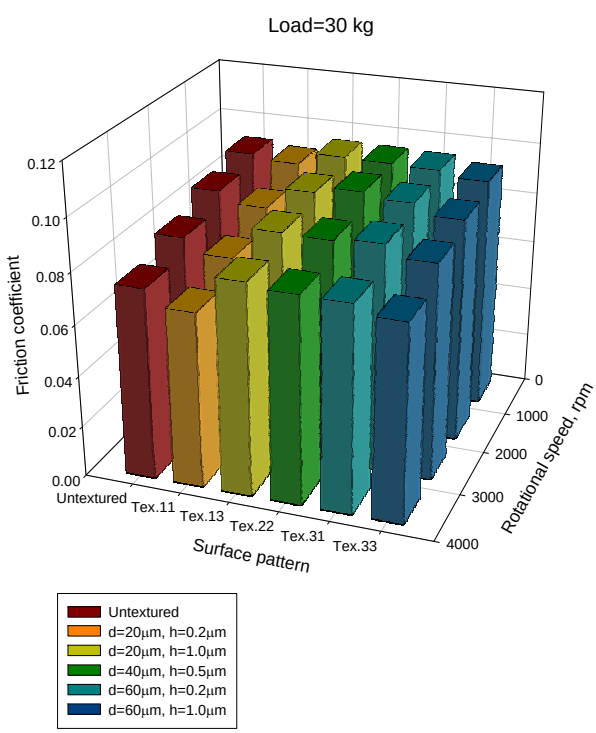

Fig.3. Friction coefficient of untextured and textured surface at the load of 30 kg

In summary, we have successfully developed a rapid low cost chemical etching process that can partially duplicate the results from those fabricated using a triboindenter.

Publications/Presentations

Presentations:

Jorn Larson Basse, X. Wang, L. Ives, S. M. Hsu, "Some friction experiments with dimpled surface texture," The fourth China International Symposium on Tribology, Xian, China, Nov. 8-11, 2004.

S. M. Hsu, "An Integrated surface modification technique to control friction: a new paradigm," Keynote speaker, the 4th China International Symposium on Tribology, November 8-11, 2004, Xian,China.

Y. Chae, X. Wang, S. M. Hsu, "The size effect of surface texture on lubricated friction," The First International Conference on Advanced Tribology, Singapore, Dec. 1-3, 2004.

Publications:

Jorn Larson Basse, X. Wang, L. Ives, S. M. Hsu, "Some friction experiments with textured surfaces," Proceedings of Nordic Symposium on Tribology, Troms, Norway, June 2004.

X. Wang, S. M. Hsu, "An Integrated surface modification technique to control friction: a new paradigm," Keynote paper, the 4th China International Symposium on Tribology, November 8-11,2004, Xian,China.